論文 / 著書情報
Article / Book Information

題目(和文)	極微光デバイス製作のための反応性イオンビームエッチングに関する研究
Title(English)	A Study of Reactive Ion Beam Etching Process for Optoelectronic Micro-Devices
著者(和文)	松谷晃宏
Author(English)	akihiro matsutani
出典(和文)	学位:博士(工学), 学位授与機関:東京工業大学, 報告番号:乙第3270号, 授与年月日:1999年2月28日, 学位の種別:論文博士, 審査員:
Citation(English)	Degree:Doctor (Engineering), Conferring organization: Tokyo Institute of Technology, Report number:乙第3270号, Conferred date:1999/2/28, Degree Type:Thesis doctor, Examiner:
学位種別(和文)	博士論文
Type(English)	Doctoral Thesis

A Study of Reactive Ion Beam Etching Process for Optoelectronic Micro-Devices

（極微光デバイス製作のための反応性イオンビームエッチングに関する研究）

by

Akihiro Matsutani

1998

Adviser: Professor Kenichi Iga

Associate Professor Fumio Koyama

Tokyo Institute of Technology

4259 Nagatsuta, Midoriku, Yokohama 226-8503, Japan

Chapter 1 Introduction

In this chapter, the background of my study is first introduced. Next, the important issues of dry etching technologies for microoptoelectronic devices are described. Then, the objective of this study is present. Finally, the outline of this thesis is described.

1.1 Background and History of Dry Etching Process

This study is the investigation on low damage microfabrication technologies of reactive ion etching for dielectric multilayers and reactive ion beam etching for InP, GaAs and related materials which are important in optoelectronics. Various laser structures have been investigated since the appearance of semiconductor lasers. In the development of semiconductor lasers, the development of the fabrication technology has been needed as well as the epitaxy technology of semiconductor crystal. So far, the wet etching was used as a microfabrication technology of semiconductor laser. This is a process that fabricate the wafer to form desired shapes by dipping itself in the solution. Although the wet etching is a simple process, the etching shape is isotropic profile dependent on crystal orientation, because of chemical reaction between the crystal and the solution. Accordingly, the anisotropic and high aspect ratio etching cannot be obtained, and the fabrication size is limited. On the other hand, the dry etching technology can overcome these difficulties of wet etching.

The dry etching technique using a discharged plasma is now widely used as a fundamental tool to fabricate various semiconductor devices such as integrated circuits, especially large scale integrated circuits (LSI) or VLSI, which are made on Si substrates, compound semiconductor devices such as GaAs FET, GaAs IC, optoelectronic integrated circuits (OEIC), Josephson effect devices and so on. In these devices, the fabrication of submicron sized patterns are becoming more and more with increasing memory capacities.

In an earlier state of dry etch, non-reactive gases such as Ar discharged plasma were used. This dry etching characteristics are mainly physical sputtering. This technique is called ion beam etching (IBE). The mechanism of ion beam etching is cutting of the ion bombardment of substrate atom by ion collision. However, a high ion energy is required to obtain the

useful etching rate. Therefore, in IBE, the substrate surface is damaged by high energy ions. This is a disadvantage in devices characteristics. However, in early 1970's, new dry etching technique with a halogen gas was firstly used in microfabrication of Si. This new technique was noticed immediately and the investigation has started [1]. Then, the model of plasma etching process was proposed by Coburn and Winters in 1978 [2], and the dry etching of Si have been investigated in many ways. At present, in the dry etching of Si, reactive ion etching (RIE) is widely and commercially used. Figure 1-1 shows the model of plasma etching process that Coburn and Winters proposed.

On the other hand, III-V semiconductor materials such as GaAs, InP and related compounds have been widely used for semiconductor lasers, integrated optoelectronic devices and high speed electronic devices. In order to fabricate stripe geometry semiconductor lasers and optical waveguides, a wet etching technique has been commonly employed. However, the present wet etch is not necessarily suitable for making a tiny structure of several microns or even smaller sizes due to the lack of reproducibility and the existence of noticeable side etching except some particular crystal orientations. To overcome theses problems up to now, several dry etching techniques such as ion beam etching (IBE), reactive ion etching (RIE), reactive ion beam etching (RIBE), and more sophisticated techniques with assistance of laser light and electron beam have been studied. Among them, the IBE system can etch with high resolution but its etch rate is very low and it generates surface damages which is not negligible in the case of bipolar devices. On the other hand, several results on the etching characteristics of GaAs and InP using a conventional RIE system have been reported, and some semiconductor laser devices with vertically etched facets [3] or vertical circular mesas [4-6] were fabricated and light emitting diode by coaxial transverse junction [7] using the RIE. The RIE system provides a good selectivity but it is rather difficult to fully control its etching parameters.

The RIBE which includes the advantage of IBE and RIE can exhibit a high resolution and a good selectivity. Moreover, its high etch rate will be another advantage. In addition to these merits, it is possible to independently control a lot of etching parameters, such as gas pressure, plasma density, ion current density and ion energy, that are helpful for choosing a condition between the IBE like etch behavior and the RIE like etch behavior. As for GaAs,

etching characteristics using an ultrahigh vacuum RIBE system were initially studied by Asakawa *et al.* [8] in 1983. Almost equi-rate etching for both GaAs and GaAlAs was realized by eliminating residual oxygen by an ultra-high vacuum (UHV) system. In 1986, short cavity GaAs /AlGaAs multiquantum well lasers fabricated by RIBE was reported by Yuasa *et al* [9]. Moreover, in 1987, GaAs-AlAs monolithic microresonator arrays using chemically assisted ion beam etching (CAIBE) was reported by Jewell *et al* [10]. However, only a few results on InP using the RIBE technique have been published [11-13] and systematic data on etching parameters had not been fully clarified before 1988. In general, the etching of In-contained materials is difficult become the boiling point of In-products is very high. Table 1-1 shows the boiling point of halogenide for III-V group elements (at 1atm.) [14]. In 1988, ABC-diagram was proposed to classify the etching mechanism of RIBE by Tadokoro *et al* [15]. Then, this study has been started.

The background and history of this thesis is summarized in Table 1-2. In appendix A, the outline of some dry etching technique are briefly described. Moreover, Fig. 1-2 shows the applications of dry etching.

1. 2 Problems of Dry Etching for Microstructure Optoelectronic Devices

The semiconductor laser diodes have been investigated extensively since its appearance, in particular as for distributed feedback (DFB) lasers, vertical cavity surface emitting lasers (VCSELs)[16], quantum well lasers and so on. The RIE is generally used as a fabrication technology for these devices, as well as Si integrated circuits. In the dry etching of III-V semiconductor, CH_4 or CCl_2F and so on are used as an etching gas [4, 17]. Although the surface etched by these gases is generally smooth, the etched surface is contaminated by the carbon included in the etching gas. Moreover, the wafer induced damage is relatively large, because the sample is set in the plasma. Therefore, the low damage and contamination-free etching technology is needed for the device fabrication.

Next, let me consider vertical cavity surface emitting lasers (VCSELs) and microcavity lasers with etched facets. The ultralow threshold operation or spontaneous emission control [18] of VCSELs is expected by introducing a microcavity structure. In order to realize such a

microcavity laser, fabrication of a highly reflective mirror is one of the key technologies. For this purpose, dielectric multilayer reflector consisting of SiO_2/TiO_2 [19] or Si/SiO_2 and semiconductor multilayer reflector consisting of GaInAsP/InP or AlAs/GaAs [20] are used. In order to control the transverse mode of the microcavity laser as well as to inject current into the active layer, the fabrication of a very small dielectric multilayer reflector is needed [21]. Also, a steep and smooth etching profile is required for highly reflective micromirror by eliminating diffraction and scattering losses in multilayer reflectors. In the wet etching, the etching shape is not necessarily smooth and steep. On the other hand, the etching shape in dry etching is expected to be smooth and vertical without influence of crystal orientation, because of etching by fixed ions in direction. Therefore dry etching is used as an effective microfabrication technique to form etched facet lasers. But its etching characteristics for multilayered materials have not been investigated in detail.

Moreover, it is important for such a microcavity laser to reduce the etched sidewall damage. However, the sidewall induced damage has not been investigated. Also, a smooth etched facet is needed to reduce the etching-induced damage at sidewalls. However, the quantitative evaluation of sidewall roughness is has not been fully studied. The dry etching technique using Cl_2 gas causes unwanted side-etching near the bottom of etched samples, which should be avoided for submicron device fabrication such as VCSELs and microcavity lasers. So far, the origin on this side etching is not clear. Then, the application to VCSELs and microstructure optoelectronic devices is also a problem. Moreover, the plasma characteristics have not been clarified in RIBE. It is also important to investigate a suitable mask material.

These unsolved problems in the beginning of this study are summarized as follows;

(1) Microfabrication of multilayers for VCSELs

(2) Induced damage on sidewall and surface

(3) Quantitative evaluation of etched sidewall roughness and improvement of etching profile and investigation of suitable mask material

(4) Plasma Characterization in RIBE

(5) Application to VCSELs or microstructure optoelectronic devices

1.3 Objective of this study

As above mentioned, in applying dry etching process to fabrication of the micro-structure optoelectronic devices, there are some significant problems.

Therefore, on this study, I think the RIBE is one of the best technique for submicron devices such as VCSELs and microcavity lasers. The reason is that it can independently select many etching parameters, and is able to perform suitable etching behaviors such as low damage etching, fine pattern etching, etc. Also, the RIE technique is available for microfabrication of dielectric multilayer mirrors. So, I adopted the RIBE technique for semiconductor etching and the RIE for dielectric mirror etching.

Therefore the following is set up as the main object of my study.

(1) To establish microfabrication of multilayers for VCSEL fabrications

(2) To characterize and to avoid RIE and RIBE induced damage

(3) To evaluate quantitatively etched sidewall roughness and to improve etching profiles and to investigate new suitable mask material

(4) To characterize process plasma in RIBE

(5) To apply the RIBE to the fabrication of VCSELs and microstructure optoelectronic devices

1.4 Outline of This Thesis

According to these plans, the outline of this thesis was determined. The outline of this thesis is shown in Fig. 1-3. In chapter 2, I carried out the microfabrication of GaInAsP/InP multilayer reflectors for surface emitting lasers by RIBE. In this chapter, the etching characteristics of GaAs, InP and GaInAsP is discussed. Moreover, it is necessary for microfabrication to suppress mask edge fluctuations. Therefore, in this chapter, microetching by RIBE using mask written by electron beam direct patterning is described. In chapter 3, RIBE-induced damage in InP substrates was characterized by C-V and PL measurements. In addition, the removal of the induced damage by the second RIBE with different conditions for the InP wafer was demonstrated. The sidewall damage is characterized by photoluminescence emitted from the etched sidewall of a GaInAsP/InP double hetero structure

(DH) wafer. Inaddition, RIE- induced damege is discussed. In chapter 4, roughness analysis of sidewalls processed by RIBE is discussed. This roughness analysis is important for devices with etching mirrors. In chapter 5, the etching profile of RIBE and in-situ measurements of temperature variation with a radiation thermometer during Cl_2-RIBE is discussed. I found that the side-etch is caused by the temperature rise of the sample surface due to ion irradiation. I have also proposed a multistep RIBE for improving etched profiles. In chapter 6, plasma characterization in RIBE and CAIBE is presented. In chapter 7, C_{60} resist mask of electron beam lithography for RIBE is described as a new mask material. Taking account of a recent development of VCSELs in chapter 8, the application of RIBE and RIE to surface emitting lasers is presented. Finally, conclusions of this thesis are summarized in chapter 9.

References

[1] For example, James A. Bondur, "Dry process technology (reactive ion etching)," *J. Vac. Sci. Technol.*, 13, pp. 1023-1029, 1976.

[2] J. W. Coubrn and Harold F. Winters, "Ion-and electron-assisted gas-surface chemistry -An important effect in plasma etching," *J. Appl. Phys.*, 50, pp. 3189-3195, 1979.

[3] L. A. Coldren, K. Iga, B. I. Miller and J. A. Rentschler, "GaInAsP/InP stripe-geometry laser with a reactive-ion-etched facet," *Appl. Phys. Lett.*, 37, pp. 681-683, 1980.

[4] for example, R. E. Kinger and J. E. Greene, "Reactive ion etching of GaAs in CCl_2F_2," *Appl. Phys. Lett.*, 38, pp. 620-622, 1981.

[5] for example, L. A. Coldren and J. A. Rentschler, "Directional reactive-ion-etching of InP with Cl_2 containing gases," *J. Vac. Sci. Technol.*, 19, pp. 225-230, 1981.

[6] H. Yamada, H. Ito and H. Inaba, "Microprocessing of GaAs Cylindrical Columns for Integrated Optical Device Fabrication by Cl_2-Ar Reactive Ion Etching," *Electron. Lett.*, 20, pp. 591-592, 1984.

[7] H. Ito, N. Komagata, H. Yamada and H. Inaba, "Novel structure of laser diode and light-emitting diode realised by coaxial transverse junction (CTJ)," *Electron. Lett.*, 20, pp. 577-579, 1984.

[8] K. Asakawa and S. Sugata, "GaAs and AlGaAs equi-rate etching using a new reactive ion beam etching system," *Jpn. J. Appl. Phys.*, 22, pp. L653-655, 1983.

[9] T. Yuasa, T. Yamada, K. Asakawa, S. Sugata and M. Ishii, M. Uchida, "Short cavity GaAs/AlGaAs multiquantum well lasers by dry etching," *Appl. Phys. Lett.*, pp. 1007-1009, 1986.

[10] J. L. Jewell, A. Scherer, S. L. McCall, A. C. Gossard and J. H. English, "GaAs-AlAs monolithic microresonator arrays," *Appl. Phys. Lett.*, 51, pp. 94-96, 1987.

[11] M. A. Bosch, L. A. Coldren and E. Good, "Reactive ion beam etching of InP with Cl_2," *Appl. Phys. Lett.*, 38, pp. 264-266, 1981.

[12] R. A. Barker, T. M. Mayer and R. H. Burton, "Surface composition and etching of III-V semiconductors in Cl_2 ion beams," *Appl. Phys. Lett.*, 40, pp. 583-586, 1982.

[13] Y. Yuba, K. Gamo, G. He, Y. S. Zhang and S. Namba, "Ion beam etching of InP. II.

Reactive etching with halogen-based source gases," *Jpn. J. Appl. Phys.*, 22, pp. 1211-1214, 1983.

[14] R. C. Weast and M. J. Astle, *CRC Handbook of chemistry and physics, CRC Press. Boca.*, pp. B-73, 1980.

[15] T. Tadokoro, F. Koyama and K. Iga, "Classification of etching mechanism in reactive ion beam etching," *J. Vac. Sci. Technol.*, B7, pp. 1111-1114, 1989.

[16] K. Iga, F. Koyama and S. Kinoshita, "Surface Emitting Semiconductor Lasers," *IEEE Journal of Quantum. Electron.*, 24, pp. 1845-1855, 1988.

[17] R. Cheumg, S. Thomas, S. P. Beaumont, G. Doughty, V. Law and C. D. W. Wilkinson, "Reactive Ion Etching of GaAs Using a Mixture of Methane and Hydrogen," *Electron. Lett.*, 23, pp. 857-859, 1987.

[18] T. Baba, T. Hamano, F. Koyama and K. Iga, "Spontaneous Emission Factor of a Microcavity DBR Surface-Emitting Laser," *IEEE J. Quantum Electron.*, 27, pp. 1347-1358, 1991.

[19] T. Sakaguchi, F. Koyama and K. Iga, "Electron Beam Evaporation of TiO_2/SiO_2 Dielectric Multi-layer Reflector for Surface Emitting Lasers," *International Meeting on Advanced Materials,* K4.6, *Tokyo,* 1988.

[20] T. Sakaguchi, F. Koyama and K. Iga, "Vertical Cavity Surface-Emitting Laser with an AlGaAs/AlAs Bragg Reflector," *Electron. Lett.*, 24, pp. 928-929, 1988.

[21] M. Shimizu, F. Koyama and K. Iga, "BPM Analysis for Transverse Mode Stabilization of Surface Emitting Laser," *Dig. 3rd Optoelectronic Conf.*, 13B1-5, pp. 196-197, 1990.

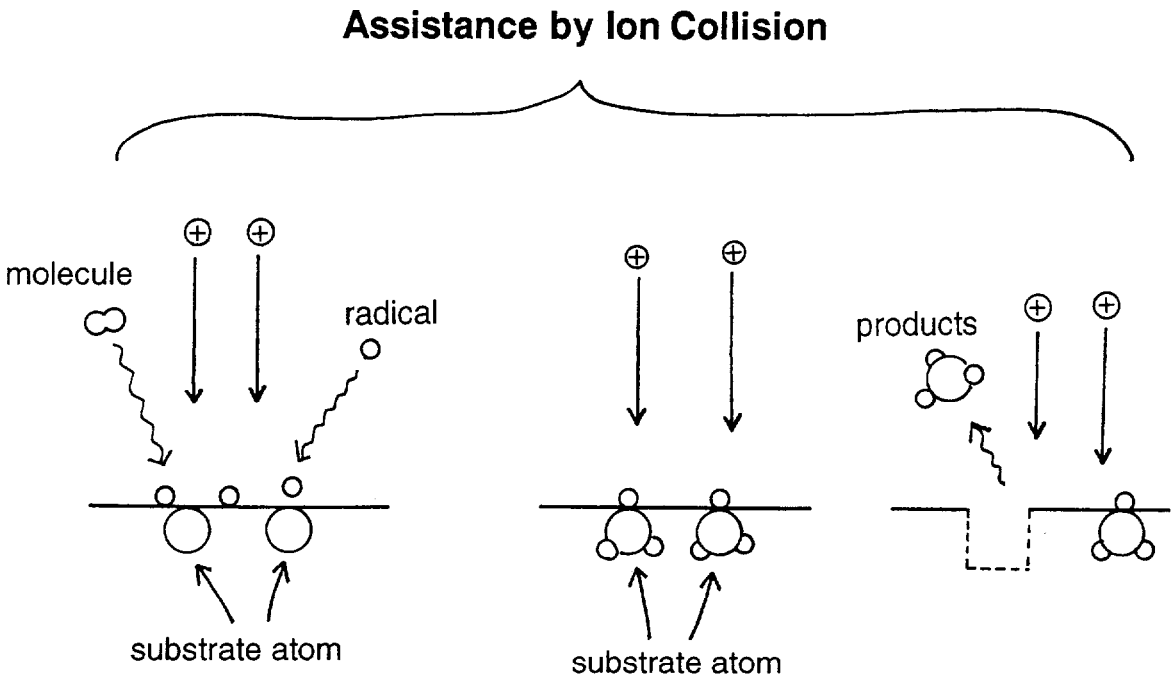

Fig. 1-1 Model of plasma etching process

Table 1-1 Boiling points of halogenide for III-V group elements (@ 1 atm.) [14]

Products	Boiling Point	Products	Boiling Point
AlF_3	1291°C	PF_5	- 75°C
$AlCl_3$	183°C	PF_3	- 101°C
$AlBr_3$	263°C	PCl_5	162°C
GaF_3	1000°C	PCl_3	76°C
$GaCl_2$	535°C	PBr_5	106°C
$GaCl_3$	201°C	PBr_3	173°C
$GaBr_3$	279°C	AsF_5	- 53°C
$In F_3$	>1200°C	AsF_3	- 63°C
InCl	608°C	$AsCl_3$	130°C
$InCl_2$	560°C	$AsBr_3$	221°C
$InCl_3$	600°C		
$InBr_2$	632°C		

Table 1-2 History of Reactive Dry Etching

	Dry Etching	R I E	R I B E	Dry Etch in Tokyo Inst. Tech.
1970	Si (halogen gas)			
1978	Mechanism of Plasma Etch (Coburn and Winters, IBM)			
1980		InP etched mirror LD		
1981		(L. A. Coldren, K. Iga *et al*, AT&T Bell)	InP of Cl_2-RIBE (K-type) (M.A.Bosch, Bell Lab.)	
1983			GaAs,GaAlAs (Cl_2-RIBE) (K. Asakawa, OTRJ)	
1984		GaAs Cylindrical Etching (Cl2-Ar) (H.Ito etal, Tohoku Univ.)		
1985	GaAs/GaAlAs BH LD (IBE) (N. Bouadma *et al*, CNET)			
1986			Short Cavity LD (Cl_2-RIBE) (T. Yuasa *et al* OJRL & NEC)	
1987	GaAs/AlAs microresonator arrays (CAIBE)(J. L. Jewell AT&T Bell)			
1988			Mechanism of Cl_2-RIBE (T. Tadokoro *et al*)	
1989				This Work ↓

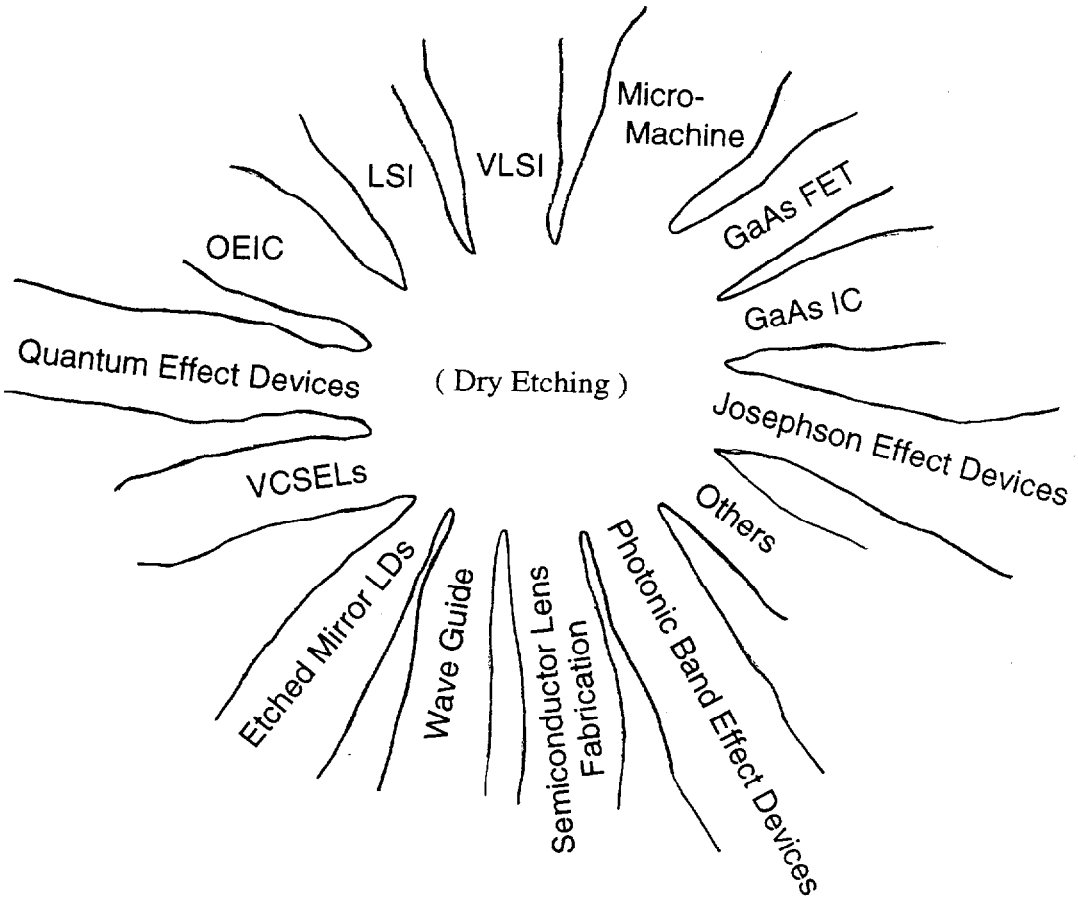

Fig. 1-2 Applications of Dry Etching

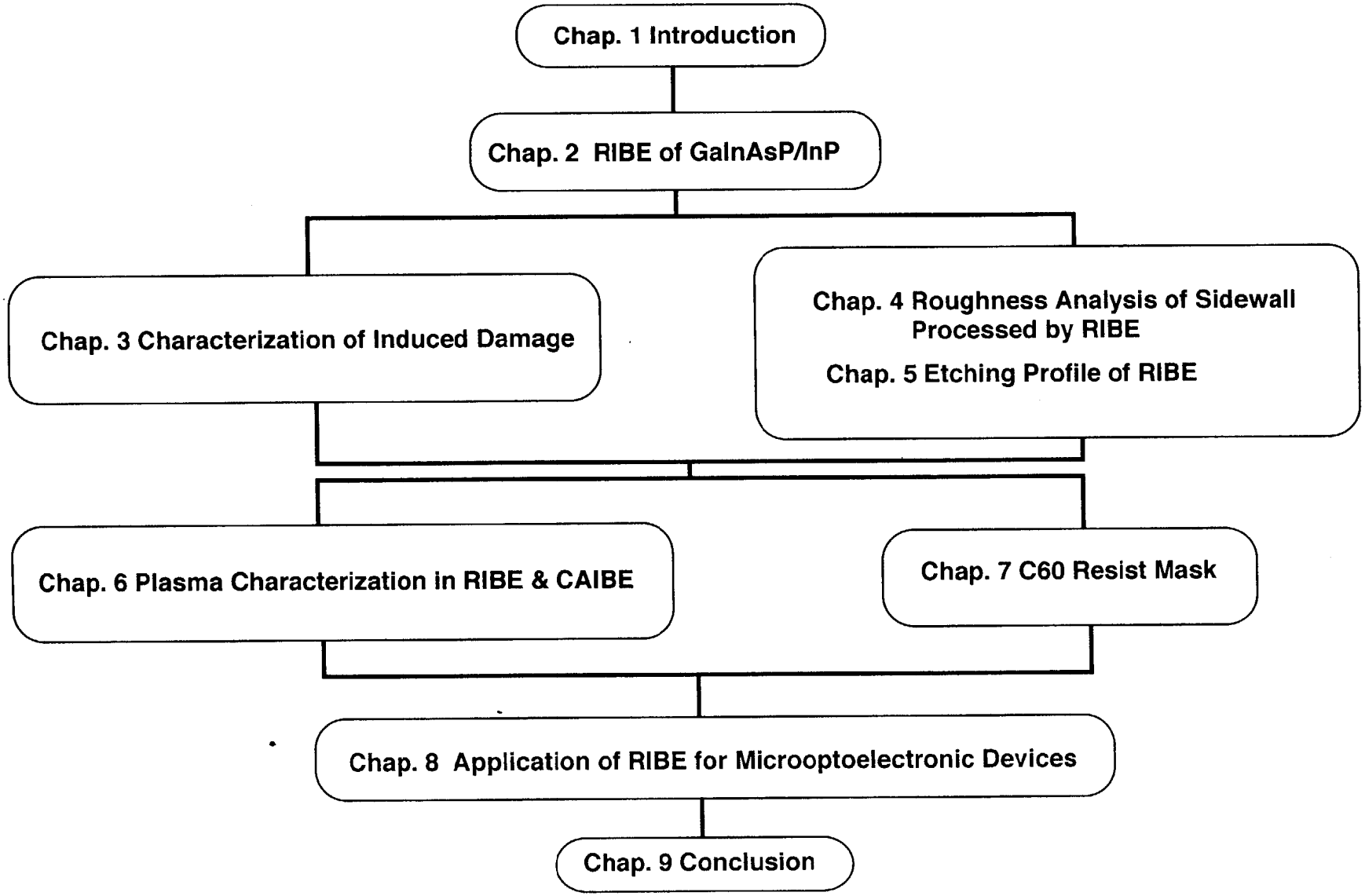

Fig. 1-3 Outline of my thesis

Chapter 2 Reactive Ion Beam Etch of InP/GaInAsP

2.1 Introduction

In order to realize such a low-threshold VCSEL, a microfabrication technology which provides a low-damage etch is becoming an important issue. I have investigated a reactive ion beam etch (RIBE) technique to fabricate a semiconductor microresonator for surface emitting lasers in chapter 8. In most VCSEL structures, a dielectric multilayer reflector such as SiO_2/TiO_2 or semiconductor multilayer mirror is used as a highly reflective mirror. However, it has been difficult to fabricate a GaInAsP/InP microcavity with steep side walls by wet chemical etching since each material has different etching rates. Up to now, some RIBE etching conditions for GaAs and InP have been studied[1-4], but data for GaInAsP, or especially for GaInAsP/InP semiconductor multilayers, have not been fully clarified yet.

In this chapter, etching characteristics of GaInAsP/InP multilayers are studied. The dependence of the etching rate of GaInAsP, InP and GaAs on the ion extraction voltage and the etching temperature are discussed. Circular array patterns of GaInAsP/InP multilayers and DH wafers were fabricated.

2. 2 Reactive Ion Beam Etching (RIBE) System

Figure 2-1 and 2-2 show a photograph and a schematic diagram of an ultra high vacuum reactive ion beam etch (RIBE) system. This system has an electron cyclotron resonance (ECR) ion source, and the ECR plasma is generated by introducing 2.45GHz microwaves into a horizontal discharge chamber on which a magnetic field is superimposed. The etching chamber is exhausted by a cryopump and a load-lock chamber is evacuated by a turbomolecular pump. The back pressure is usually less than 2×10^{-8} Torr. A sample can be heated up to 600°C. The gas flow rate can be controlled by a variable orifice of the cryopump. The etching gas examined in this study is pure chlorine and Ar. Ions are extracted through two circular multi-aperture grids (Figure 2-3). The diameter of the circular grids is 15 cm and the distance between these two grids is 1.5 mm. The diameter of apertures is 2 mm. One grid, which is located far from the plasma, is dropped to ground potential. The extraction

voltage is applied between this grid and the discharge chamber.

This RIBE system has an ion current monitor near the sample holder. Therefore the ion current in the plasma can be measured. In this section, the measured relationships between the ion current and the etching gas pressure with this ion current monitor are described. Figure 2-4 shows the measurement result for Cl_2 and Fig. 2-5 shows the measurement result for Ar. Where the V_e is the ion extraction voltage. The vertical axis shows the ion current density. These measurement results show that the ion current is maximum at gas pressure of $1\sim3\times10^{-4}$Torr in ion each extraction voltage, and the ion current decreases at 10^{-3}Torr because ECR condition is not satisfied.

The RIBE system can be used as a chemically assisted ion beam etching (CAIBE) system. The general description of the CAIBE process, is as follows: Ar ions are accelerated in an ion source and directed toward the substrate while chlorine gas is made to flow on the surface. The chlorine molecules are adsorbed chemically on the sample surface. The chlorine atoms can then react with the substrate atoms, spontaneously or stimulated by striking ions, to from chlorides. When the surface is exposed to a flux of high energetic Ar ions, collisional cascade removal of chloride products and thermal desorption as well as collisional cascade removal products are dominant removal mechanisms. These chlorides are volatile and do not significantly redeposit on the substrate. This is a major advantage of CAIBE compared to straight ion milling where a substantial fraction of the sputtered material redeposits.

2. 3 Etching Rate of GaInAsP, InP and GaAs under Different Etching Conditions

Figure 2-6 shows measured etching rates for GaInAsP, InP and GaAs against extraction voltage and various substrate temperatures. A quaternary semiconductor $Ga_{0.27}In_{0.73}As_{0.6}P_{0.4}$ (λ_g = 1.3 μm) was prepared by liquid phase epitaxy (LPE). The etching mask materials were a positive-type photoresist OFPR-8600 (Tokyo Ohka Inc.) and SiN. The SiN film was deposited using a plasma-chemical vapor deposition (plasma-CVD) method. The stripe photoresist pattern was prepared on the SiN film using a conventional photolithographic process, and then the SiN film was etched in a buffered hydrofluoric acid. The sample was etched with a

gas pressure of 8×10^{-4} Torr and Cl_2 gas flow rate of 10 sccm.

The etch rates of GaInAsP, InP and GaAs increase with the increase in both the extraction voltage and etching temperature. The etch rate of GaInAsP was found to be between those of InP and GaAs at each temperature. The etch rate of GaInAsP is close to that of InP at 100°C, however, it approaches that of GaAs at 250°C. The classification of the etching mechanism in RIBE has been studied on GaAs and InP[2]. These etching rates are expressed as the sum of these three parameters.

$$R = A \cdot V^{3/2} \text{ (RIE-like)} + B \cdot V^{5/2} \text{ (IBE-like)} + C \text{ (chemical-etch-like)} \qquad (2\text{-}1)$$

In this experiment, the etching rates of GaInAsP at 100°C, 170°C and 250°C are in proportion to $V^{3/2}$, $V^{5/2}$ and V, respectively. Therefore, the etching mechanism of GaInAsP is IBE-like and RIE-like at 100°C and 170°C, respectively. In addition, that of GaInAsP at 250°C is between chemical-etch-like and RIE-like. The etching profile shows anisotropy at 100°C and isotropy to some extent at 250°C. For device applications, we must etch the semiconductor multilayer with a relatively high etch rate and anisotropic profile. Thus, we adopted the conditions of temperature: 170°C, extraction voltage: 400V, and gas pressure: 8×10^{-4}Torr. Under these conditions, the etching rates for InP, GaInAsP and GaAs are 940Å/min, 12000Å/min and 13000Å/min, respectively. This RIBE condition corresponds to a RIE-like classification for GaInAsP.

2. 4 Microetching of GaInAsP/ InP Multilayer by Cl_2-RIBE

Figure 2-7 shows a cross section of a strip of a 15-pair GaInAsP/InP semiconductor multilayer etched by RIBE. This multilayer consisting of quarter-wavelength layers of GaInAsP (1589Å) and InP (1055Å) was prepared by chemical beam epitaxy (CBE)[5]. The etching time of the GaInAsP/InP multilayer was 15 min. The total etching time of the multilayer corresponds to the sum of that of each layer. The straight side wall was obtained, although the etch rate of GaInAsP is quite different from that of InP, as described above. This result shows that there is not necessarily a requirement of equal etch rates to etch multilayers to a smooth and anisotropic shape. I can simply etch the semiconductor multilayer under the anisotropic etching condition. I can also fabricate the mesa of a GaInAsP/InP multilayer with

a 1.5 μm width using the same condition. Figure 2-8 (a) shows an scanning electron microscope (SEM) photograph of circular array patterns made on a GaInAsP/InP DH wafer with a 1.7-μm-thick GaInAsP active layer. The diameter is 5 μm and the pattern pitch is 10 μm. This wafer was grown by LPE. The RIBE conditions are the same as indicated in Fig.2-7. The circular patterns have no side etching. However, the profile near the edge of the array pattern shows a reasonably vertical shape and the side wall near the center appears tapered near the bottom. In other words, the etching rate of the center is lower than that of the outside. This is a type of loading effect. This effect originates from the high-mask-pattern density. Figure 2-8 (b) shows an SEM photograph of the circular array pattern of the GaInAsP/InP multilayer. The diameter is 5 μm and the pitch is 15 μm. In this case, the etching profile is more vertical than that of the 10 μm pitch. It is obvious that the taper shape in Fig. 2-8(a) is improved.

2. 5 Summary

In this chapter, I have established GaInAsP/InP RIBE dry etching processes for forming microcavity VCSELs. I have examined a Cl_2-RIBE for GaInAsP for the first time, in order to fabricate a microresonator composed of semiconductor multilayers.

(1) The straight side wall of the GaInAsP/InP multilayer was obtained.

(2) However, a type of loading effect derived from the high-density pattern was observed in the etching of the GaInAsP/InP wafer.

References

[1] K. Asakawa and S. Sugata, "GaAs and AlGaAs Anisotropic Fine Pattern Etching using a New Reactive Ion Beam Etching System," *J. Vac. Sci. & Technol.* B3 (1985) 402.

[2] T. Tadokoro, F. Koyama and K. Iga, "A Study on Etching Parameters of a Reactive Ion Beam Etch for GaAs and InP," *Jpn. J. Appl. Phys.* 27 (1988) 389.

[3] M. A. Bosch, L. A. Coldren and E. Good, "Reactive Ion Beam Etching of InP with Cl_2," *Appl. Phys. Lett.*, 38, pp. 264-266, 1981.

[4] S. J. Pearton, U. K. Chakrabarti, and F. A. Baiocchi, "Electrical and Structure Changes in the Near Surface of Reactively Ion Etched InP," *Appl. Phys. Lett.*, 55, pp. 1633-1635.

[5] T. Uchida, T. K. Uchida, N. Yokouchi, T. Miyamoto, F. Koyama and K. Iga: *The Japan Society of Applied Physics 51st Autumn Meeting* , 27aV8 (1990).

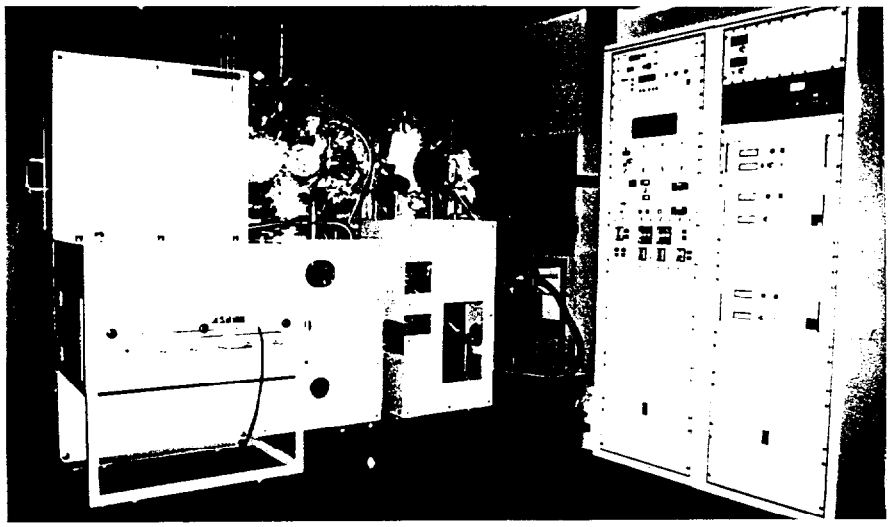

Figure 2-1 Photograph of Reactive Ion Beam Etching System

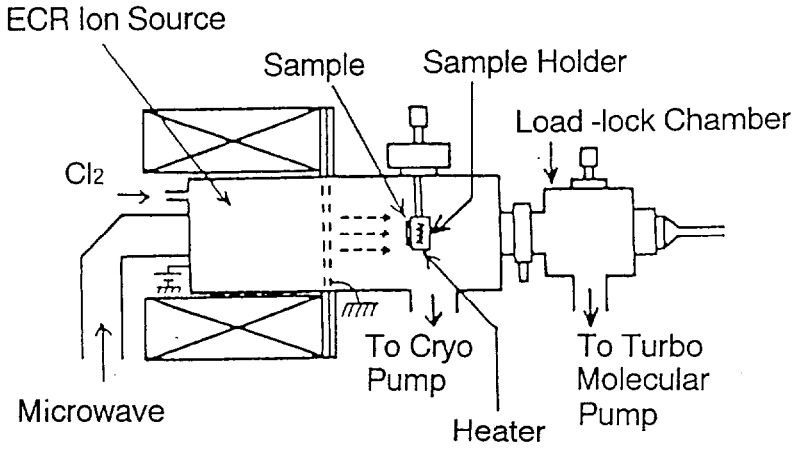

Figure 2-2 Schematic Diagram of Reactive Ion Beam Etching System

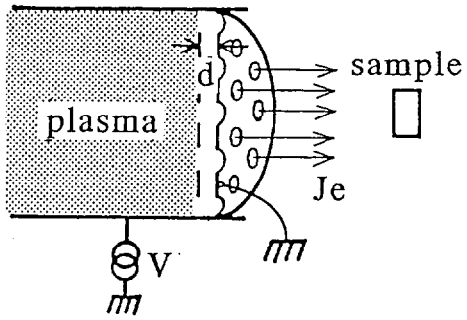

Figure 2-3 Ion Extraction Mechanism

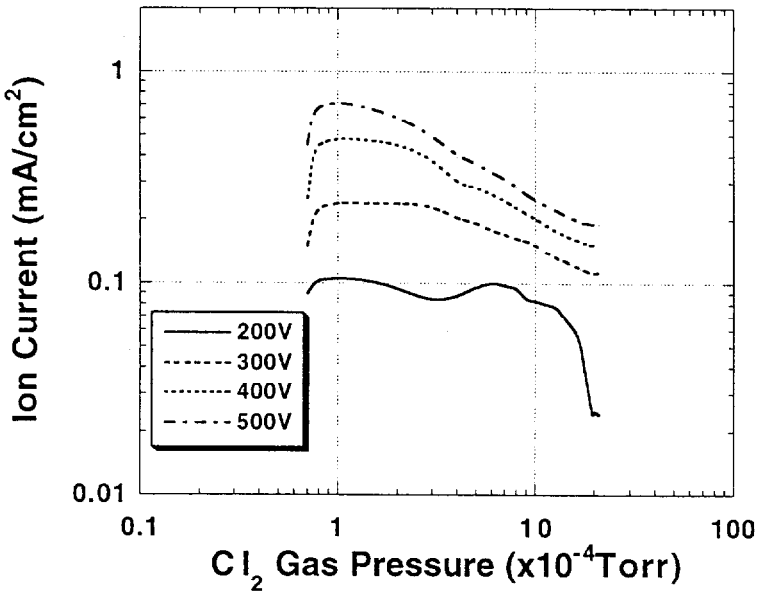

Figure 2-4 Ion Current as a function of Cl_2 Gas Pressure

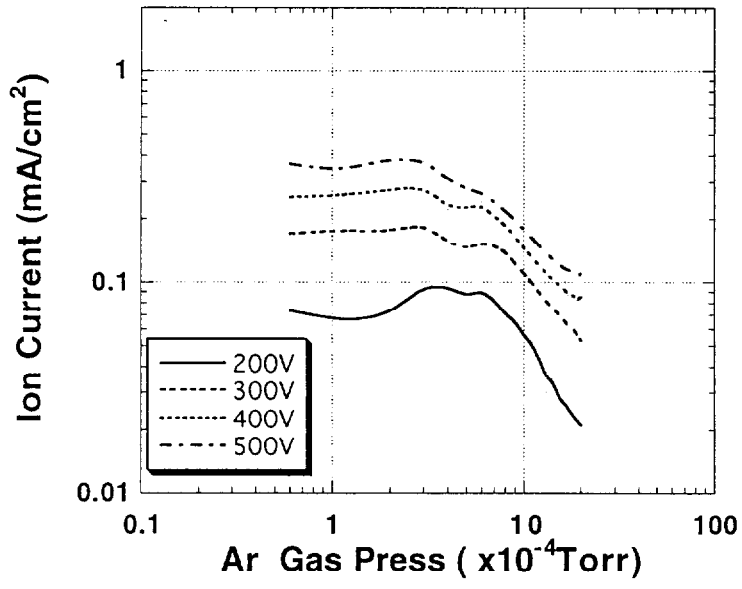

Figure 2-5 Ion Current as a function of Ar Gas Pressure

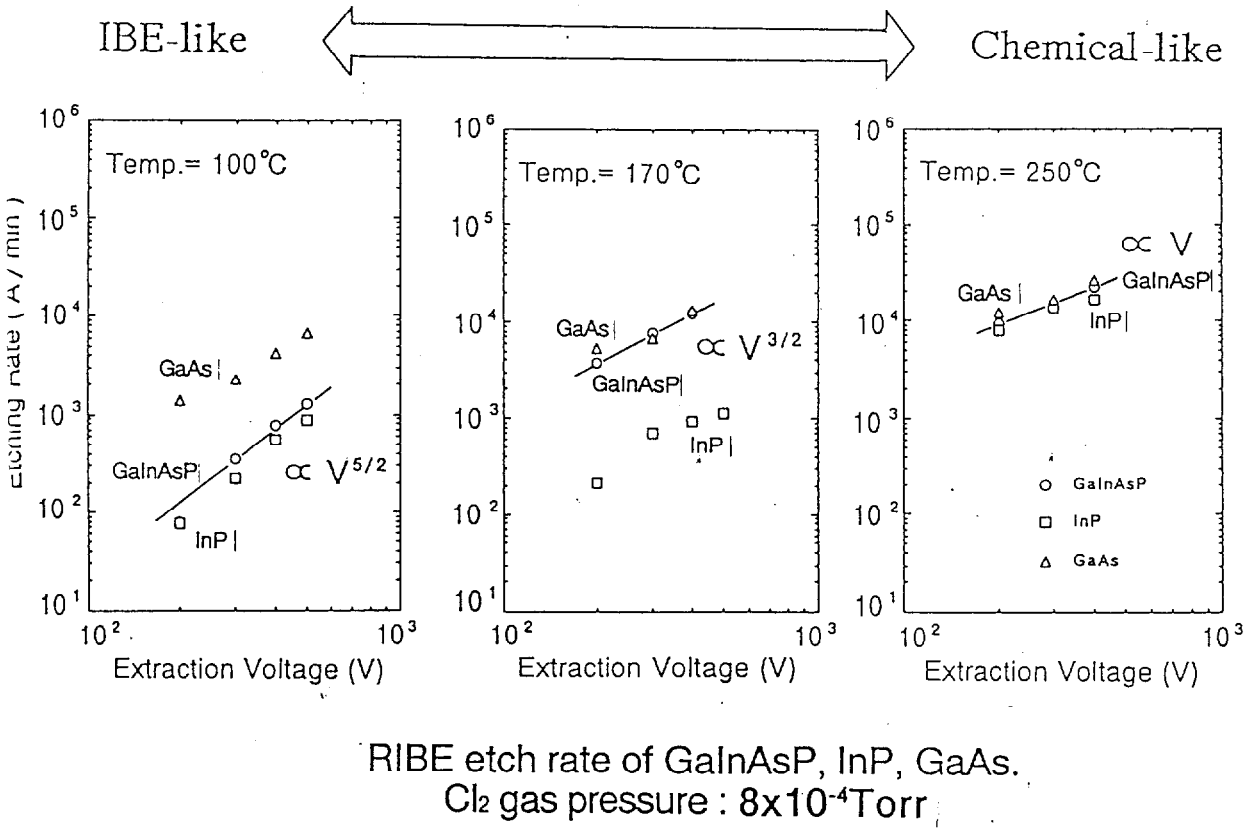

Fig. 2-6 Etching rate for GaInAsP, InP and GaAs. Cl_2 gas pressure: 8×10^{-4}Torr.

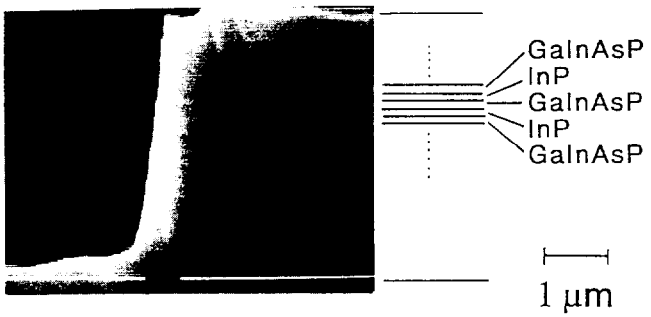

Fig. 2-7 GaInAsP/InP multilayer etched by RIBE. extraction voltage: 400V, temperature: 170°C, Cl_2 gas pressure: 8×10^{-4}Torr.

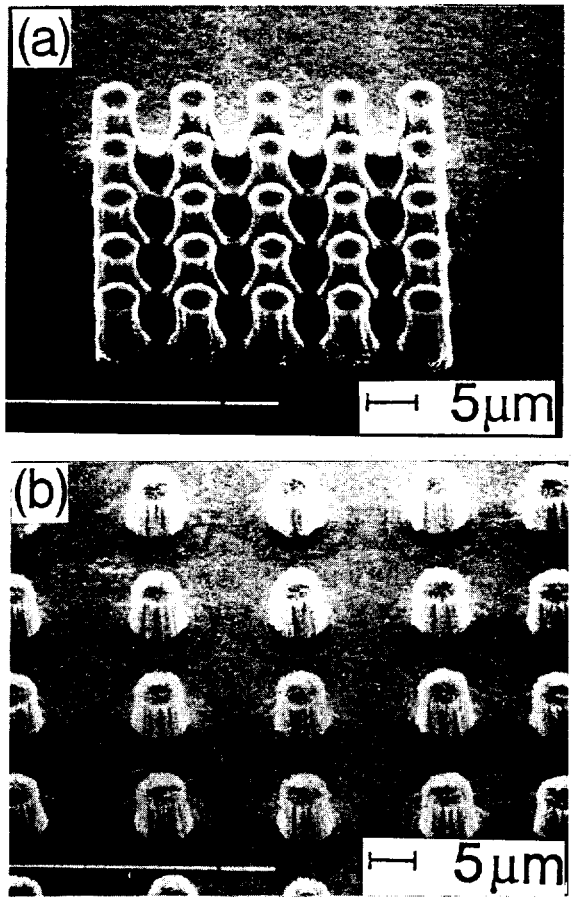

Fig. 2-8 (a) GaInAsP/InP DH-structure wafer etched by RIBE (D=5μm, pitch=10μm). (b) GaInAsP/InP multilayer etched by RIBE (D=5μm, pitch=15μm), extraction voltage: 400V, temperature: 170°C, Cl_2 gas pressure: 8×10^{-4}Torr.

Chapter 3 Characterization of Induced Damage by RIBE

3.1 Introduction

It is well-known that semiconductors are damaged during the dry etching processes. It is important to reduce or remove the damage for fabrication of microsized optoelectronic devices. However, the origin of induced damage by dry etching has not been fully clarified yet. In this chapter, RIBE-induced damages in InP substrates is discussed by capacitance-voltage (C-V) measurement. In addition, the removal of the induced damage by the second RIBE with different conditions for the InP wafer is proposed. The sidewall damage induced by reactive ion-beam etching (RIBE) with Cl_2 is studied. The sidewall damage depth is estimated from the ion-beam-angle dependence, and the photoluminescence (PL) emitted from the etched sidewall of a GaInAsP/InP DH wafer is directly measured.

3. 2 Bottom Surface Damage

3. 2. 1 Damage Depth of Bottom Surface

I have investigated the RIBE-induced damage of a Sn-doped ($2 \times 10^{18} cm^{-3}$) n-type InP substrate by a C-V measurement. In this measurement, I used a semiconductor profile plotter (Bio-Rad Laboratories, POLARONS PN4210). The carrier profile of RIBE-etched InP is denoted by the dotted line in Fig. 3-1.The etching was conducted at a Cl_2 gas pressure of 8×10^{-4} Torr, a gas flow rate of 10 sccm, an etching temperature of 170℃, an ion extraction voltage of 400V and an etching time of 10 min. An increase in carrier concentration was observed in the range extending to ~1000Å or more from the surface. It is considered that this phenomenon originates from phosphorus vacancy-related donors[1].

3. 2. 2 Removal of Damaged Layer by Two-step Etching

I conducted a two-step RIBE to remove the damaged layer. The principle of the two-step RIBE for removal of the damaged layer is shown in Fig. 3-2. The process is as follows: (a) the sample is etched in the RIE-like condition, where the ~1000Å-thick damaged layer is generated after RIBE; (b) the second RIBE is conducted at a Cl_2 gas pressure of $8 \times$

10^{-4} Torr, a gas flow rate of 10 sccm, an etching temperature of 250°C, an ion extraction voltage of 200V and an etching time of 10 sec. Since the RIBE condition at higher temperatures exhibits a chemical-etch characteristic to some extent . I may expect to achieve a somewhat lower damage etch.

Also, the side wall damage may be removed due to its isotropic etching behavior. The etching depth in this experiment is ~1300Å, which is chosen to be slightly deeper than the damage depth. The solid line in Fig. 3-3 shows the carrier profile after the second RIBE. It is obvious that the increase in carrier concentration is removed after the second RIBE. Figures 3-4(a) and 3-4(b) show etching profiles before and after the second RIBE, respectively. The etching profile changed slightly after the second RIBE. However, in the future, a damageless dry etching process with negligible change of shape may be achieved by adopting the optimized condition of the two-step RIBE. I consider that smoothing of surface roughness after the second soft dry etch is also expected.

3. 3 Sidewall Damage

Until recently, there have been some reports on dry-etching-induced damage[2, 3]. For example, Wong *et al.* [2] investigated reactive ion etching (RIE)-induced damage on the bottom surface in a GaAs-GaAlAs multi-quantum well (MQW) structure. They concluded that the range of defects extended to 1000Å or more from the sample surface. As for its application to devices, a 1.3 μm buried heterostructure laser diode was fabricated by RIBE [4]. However, there are few reports on sidewall damage, especially on damage by RIBE. Pang *et al.* studied sidewall damage of GaAs by ion-beam etching (IBE) [3]. They have shown that impurities or defects generated during etching remain on the vertical sidewall. However, sidewall damage has not yet been fully clarified. Moreover, the reduction of sidewall damage is one of the most important subjects when considering microdevices.

In this study, the relationship between the incidence ion-beam angle and damage depth on InP is clarified through capacitance-voltage (C-V) measurements. The incidence-angle dependence of the photoluminescence intensity of a GaAs substrate is also discussed. In addition, the photoluminescence (PL) spectrum emitted from the etched sidewall of a

GaInAsP/InP double-heterostructure wafer was directly measured.

3. 3. 1 Ion Beam Incident Angle Dependence of Cl_2-RIBE Induced Damage

The incident angle of the ion beam was changed by tilting the sample stage. We used a Sn-doped ($2 \times 10^{18} cm^{-3}$) n-type InP substrate as the sample. The following etching conditions were adopted: temperature 170℃; extraction voltage 400V; and gas pressure 8×10^{-4}Torr. Under these conditions, the etching rates for InP, GaInAsP and GaAs were 1300Å/min, 12000Å/min and 13000Å/min, respectively.

Figure 3-5 shows the etching rate of InP as a function of the incidence angle θ of the ion beam. Clearly the etch rate decreases as the incidence angle θ is increased. As can be seen, the etch rate decreases with cosine dependence of the incidence angle θ. This result is explained by the fact that InP is etched mainly by physical sputtering (IBE~RIE-like etch) at this temperature. This measured etch rate has the same tendency as that reported by Mutoh *et al* [5, 6].

It is well-known that the surface of semiconductors is damaged during dry etching processes. It is important to understand sidewall damage, in particular, for the microfabrication of optoelectronic devices. We have investigated sidewall damage induced by RIBE by tilting the substrate relative to the ion flux. The RIBE-induced damage is indicated by the increase of carrier concentration of the InP substrate. We judged the damage depth from the increase of carrier density induced by the damage. The carrier profile was measured using a semiconductor profile plotter (Bio-Rad Laboratories, POLARONS PN4210).

Figure 3-6 shows the carrier profile against the incident angles from 0° to 180° after RIBE as a function of the depth from the substrate surface. The etching time of all the samples is 2 min. In this figure, each triangular symbol represents the estimated damage depth. The damage depth decreases with an increase in the incident angle θ. Damage does not accumulate with increasing etching time[7]. The damage depth is almost independent of the etching rate. It is obvious that the heaviest damage is caused at $\theta = 0^\circ$, where the ion flux is normal to the etched surface.

Figure 3-7 shows the damage depth as a function of the incident angle of the ion

beam. It is obvious that the damage depth decreases with an increase in the incident angle. The $\cos\theta$ dependence is shown by the dotted line. The damage depth decreases with cosine dependence from 0° to 50°. However, it is different from the cosine dependence from 70° to 90°. In addition, the damage depth is not observed in this measurement at 90° or 180°. Hence, the damage is less than 200Å (resolution limit) at $\theta > 90^{\circ}$. These results show that the sample is damaged when placed at an angle $\theta \sim 90^{\circ}$. The estimated damage depth is much larger than the penetration depth of the Cl ion calculated by the LSS theory. We think that the damage may be due to channeling, high-order collision, propagation of defects, and so on. In other words, the sample is damaged whenever the ion beam collides with it.

Figure 3-8 shows the relationship between the incident angle θ and PL intensity of the etched GaAs substrate. The PL intensity was normalized by an undamaged sample. The sample is etched at the substrate temperature of 100℃ and extraction voltage of 400V. The etching time is 2 min. A He-Ne laser (λ =633nm) is used as a pumping source. The PL intensity is decreased by RIBE. However, the PL intensity reaches ~90% of the nonetched substrate when $\theta > 30^{\circ}$. Also, damage is caused by RIBE even at the shallow angle of $\sim 85^{\circ}$. Therefore, the wafer is also damaged due to the collision.

3. 3. 2Evaluation of Sidewall Damage by Photoluminescence Observation and Effect of Sulfur Passivation

In the above-mentioned experiment, the sidewall damage after RIBE was estimated by varying the incident angle of the Cl_2 ion beam. However, this is not direct observation of sidewall damage. Hence, I tried to measure the photoluminescence emitted from the sidewall etched by RIBE. This experimental procedure is shown in Fig. 3-9. The sample is a GaInAsP/InP double-heterostructure (DH) wafer grown by liquid phase epitaxy (LPE). This wafer has one GaInAsP(λg=1.3 μm) and two GaInAsP(λg=1.25 μm) layers. Next, the wafer is etched by RIBE under the following conditions: extraction voltage 400V; substrate temperature 170℃ Cl_2 gas pressure 8×10^{-4}Torr; etching time 15 min. Then, excited light is irradiated on to the etched sidewall. In this experiment, a Nd:YAG laser (λ=1.06 μm) is used as a pumping source. The beam spot size is <500μm, and the beam divergence is a few degrees. Therefore,

the pumping light can be treated in a manner approximately the same as a parallel plane wave. Figure 3-10 shows the PL spectra at room temperature from the etched and cleaved sidewalls. The bold line represents the spectrum after RIBE and the thin line represents the spectrum of the cleaved sidewall. I compare the PL intensity before and after RIBE at the peak wavelength (λ=1.25μmm, 1.33μm), emitted from two GaInAsP layers. This figure shows that the PL intensity of RIBE sample was deteriorated in comparison with that of the cleaved sidewall. It is estimated that the pumping light penetrates into GaInAsP layer to $\sim$ 1μm deep from sidewall surface by taking into account the absorption coefficient of about 10^4cm-1. The photoluminescence from the GaInAsP layer well expresses the information of minority carriers near the sidewall. Thus, it can be considered that the deterioration of PL intensity is expressing the existence of some sidewall damages. Accordingly, it is clear that the nonradiative recombination of RIBE treated active layer facet is larger than that of the cleaved facet.

Next, I passivate these samples with $(NH_4)_2S_x$. These samples are dipped in $(NH_4)_2S_x$ at 23℃ for 20 hours. The etching depth with $(NH_4)_2S_x$ is estimated to be a few tens of angstroms. In this figure, the spectrum of the etched sidewall after passivation and the cleaved sidewall after passivation are shown by the bold and thin dotted lines, respectively. Both spectral intensities increased considerably. The etching effect of passivation is very small because the etching depth extends to only a few monolayers. Hence, I believe that passivation with $(NH_4)_2S_x$ is an effective technique for reduction of nonradiative surface recombination induced by RIBE and oxidation. Furthermore, I can distinguish the damage contribution relative to a nondamaged reference.

3. 3. 3 Quantitative Evaluation of Sidewall Damage by Photoluminescence Observation and Br-methanol Etching

Figure 3-11 shows the experiment processes of measurement of sidewall damage. I used a double-hetero (DH) structure GaInAsP/InP wafer grown by a CBE as a sample. First, the wafer was etched by RIBE to a depth of appearance the lower GaInAsP (λ_g=1.55μm) layer. After that, I measured the photoluminescence (PL) emitted from the GaInAsP layer by

pumping at the sidewall of the sample. I used a Nd:YAG laser (λ_g=1.06μm) as a pumping source. Then, in order to clarify the damage depth of the etched sidewall, I measured the PL intensity by etching the sample slowly. The extremely slow-rate etchant Br-CH_3OH was used. The etch rate of etchant was 170Å/min. Figure 3-12 gives the actual measured plots of etch rate vs. θ by L. A. Coldren *et al*[8]. The Br-CH_3OH etchant I used has sufficient etch rate at θ=90°, *i. e.*, a crystal orientation of (011). Figure 3-13 shows the PL spectra at room temperature from the etched sidewall. In this figure, the spectrum of the etched sidewall after RIBE and after Br-methanol etching and the cleaved sidewall are shown. After Br-methanol etching, the spectral intensities increased considerably. Figure 3-14 summaries the relationship the PL intensity of a GaInAsP sidewall etched by RIBE and the distance from the sidewall surface. The PL intensity was normalized with the PL intensity of cleaved facet. In this figure, it is found that the PL intensity is recovered to that of cleaved facet by a slightly wet etching by Br-CH_3OH of 8-10 sec. The wet etching time of 8-10 sec corresponds to the etched depth of 20-30Å. Therefore, the damage depth of etched sidewall is estimated to be 20-30Å. Figure 3-15 shows the relationship PL intensity and ion extraction voltage. From this figure, the PL intensity is the same in the region of ion extraction voltage of 300V-500V. Therefore, I think the sidewall damage is almost the same in the region. It was observed that the PL intensity changed with time in irradiation with relatively high laser power as shown in Fig. 3-16. The applied laser power was about 50mW, and the spot diameter on the sample was 500μm. In this figure, the PL intensity saturated after irradiation of about 8 min. This phenomenon is caused by the annealing of the crystal by irradiation [9].

3. 4 Reactive Ion Etching Induced Damage and Its Reduction

3. 4. 1 Reactive Ion Etching (RIE) System

Generally speaking, the limitation of wet chemical etching in pattern width is about 3μm due to the isotropic etching profile. While Ar plasma etching can decrease the pattern size. However the etching rate ratio between substrate and etching mask is small, and the induced damage by ion collision is serious. Also, in reactive gas etching, the etching rate ratio between substrate and etching mask is large, but the pattern size is limited due to the

isotropic etching profile by side etching. Hosokawa *et al* have reported a new etching manner that has anisotropic etching profile, large etching rate ratio and good productivity [10]. The new etching technique is called reactive ion etching (RIE). The mechanism of RIE is as follows. The sample is set on the plane electrode and the sample is etched by sputtering effect of ion that is accelerated in the plasma sheath and the surface reaction between the sample and activated particle generated in the plasma [11, 12]. At present, RIE is main technology in the Si-LSI fabrication due to good mass productivity and easy operation [13].

Figure 3-17 (a) and (b) show a schematic diagram and photograph of an RIE system (Samco International: RIE10N), respectively. This system has parallel planar electrodes.. The diameter of these electrodes is 210mm. The effective diameter providing uniform etching is 160mm and the space of both of electrodes is 65mm. The etching characteristics of RIE depend on some conditions, i. e., etching pressure, gas flow rate, RF power and so on. This system can control these conditions automatically. This system has two etching gas lines (CF_4 and O_2). these gas flow rate are controlled by mass flow controllers. A 13.56MHz RF power supply is used to generate plasma, and the input RF power is matched automatically. The etching chamber is evacuated by a diffusion pump after loading samples. The back ground pressure is 10^{-6}Torr. Samples are set on the etching table that is placed on the lower electrode, and cooled by water. The materials of used etching table are Teflon (CF_{2n}) and Quartz. The electric discharge plasma generates in the space of electrodes that are face each other. In this case, the cathode fall is generated on these electrodes surface due to the difference of mobility for ion and electron. In this cathode fall space, the ion of activated gas incidence along the vertical electrical field on the electrode and sample surface, and the ion etch the sample reactively, in the incident direction. Figure 3-18 shows the phenomenon on the sample surface. The sample was etched by vaporizing the product that is generated by chemical reaction between the atom of sample surface and activated ion (or neutral radical). The incidence ion energy is controlled by gas pressure and applied power. Therefore the physical sputtering due to ion collision effect is caused by decreasing gas pressure and increasing applied power. In the opposite conditions, the chemical-like etching which has few ion collision effect is possible. The electrode structure used in this study is shieldless type.

Generally speaking, in this type, it is known that the etching rate increase and the uniformity of etching better with increasing the interval of two electrodes [14].

3. 4. 2 RIE Induced Damage and Its Reduction

The RIE process might induce damage of laser wafers. We have investigated the induced damage of a GaAs substrate by PL measurement. Figure 3-19 shows the relation between the PL intensity of 0.87 μm of the GaAs substrate and GaAs active layer in the DH structure and reactive ion etching time. In this experiment, the sample was etched by RIE with a pressure of 0.12Torr and an rf power of 100W and an etching table of Teflon. A He-Ne laser (λ = 633nm) was used as a pumping source. The PL intensity of the GaAs substrate decreased with increase of etching time, and it was saturated. However, the damage was recovered to some degree by thermal annealing in H_2 at 400℃ for 10 min. Furthermore, the degradation of the PL intensity of the DH wafer was not observed thoroughly. This is because the GaAs active layer in the DH structure was located 1 μm from the surface. In order to clarify the damage depth, we measured the PL intensity by etching the sample slowly. The extremely slow-rate etchant H_2SO_4:H_2O_2:H_2O in the ratio of 6:1:18 was used. The etch rate was 1.2 μm/min. Figure 3-20 shows the change of PL intensity of a GaAs substrate etched by RIE versus the distance from the surface. The etching time of the GaAs substrate by RIE is 10 minutes. In this figure, three depressions of PL intensity were observed. The origin of this phenomenon is now under investigation. The damage depth is estimated to be 0.3 μm.

3. 5 Summary

I investigated sidewall and bottom surface damage induced by Cl_2-RIBE.

(1) The induced damage of the InP substrate was studied by C-V measurement. The damaged layer thickness was estimated to be ~1000Å.

(2) In order to eliminate this induced damage, I have proposed a two-step RIBE.

(3) The ion-incident-angle dependence of the sidewall damage indicates that sidewall damage was <200Å at 400V.

(4) Also, I measured the PL spectrum of the etched sidewall of a GaInAsP/InP DH wafer after RIBE. We found that the PL intensity of the etched sidewall decreased considerably.

(5) In addition, I demonstrated that the PL intensity of the sidewall recovers after passivation with $(NH_4)_2Sx$.

(6) In order to clarify the damage depth of the etched sidewall, I measured the PL intensity by etching the sample slowly. The damage depth of etched sidewall is estimated to be 20-30Å.

(7) The sidewall damage is the same in the region of 300V-500V.

(8) It was observed that the sample PL intensity changed with time in irradiation with relatively high laser power. This phenomenon is caused by the annealing of the crystal by irradiation, not by the filling up of some deep levels.

9) The damage of a wafer induced by RIE was investigated by PL study. The active layer in the DH wafer was not affected by the RIE process. Also, the damage of the cladding layer can be relaxed by thermal annealing.

Thus, sidewall damage by RIBE is relaxed by optimizing the etching condition and introducing passivation. RIBE is an effective low-damage dry-etching technique for the fabrication of microsized SE lasers and optoelectronic devices, if the induced damage can be properly eliminated and the bared surface passivated. It is expected that RIE is very effective for producing a microcavity resonator. The fabrication of a surface emitting laser with such a RIE-patterned dielectric mirror is under way.

References

[1] S. J. Pearton, U. K. Chakrabarti, and F. A. Baiocchi, "Electrical and structural changes in the near surface of reactively ion etched InP," *Appl. Phys. Lett.*, 55, pp. 1633-1635, 1989.

[2] H. F. Wong, D. J. Green, T. Y. Liu, D. G. Lishan, M. Bellis, E. L. Hu, P. M. Petroff, P. O. Holtz and J. L. Merz, "Investigation of reactive ion etching induced damage in GaAs-AlGaAs quantum well structure," *J. Vac. Sci. & Technol.* , B6, pp. 1906-1910, 1988.

[3] S. W. Pang, W. D. Goodhue, T. M. Lyszczarz, D. J. Ehrlich and R. B. Goodman, "Dry etching induced damage on vertical sidewalls of GaAs channels," *J. Vac. Sci. & Technol.*, B6, pp. 1916-1920, 1988.

[4] N. Bouadma, C. Kazmierski and J. Semo, "Over 245mW 1.3μm buried rudge stripe laser diode on n-substrate fabricated by the reactive ion beam etching technique," *Appl. Phys. Lett.* , 59, pp. 22-24, 1991.

[5] K. Mutoh, M. Nakajima and M. Mihara, "Reactive Ion-Beam etching of InP with Cl_2," *Jpn. J. Appl. Phys.*, 29, pp. 1022-1026, 1990.

[6] K. Mutoh, S. Wakabayashi, Y. Toyoda and M. Nakajima, "Simultaneous Fabrication of Vertical and 45° Mirrors of InP for Surface-Emitting Lasers Using Inclined Cl Ion Beam," *Jpn. J. Appl. Phys.*, 30, pp. 67-71, 1991.

[7] M. A. Bosch, L. A. Coldren and E. Good, "Reactive ion beam etching of InP with Cl_2," *Appl. Phys. Lett.* , 38, pp. 264-266, 1981.

[8] L. A. Coldren, K. Furuya and B. I.Miller, "On the Formation of Planar-Etched Facets in GaInAsP/InP Double Heterostructures," *J. Electrochem. Soc.: Solid-State Science and Technology,* vol. 130, No. 9, pp. 1918-1926, 1983.

[9] T. Tadokoro, F. Koyama and K. Iga, "Comparison of Luminescence from InP Processed by Reactive Ion Beam Etching," *Jpn. J. Appl. Phys.*, 29, pp. 242-243, 1990.

[10] N. Hosokawa, R. Matuzaki and T. Asamaki, "RF Sputter-Etching by Fluoro-chloro-hydrocarbon Gases," *Jpn. J. Appl. Phys.,Suppl.* 2, Pt 1, pp. 435, 1974.

[11] J. A. Boundur, "Dry process technology (reactive ion etching)," *J. Vac. Sci. Technol.*, vol. 13, No. 5, pp. 1023-1029, 1976.

[12] R. A. Heinnecke, "Control of Reactive Etch Rates of SiO_2 and Si in plasma Etching,"

Solid State Electron., 18, pp. 1146-1147, 1975.

[13] R. Cheumg, S. Thomas, S. P. Beaumont, G. Doughty, V. Law and C. D. W. Wilkinson, "Reactive Ion Etching of GaAs Using a Mixture of Methane and Hydrogen," *Electron. Lett.*, 23, pp. 857-859, 1987.

[14] T.Sugano, *"Semiconductor Plasma Process Technology," Sangyo Tosyo,* pp. 160, 1980.

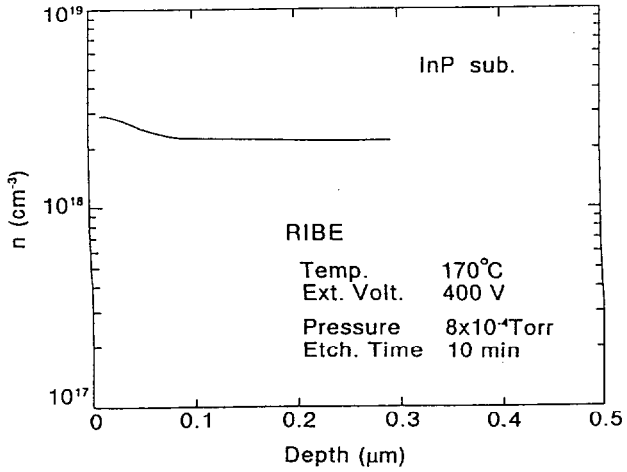

Fig. 3-1 Carrier profile of RIBE-etched InP. Etching was conducted at a Cl_2 gas pressure of 8 $\times 10^{-4}$ Torr, a gas flow rate of 10 sccm, an etching temperature of 170℃, an ion extraction voltage of 400V and an etching time of 10 min. An increase in carrier concentration was observed in the range extending to ~1000Å or more from the surface.

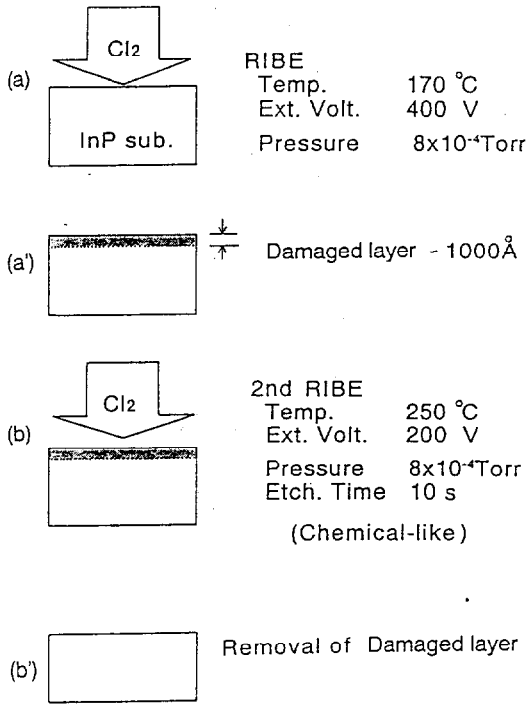

Fig. 3-2 The principle of the two-step RIBE for removal of the damaged layer. The process is as follows: (a) the sample is etched in the RIE-like condition, where the ~1000Å-thick damaged layer is generated after RIBE; (b) the second RIBE is conducted at a Cl_2 gas pressure of 8 $\times 10^{-4}$ Torr, a gas flow rate of 10 sccm, an etching temperature of 250°C, an ion extraction voltage of 200V and an etching time of 10 sec.

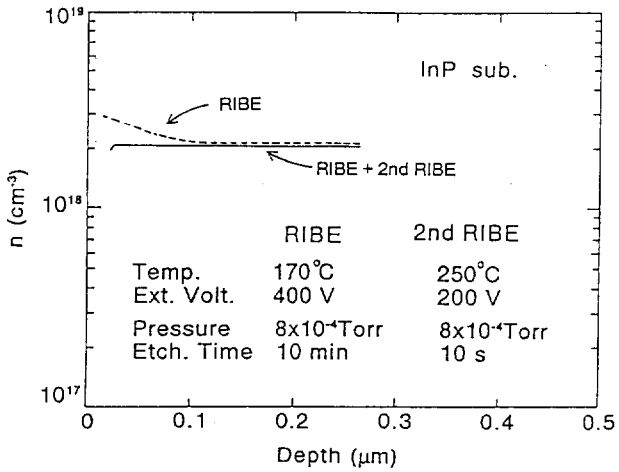

Fig. 3-3 Carrier profile after the second RIBE. It is obvious that the increase in carrier concentration is removed after the second RIBE.

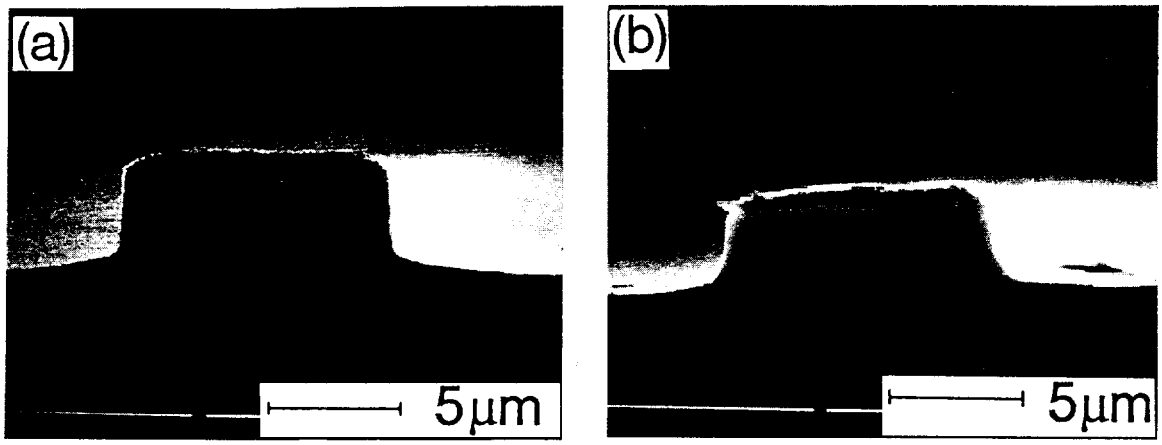

Fig. 3-4 Etching profiles before (a) and after (b) the second RIBE, respectively. The etching profile changed slightly after the second RIBE.

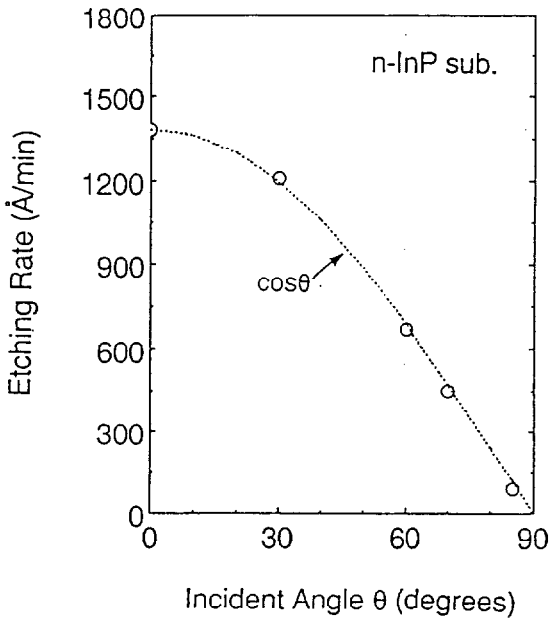

Fig. 3-5 Eching rate of InP as a function of the incidence angle θ of the ion beam. Clearly the etch rate decreases as the incidence angle θ is increased. As can be seen, the etch rate decreases with cosine dependence of the incidence angle θ.

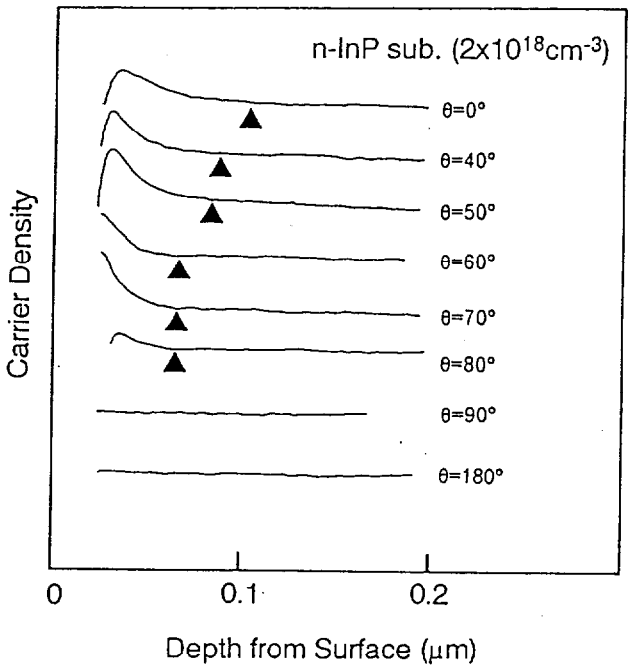

Fig. 3-6 Carrier profile against the incident angles from 0° to 180° after RIBE as a function of the depth from the substrate surface. The etching time of all the samples is 2 min.

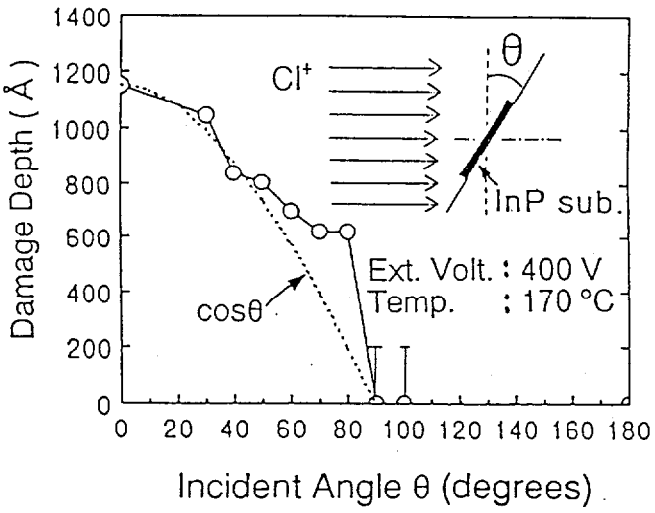

Fig. 3-7 Damage depth as a function of the incident angle of the ion beam. It is obvious that the damage depth decreases with an increase in the incident angle.

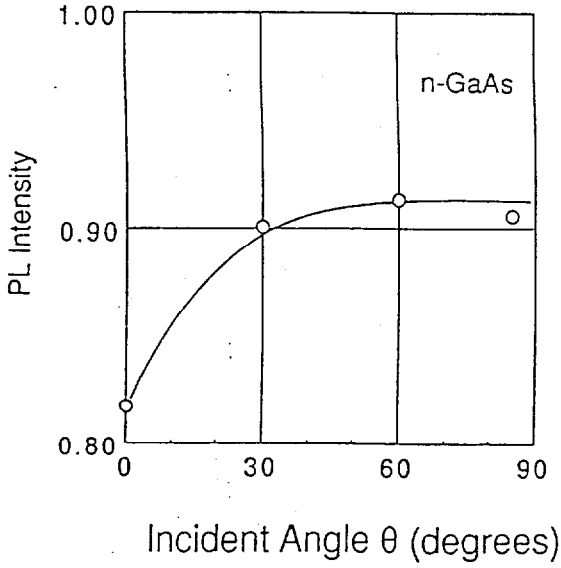

Fig. 3-8 Relationship between the incident angle θ and PL intensity of the etched GaAs substrate.

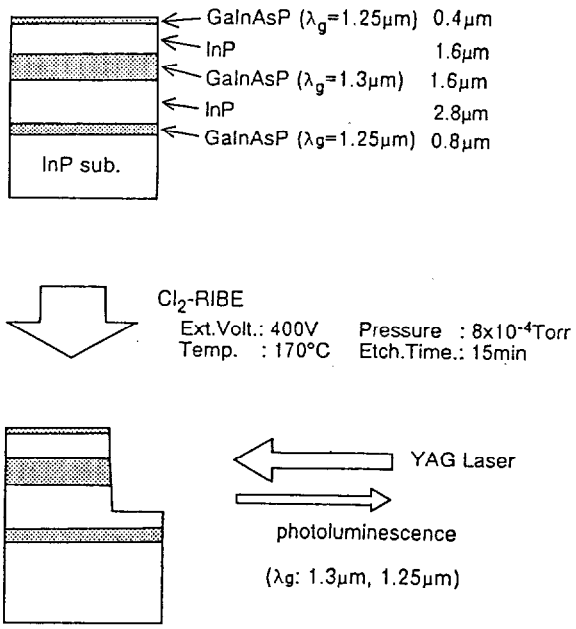

Fig. 3-9 Measurement of the photoluminescence emitted from the sidewall etched by RIBE.

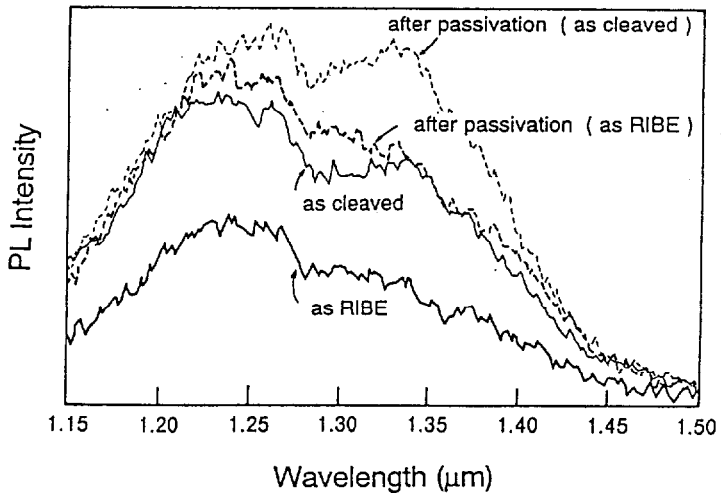

Fig. 3-10 PL spectra at room temperature from the etched and cleaved sidewalls. The bold line represents the spectrum after RIBE and the thin line represents the spectrum of the cleaved sidewall. The spectrum of the etched sidewall after passivation and the cleaved sidewall after passivation are shown by the bold and thin dotted lines, respectively.

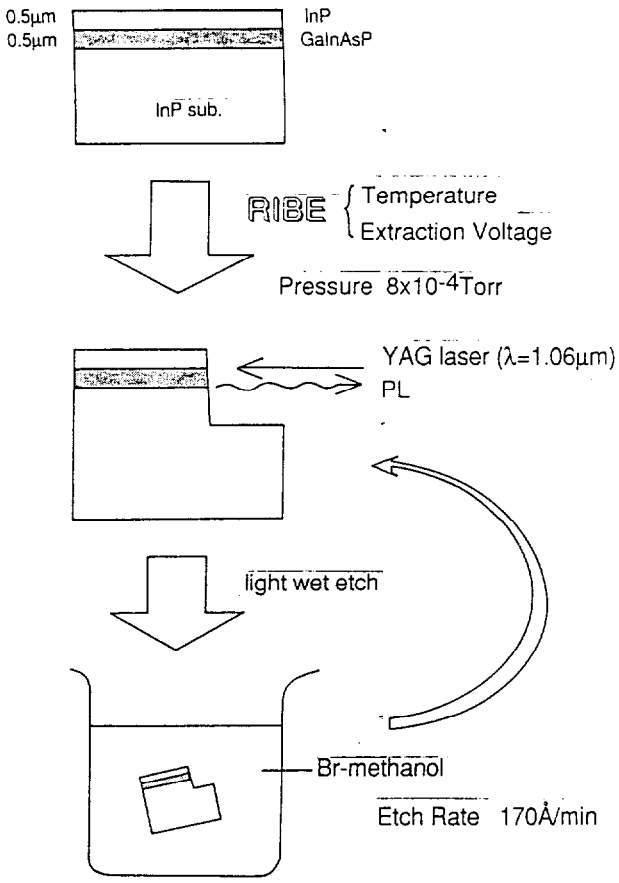

Fig. 3-11 Experiment processes of measurement of sidewall damage. The etch rate of slow-rate etchant Br-CH_3OH etchant was 170Å/min.

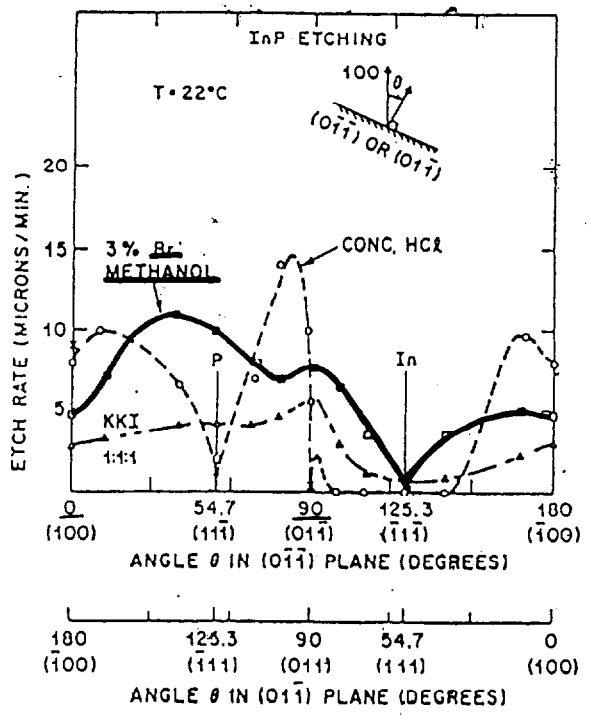

Fig. 4. Measured etch rate vs. InP substrate orientation angle from the (100) for rotation about either the [0$\bar{1}$1] or [011] axes.

Fig. 3-12 Actual measured plots of etch rate vs. θ by L. A. Coldren *et al*[8].

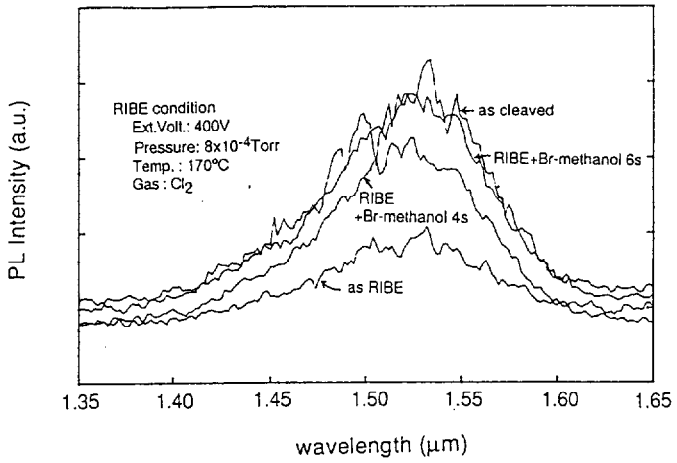

Fig. 3-13 PL spectra at room temperature from the etched sidewall. In this figure, the spectrum of the etched sidewall after RIBE and after Br-methanol etching and the cleaved sidewall are shown. After Br-methanol etching, the spectral intensities increased considerably.

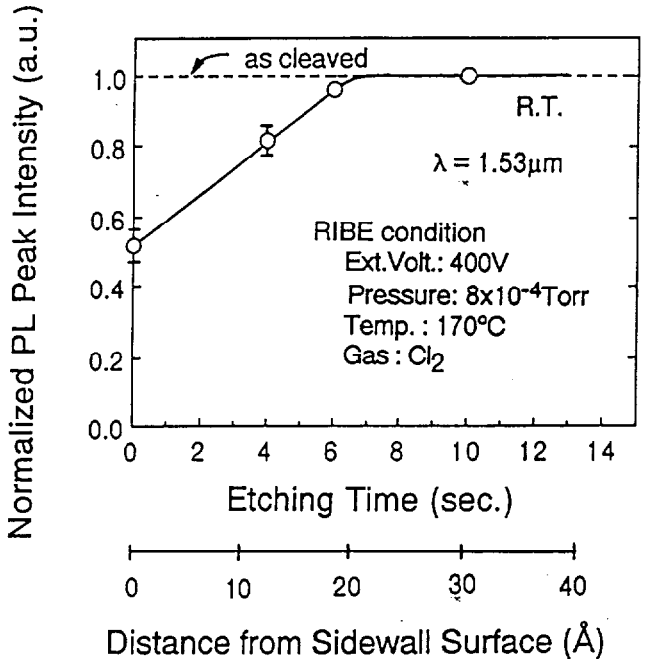

Fig. 3-14 Relationship the PL intensity of a GaInAsP sidewall etched by RIBE and the distance from the sidewall surface. The PL intensity was normalized with the PL intensity of cleaved facet. In this figure, it is found that the PL intensity is recovered to that of cleaved facet by a slightly wet etching by Br-CH_3OH of 8-10 sec. The wet etching time of 8-10 sec corresponds to the etched depth of 20-30Å.

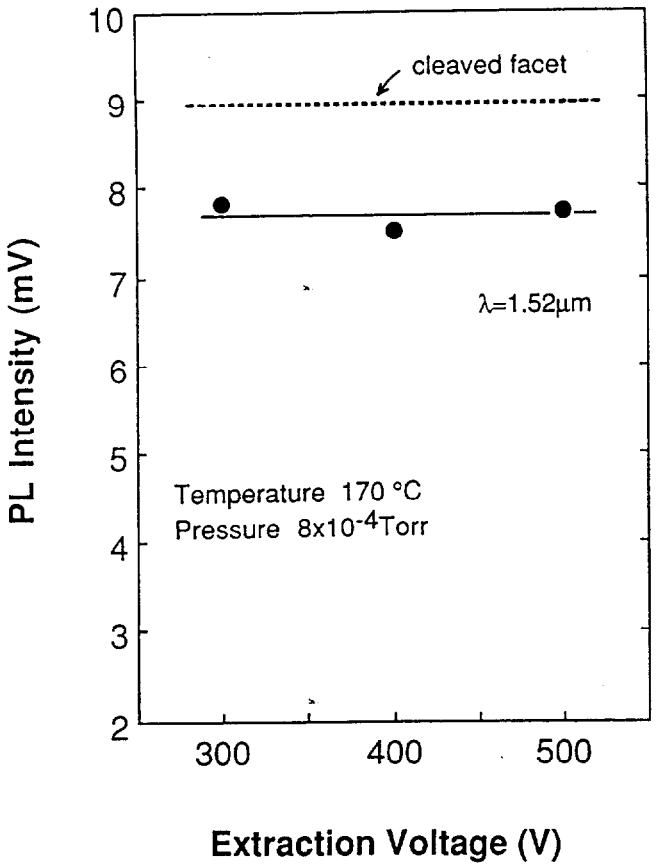

Fig. 3-15 Relationship PL intensity and ion extraction voltage. From this figure, the PL intensity is the same in the region of ion extraction voltage of 300V-500V.

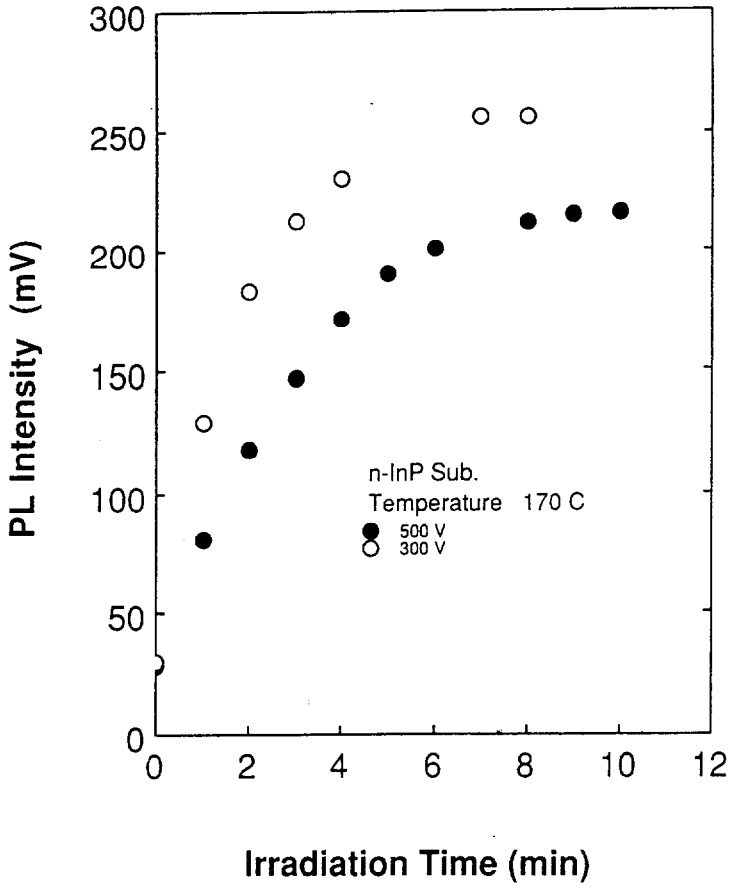

Fig. 3-16 PL intensity changed with time in irradiation with relatively high laser power. The applied laser power was about 50mW, and the spot diameter on the sample was 500μm.

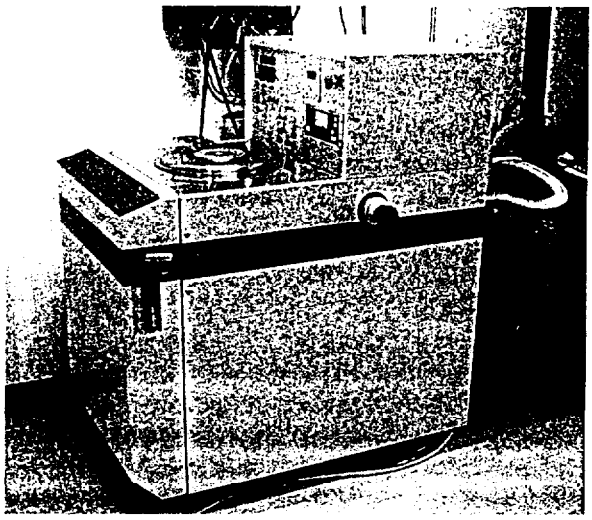

Fig. 3-17 (a) Photograph of Reactive Ion Etching System

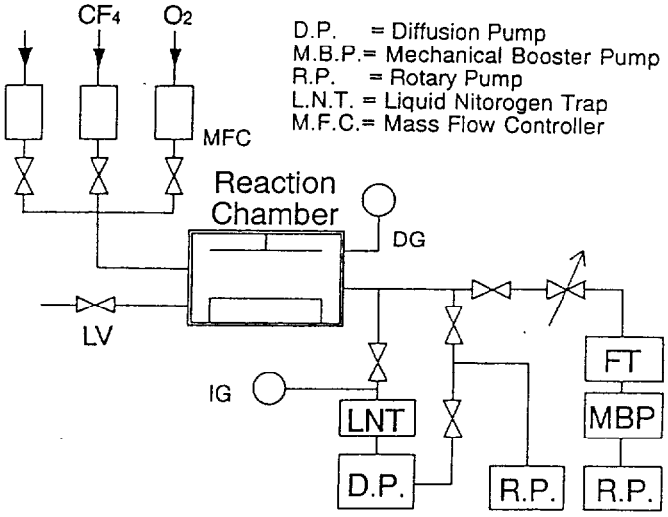

Fig 3-17 (b) Schematic Diagram of Reactive Ion Etching System

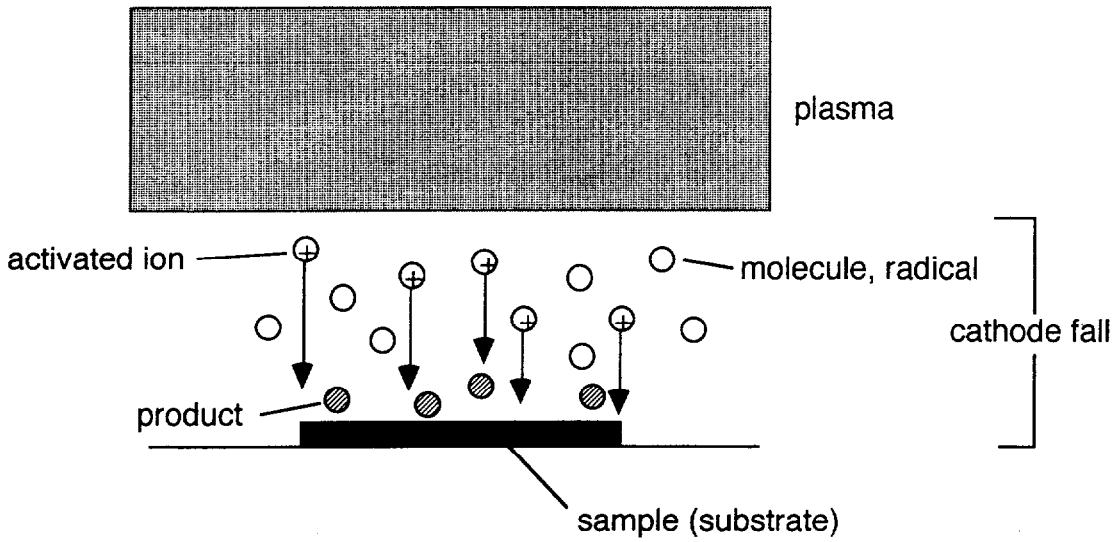

Figure 3-18 Phenomenon near the sample surface

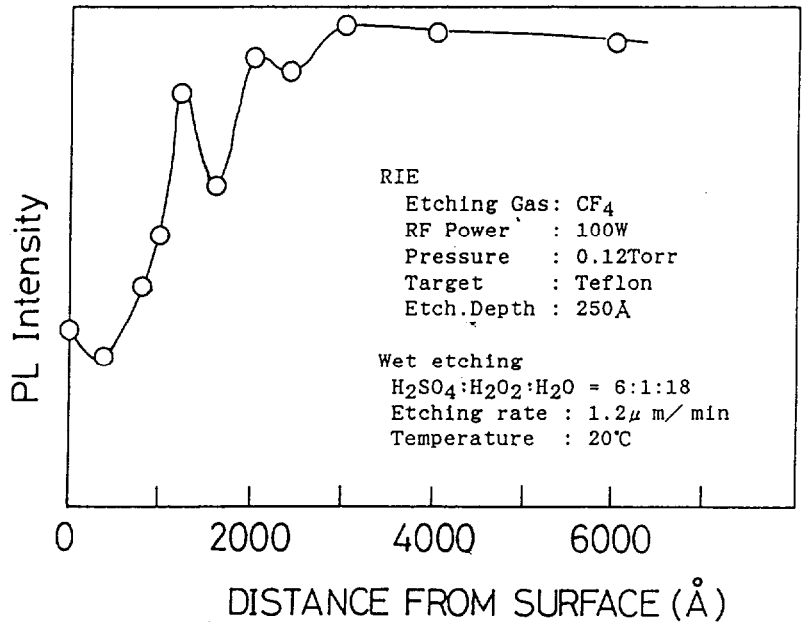

Fig. 3-19 Relation between etching time and photoluminescence intensity. RF power: 100W, Etching gas: CF_4, Etching pressure: 0.12Torr, Etching table: Teflon.

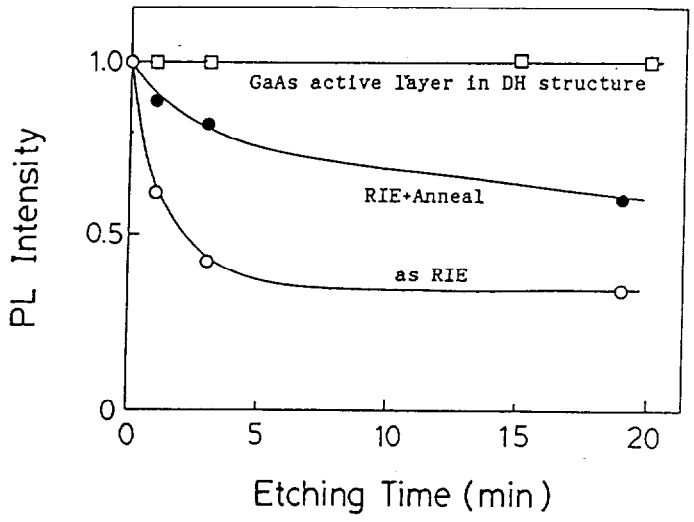

Fig. 3-20 Relation between distance from surface and PL intensity of GaAs substrate etched by RIE.

Chapter 4 Roughness Analysis of Sidewalls Processed by RIBE

4.1 Introduction

In this chapter, a quantitative 3-dimensional measurement of sidewall roughness of InP etched by chlorine-based reactive ion beam etching (RIBE) is presented. Recently, the dry etching began to be used as an effective microfabrication technique to form micro-optical devices such as VCSELs and etched facet lasers [1-3]. In these device applications, the etched facets should be vertical and smooth as to avoid light scattering and keep high reflectivity that is sensitive to the facet roughness[1]. Also, the smooth etched surface is needed to reduce an etching induced damage[4] on sidewalls. There are a lot of reports on InP reactive ion beam etching (RIBE) with Cl_2 electron cyclotron resonance (ECR) plasma [4-7]. In these works, the etched bottom roughness was measured by scanning tunnel microscope (STM) to be, for example, 1.4 nm (rms) at a high ion extraction voltage of about 1 kV[6]. So far, the quality of the etched mirror reflectivity has been estimated mainly by scanning electron microscope (SEM) observation and by measuring the external differential quantum efficiency and the threshold of etched-facet semiconductor lasers [1-3]. Also, the quantitative evaluation of etched sidewalls of various materials, for example, SiO_2 , AlGaAs/GaAs, photo-resist, etc., has been reported by a scanning probe microscope (SPM) [8-13]. However, the analysis of InP sidewalls processed by RIBE has not been reported. In this chapter, the sidewall roughness measurement of InP using an electron probe surface roughness analyzer is performed.

4. 2 Electron Probe Roughness Analyzer System

The sidewall roughness is measured by a field emission electron probe surface roughness analyzer (ELIONIX: ERA-8000FE). The roughness measurement by this system can be performed by a noncontact manner, therefore, the sample is not damaged by this measurement. Figure. 4-1 shows the principle of the measurement. This instrument has four secondary electron detectors which are set facing each other. I can detect the distribution of secondary electron intensity corresponding to the surface inclination of roughness. The surface inclination

of roughness at the electron beam incident point can be found quantitatively from the intensity of the output signals of the four detectors. The roughness profile is obtained by the scanning electron beam in the xy-plane. Figure. 4-2 shows the principle of the roughness measurement , in detail. Provided the sample is placed horizontally and two secondary electron detectors are set facing each other in a scanning electron microscope, we can detect the distribution of secondary electron corresponding to the surface inclination of roughness. When the difference in the output signal (A-B) is observed, the signals have polarities and a contrast by the illumination effect in the direction of detector A . Then the profile information can be obtained. The roughness of the sample surface can be determined qualitatively by this different signal image. The surface inclination of roughness at the electron beam incident point can be found quantitatively from the intensity of the output signals of detectors A and B. The roughness profile is obtained by the integration of the electron beam scanning at any intervals.

Before measurement, I examined the precision of this instrument using a SiO_2 step height standard (15 nm ± 0.5 nm) made by VLSI Standards Incorporated. The measured roughness is 15.5 nm. The measured value is in good agreement with the data (15 nm) provided by the manufacturer (Figure. 4-3). The roughness is measured with an electron beam acceleration voltage of 5 kV. This electron beam energy is low enough for high resolution measurements. The theoretical roughness resolution of this system is 1 nm.

4. 3 Measurement of InP Sidewall Etched by RIBE

The samples prepared here were InP substrates with an electron beam resist mask which was patterned directly by an electron beam lithography system (ERIONIX: ELS3300PWM) to avoid the mask edge fluctuations. I have optimized the substrate temperature for anisotropic etching in our instrument. Therefore, I adopted the substrate temperature of 140°C, in this experiment. The etching pressure changed from 4×10^{-4} Torr to 1.2×10^{-3} Torr. The ion extraction voltage is 300 or 400V.

Figures 4-4 show the overview SEM image and the 3-dimensional plot of sidewall roughness of etched sample. This wafer was etched at an ion extraction voltage of 300V and

a gas (Ar : Cl_2= 1 : 2) pressure of 4.5 x 10^{-4}Torr. The roughness of the etched sidewall is 3nm in center line average (R_a) and 10 nm in peak to peak roughness (R_{max}). The R_a is really corresponding to root mean square (rms). And then, the roughness is measured with electron beam acceleration voltage of 5kV. This electron beam energy is low enough for high resolution measurement.

Figure. 4-5 shows the 3-Dimensional plot of sidewall and bottom surface roughness of etched sample. This wafer was etched at 300V and a gas pressure of 4.5 $\times 10^{-4}$Torr. The Ra of the etched sidewall is 2.5nm and the Rmax is10.3nm. The Ra of the etched bottom surface is 2.1nm and the Rmax is 11.4nm. The roughness of sidewall is as smooth as that of surface.

4.4 Sidewall Roughness under Different Etching Conditions

Figure. 4-6 shows the etching pressure dependence of sidewall roughness. The upper figure shows the 3-dimensional plot of wafer etched at 400V and a gas pressure of 8 $\times$ 10^{-4}Torr. The Ra of the etched sidewall is 1.7nm and the Rmax is 9.7nm. The lower figure shows the 3-dimensional plot of wafer etched at a gas pressure of 4 $\times 10^{-4}$Torr. The Ra is about 15nm and the Rmax is about 50nm.

Figure. 4-7shows the ion extraction voltage dependence of sidewall roughness. The upper figure shows the 3-dimensional plot of wafer etched at 400V and a gas pressure of 8 $\times$ 10^{-4}Torr. The Ra is 1.7nm and the Rmax is 9.7nm. The lower figure shows the 3-dimensional plot of wafer etched at 500V. The Ra is about 10nm and the Rmax is about 35nm.

Figure. 4-8 shows the roughness of InP cleaved facet. The upper figure shows the 3-dimensional plot of InP cleaved facet. The lower figure shows the roughness measured at the middle of the etched sidewall along the y axis. The roughness of the cleaved sidewall is 0.9nm in average and 5.8nm in peak to peak roughness. From now, we call roughness average Ra and peak to peak roughness Rmax.

Figure. 4-9 summarizes the typical example of measurement of the sidewall roughness under different etching conditions. The roughness was measured at the middle of the etched wall along the y axis shown in Fig. 4-4. Fig. 4-9 summarizes the measured roughness of the

samples under various etching conditions. The measured area is 2 μm in the x direction by 1.5 μm in the y direction. Fig. 4-9 shows that the etched sidewall roughness increased when the ion extraction voltage was high. The R_a is 15nm and the R_{max} is 50 nm. The data (c) shows the minimum value among our measurements. The R_a is about 1nm and the R_{max} is 6 nm at an ion extraction voltage of 400V and a gas pressure of 1.2×10^{-3} Torr . The low ion extraction voltage and higher gas pressure are desirable for anisotropic etching of InP. The etching condition suitable for smooth etching is the acceptable for vertical etching.

4. 5 Summary

In summary, the sidewall roughness of InP etched by RIBE was measured using the electron probe surface roughness analyzer.

(1) The minimum value of the sidewall roughness average was 1nm. The peak to peak roughness was 5.8nm. Theses are obtained at 400V and a gas pressure of 1.2×10^{-3}Torr. This roughness is much smaller than the wavelength of semiconductor laser light. I think that the main origin of roughness is produced by a chemical reaction, not due to the fluctuation and undulation of mask edge.

(2) Also, for a smooth InP etching, we should reduce ion extraction voltage and increase gas pressures as far as we could, while maintaining anisotropic etching profiles.

If the etching mask edge fluctuation or undulation can be decreased, Reactive Ion Beam Etching is an effective dry etching technique for the fabrication of microsized Surface Emitting lasers and optoelectronic devices.

References

[1] H. Saito, Y. Noguchi, "HIGH-PERFORMANCE InGaAsP/InP 1.3μm LASER STRUCTURES WITH BOTH FACETS ETCHED," *Electron. Lett.*, vol. 22, pp. 1157-1158, 1986.

[2] N. Boudama, J. Riou and A. Kampfer, "LOW THRESHOLD GaAs/GaAlAs BH LASERS WITH ION-BEAM-ETCHED MIRRORS," *Electron. Lett.* 21, pp. 566-567, 1985.

[3] K. Mutoh, S. Wakabayashi, Y. Toyoda and M. Nakajima, "Simultaneous Fabrication of Vertical and 45° Mirrors of InP for Surface-Emitting Lasers Using Inclined Cl Ion Beam," *Jpn. J. Appl. Phys.*, 30, pp. 67-71, 1991.

[4] A. Matsutani, T. Tadokoro, F. Koyama and K. Iga, *Material Science Forum, 1993 Trans Tech Publications, Switzerland,* vol. 140-142, pp. 641-658 , 1993.

[5] K. Mutoh, M. Nakajima and M. Mihara, "Reactive Ion Beam Etching of InP with Cl_2," *Jpn. J. Appl. Phys.* 29, pp. 1022-1026, 1990.

[6] T. Yoshikawa, S. Kohmoto, Y. Sugimoto and K. Asakawa, "Cl_2-ECR Plasma Etching of III/V Semiconductor and Its Application to Photonic Devices," *IEICE Trans.* vol. J77-C-1, pp. 260-267, 1994.

[7] K. G. Ravikumar, K. Kudo, S. Arai and Y. Suematsu, "Low-Damage GaInAs(P)/InP Nanometer Structure by Low-Pressure ECR-RIBE," *Jpn. J. Appl. Phys.* 29, pp. L1744-1746, 1990.

[8] R. W. Herrick, Lori G. Sabo and Joseph L. Levy, *Proceedings of LEOS 1991 Summer Topical Meeting on Microfabrication for Photonics and Optoelectronics, Newport Beach,* California, pp. 43-44, 1991.

[9] R. W. Herrick, Lori G. Sabo and Joseph L. Levy, "Novel technique for the analysis of surface roughness on semiconductor laser etched facets," *J. Vac. Sci. and Technol.* B, vol. 9, pp. 2778-2783, 1991.

[10] S. Matsui, T. Ichihashi, M. Baba and A. Satoh, "Electron Beam Induced Selective Etching and Deposition Technology," *Supperlattice and Microstructures, vol. 7, #4,* pp. 295-301, 1990.

[11] A. Satoh, Y. Tsukamoto, M. Baba and S. Matsui, "Measurement of Sidewall Roughness

by Scanning Tunneling Microscope," *Jpn. J. Appl. Phys.* 30, pp. 3298-3301, 1991.

[12] C. F. Lin, "The Influence of Facet Roughness on the Reflectivities of Etched-Angled Facets for Superluminescent Diodes and Optical Amplifiers," *IEEE Photonics Technol. Lett.* vol. 4, pp. 127-129, 1992.

[13] Y. Martin and H. K. Wickramasinghe, "Method for imaging sidewalls by atomic force microscopy," *Appl. Phys. Lett.* 64, pp. 2498-2500, 1994.

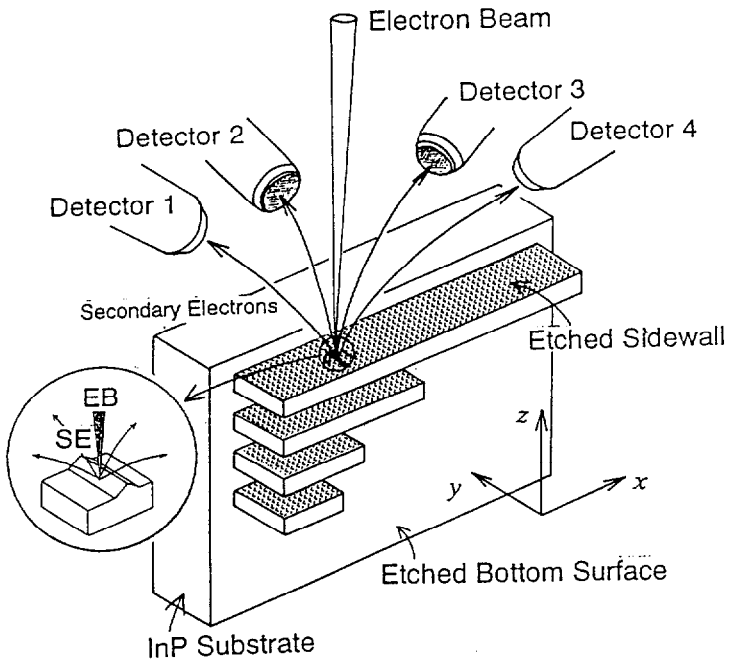

Fig. 4-1 The principle of measurement. This instrument has four secondary electron detectors which are set facing each other.

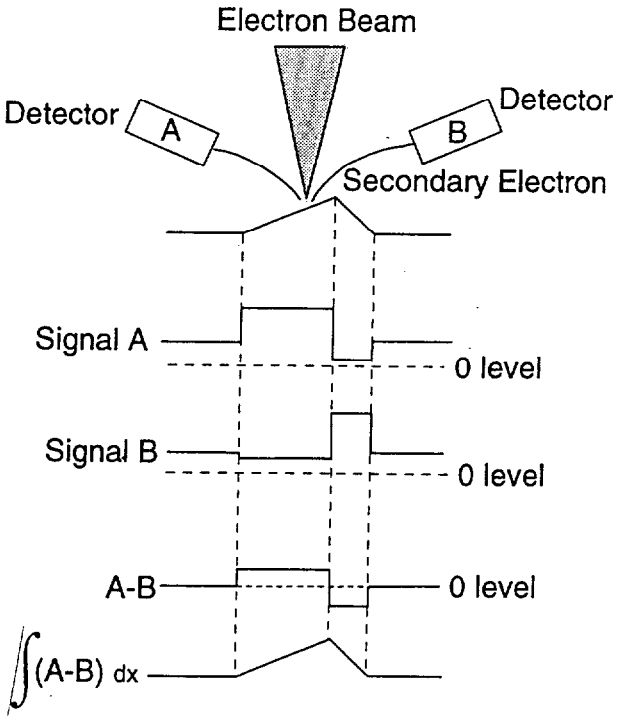

Fig. 4-2 Principle of the roughness measurement.

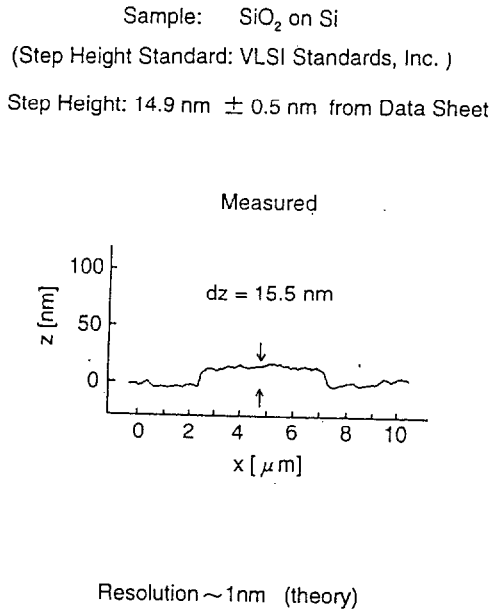

Fig. 4-3 Precision of field emission electron probe surface roughness analyzer.

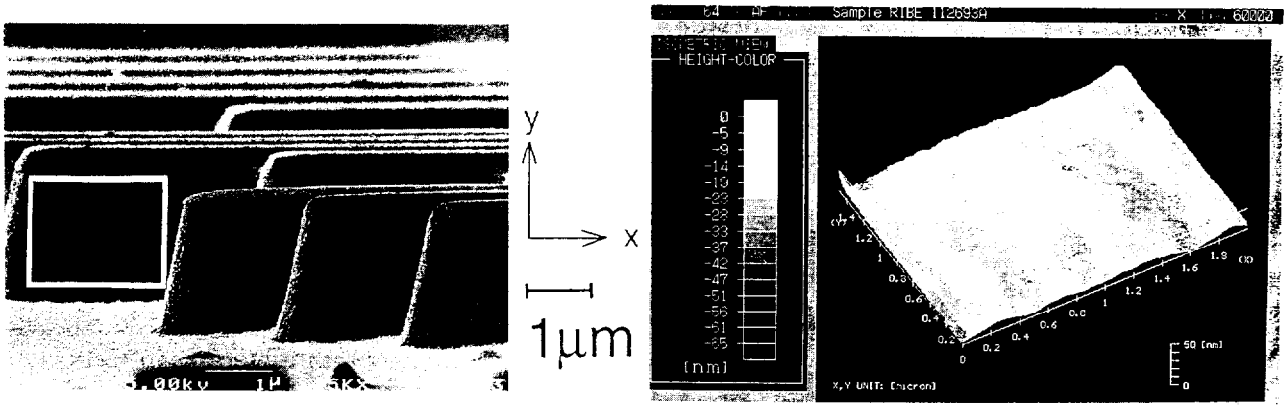

Fig. 4-4 SEM image and 3-dimensional plot of sidewall roughness of etched sample.

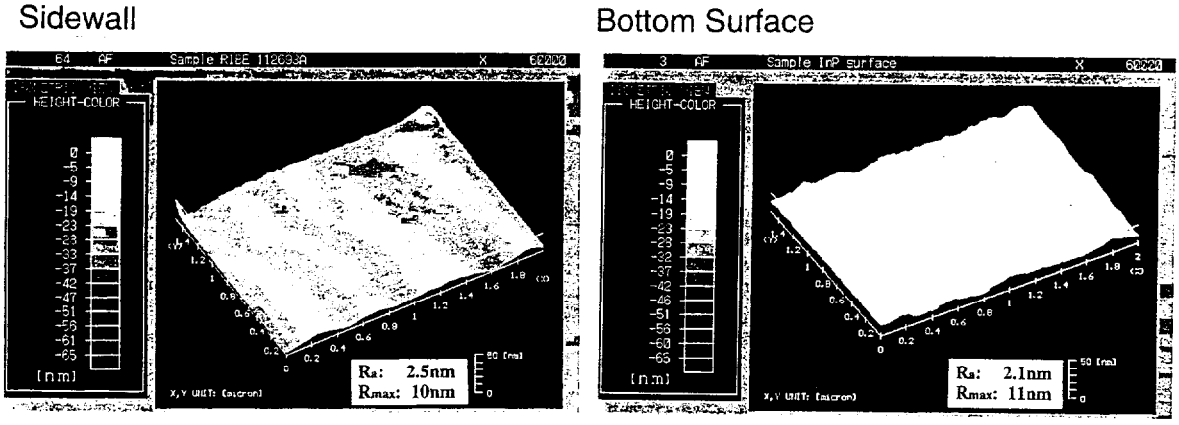

Ion Ext. Voltage: 300V, Etching Pressure: 4.5×10^{-4}Torr
Etching Gas: Cl_2+Ar (2:1), Etching Temperature: 140℃

Fig. 4-5 3-Dimensional plot of sidewall and bottom surface roughness of etched sample.

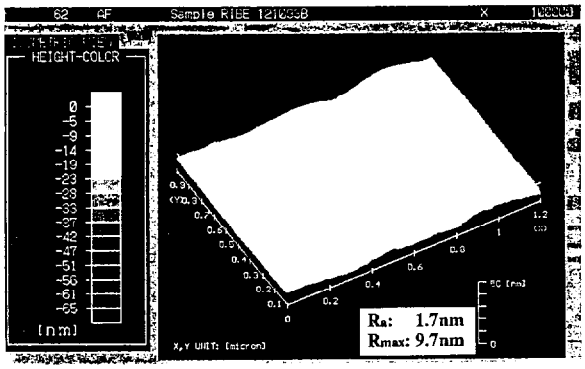

Ion Ext. Voltage: 400V, Etching Pressure: 8×10^{-4}Torr
Etching Gas: Cl_2, Etching Temperature: 140℃

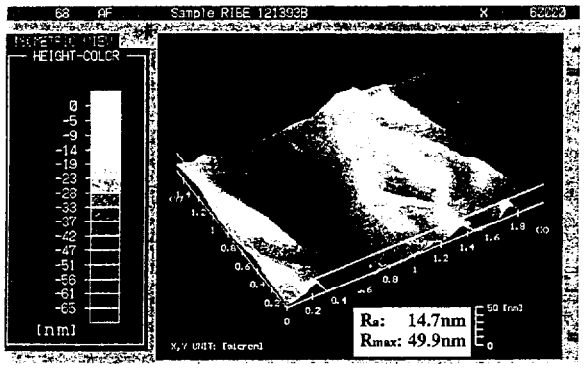

Ion Ext. Voltage: 400V, Etching Pressure: 4×10^{-4}Torr
Etching Gas: Cl_2, Etching Temperature: 140℃

Fig. 4-6 Etching pressure dependence of sidewall roughness.

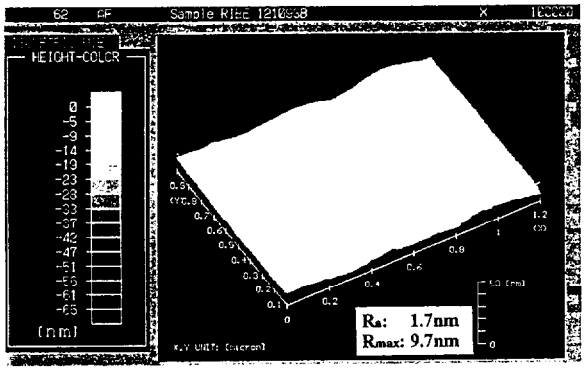

Ion Ext. Voltage: 400V, Etching Pressure: 8×10^{-4}Torr
Etching Gas: Cl_2, Etching Temperature: 140℃

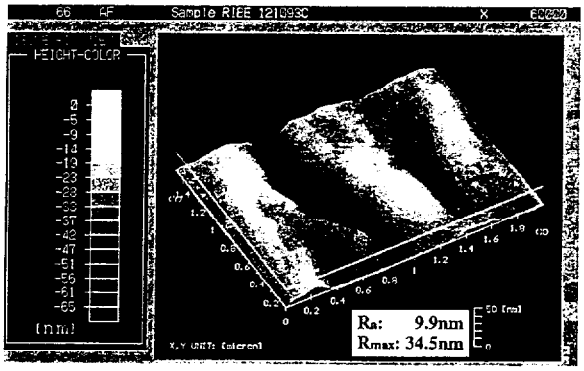

Ion Ext. Voltage: 500V, Etching Pressure: 8×10^{-4}Torr
Etching Gas: Cl_2, Etching Temperature: 140℃

Fig. 4-7 Ion extraction voltage dependence of sidewall roughness.

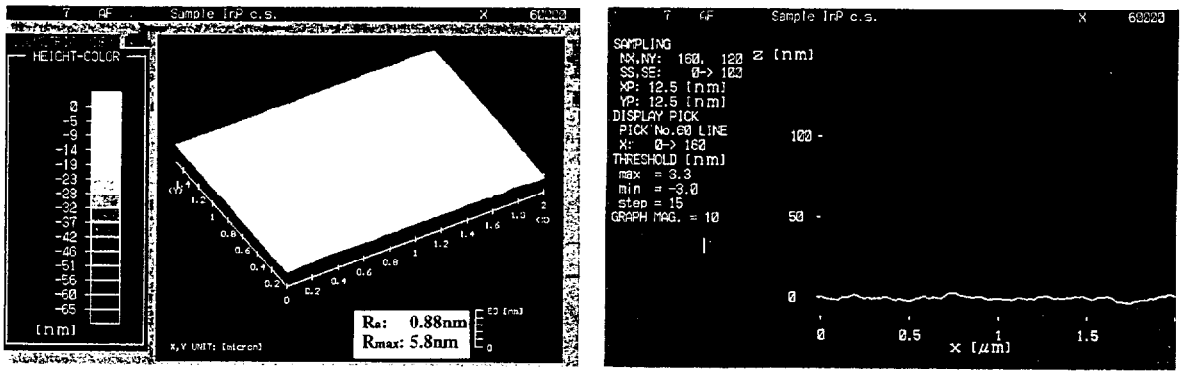

Fig. 4-8 Roughness of InP cleaved facet. The upper figure shows the 3-dimensional plot of InP cleaved facet. The lower figure shows the roughness measured at the middle of the etched sidewall along the y axis.

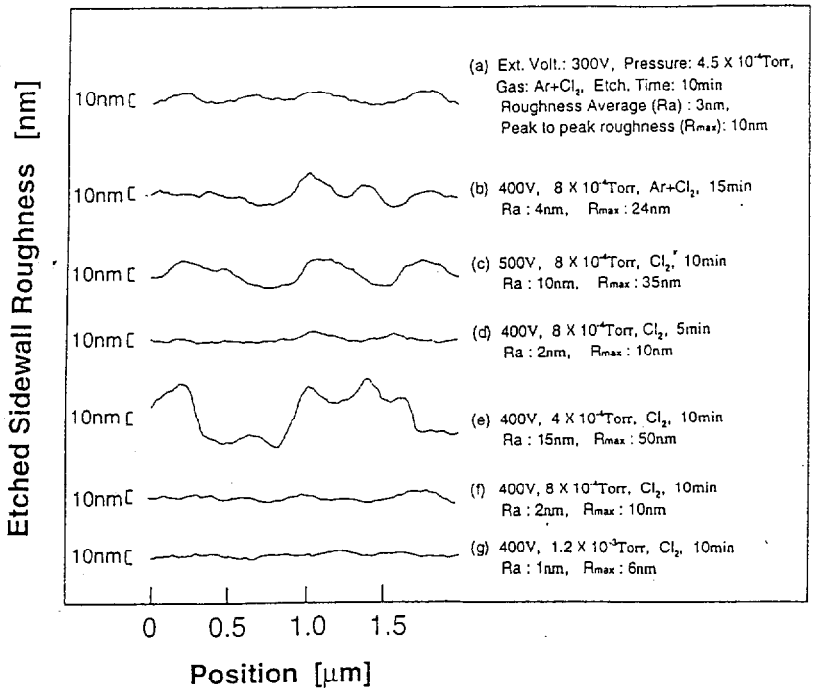

Fig. 4-9 Sidewall roughness under different etching conditions.

Chapter 5 Etching Profile of Reactive Ion Beam Etching

5.1 Introduction

Reactive ion beam etch (RIBE) is one of the most important dry etching techniques for microfabrication of semiconductor devices[1]. However, the dry etching technique using Cl_2 gas causes unwanted side-etching near the bottom of etched samples, which should be avoided, particularly, for submicron device fabrication. For example, some microsized VCSELs made by CAIBE or RIBE have a side-etched shape near the bottom of the mesas[2, 3]. The rise of surface temperature under dry etching has been observed by monitoring with a thermocouple gauge. It is considered that temperature rise might be caused by ion irradiation, but this assumption has not been experimentally confirmed yet. The temperature of the rear side of the sample holder was measured with a thermocouple gauge, and the actual surface temperature change has not been directly measured so far. There may be a large difference in temperature between the sample surface and the sample holder.

In this paper, the measurement of surface temperature by a radiation thermometer during RIBE is carried out for the first time. In addition, I propose multistep RIBE to improve the etching profile in order to alleviate the temperature rise. Also, I propose a multistep RIBE process for smoothing microneedles usually appearing on the etched surface of InP substrate.

5. 2 Surface Temperature Increase in Reactive Ion Beam Etch

I monitor the surface temperature through a transparent BaF_2 window with a radiation thermometer from the direction of ion irradiation. The BaF_2 window has sufficient transmissibility for the infrared wavelength corresponding to room temperature. The accuracy of the radiation thermometer is ± 2°C. The measurement area is nearly equal to the sample holder size.

The initial temperature is one of the important etching parameters. First, I measured the rise of the surface temperature of the sample for different ion extraction voltages. Figure 5-1 shows the relationship between the ion irradiation time and the surface temperature for

different ion extraction voltages. The etching pressure is 8×10^{-4} Torr and the initial temperature is about 25°C. The plasma irradiation time is 15min. The surface temperature of the sample increases when the ion extraction voltage increases. Moreover, the surface temperature of the sample rises to 40~50°C even at an ion extraction voltage of 0V. This result indicates that the Cl ions arrive at the substrate even at 0V. The surface temperature of the sample rises to 100°C and 250~280°C at 200V and 400V, respectively. I think that the temperature rise is due to ion energy and/or ion current.

Figure 5-2 shows the relationships between the etching time and the etched depth for a GaAs substrate with etching gases of Cl_2 and Ar. The sample was etched at an ion extraction voltage of 400V and a gas (Cl_2 or Ar) pressure of 8×10^{-4} Torr. The sample is not heated and the initial temperature of the sample is about 25°C. For Ar etching, the etched depth increases in proportion to etching time. However, the etched depth shows a superliner characteristic against etching time for Cl_2-RIBE. This might be due to the rise of the sample temperature caused by ion irradiation. The difference in the etching rates of Cl_2 and Ar also originates from chemical reaction of the Cl_2. This effect is marked in a long-term etch where the surface temperature increase caused by ion irradiation is considerable.

5. 3 Improvement of Profiles by Multistep Etching

The profile of etched mesas is dependent on the etching time. It is well-known that the etching behavior is classified into three categories in Cl_2-RIBE[4]. In Ar etching, the etching profile is of overcut shape, since the etching characteristic is ion beam etching (IBE)-like. At the initial stage of Cl_2-RIBE, the etching profile is vertical in shape, since the etching characteristic is reactive ion etching (RIE)-like. However, the etching profile shows side-etching or undercut shape with increasing etching time. These etching behaviors depend on the substrate temperature. That is, in Cl_2-RIBE, the etching profile is affected by the surface temperature rise which is caused by ion irradiation. Therefore, it is difficult to realize the vertical and high-aspect-ratio etching for microsized pillar-type mesas.

I therefore propose multistep RIBE to overcome this difficulty. This new technique involves several repetitions of the etching process under the vertical etching condition

obtainable at the initial stage of Cl_2-RIBE. Figure 5-3 shows the concept of multistep RIBE and the SEM images of the etching profiles obtained by conventional one-step RIBE and multistep RIBE. I fabricated the circular pillar-type mesa as a sample for the application to VCSELs. Etching conditions common to the two process are etching pressure of 8×10^{-4} Torr, ion extraction voltage of 400V and initial substrate temperature of about 25°C. I used a GaAs substrate as a sample. The etching time for the conventional one-step RIBE is 15 min. The multistep RIBE etching time is 7 min + 7 min + 6 min (total etching time: 20 min). The cooling time of the sample between the etching steps is 60 min. After cooling, the substrate temperature is about 25°C. In Fig. 5-3, I can see that the side-etching near the bottom of the mesa is eliminated by the multistep RIBE. Thus, the multistep RIBE is an effective dry-etching technique for the microfabrication of VCSELs and optoelectronic devices.

5. 4 Origin of Side Etch Foot of Mesa

Figure 5-4 shows a model of the origin of the side-etching at the bottom of mesas and the experimental result. I think that the temperature near the bottom of mesas increased due to the ion irradiation, because the substrate surface is irradiated directly by the ions. Therefore, the substrate surface is chemically etched and the etching profile is isotropic. I carried out the following experiment to test this idea. First, I prepared the circular pillar-type mesa of GaAs. Next, I irradiated the Ar ion beam on the sample at an extraction voltage of 400V for 15 min, this time, the bottom surface of the sample was heated to ~250°C. Immediately afterwards, I irradiated the sample with Cl ions without applying extraction voltage for 2 min. Under these etching conditions, the etching behavior is similar to chemical etching and the etching profile is isotropic. As a result, the shape of the mesa near the bottom is dependent on the crystal orientation of the substrate. Observation by scanning electron microscope (SEM) after this experiment supported my model.

5. 5 Smoothing of Etched Surface by Multistep-RIBE

Many authors have reported on the reactive ion beam etching of InP with Cl_2 electron cyclotron resonance plasma. For example, Yoshikawa *et al* have reported that Cl_2 ion

energies in excess of 1kV are required to minimize the roughness and to obtain a vertical etching profile for InP[5]. I think that the ion energy should be as low as possible to reduce the induced damage. However, in the etching condition with a low pressure and a low ion energy for InP RIBE, many micro-needles appear on the etched surface due to micromasks of Indium as reported in ref 5. Up to now, the height of these microneedles of InP have not been reduced yet at low ion extraction voltage. As described in section 5. 3, I have proposed a multistep RIBE to improve etching profiles in order to alleviate the temperature rise of the surface. That is, I have obtained the vertical etching profile of GaAs without side etch and undercut by introducing the multistep RIBE. In section 5. 3, the temperature of the etched surface rises to 250°C at an ion extraction voltage of 400V for an etching time of 15 min. I think the temperature increase is due to ion energy and ion current as described in section 5. 3. So, I have predicted that the micro-needle appearing on the etched surface of InP can also be smoothed without changing the etched profile by the partial temperature increase of the surface due to the ion irradiation.

It is well-known that the etching mechanism of RIBE is classified to three types, i.e., ion beam etching (IBE)-like, reactive ion etching (RIE)-like and chemical etching-like. An etching condition with a high gas pressure, high sample temperature and a low ion extraction voltage is needed for chemical etching-like. The microneedles can be reduced by using RIBE under the chemical etching-like condition. However, the chemical etching nature causes side-etch and undercut depending on a crystal orientation. To improve this etched profile, the microneedles on the bottom surface have to been etched without etching the sidewall of the mesa. That is, the bottom surface should be only heated without heating the sidewall of the mesa. The proposed multistep RIBE enables the local heating of the surface for smoothing of these microneedles.

Under these result above mentioned, I have predicted that the micro-needle appearing on the etched surface of InP can also be smoothed without changing the etched profile by the partial temperature increase of the surface due to the ion irradiation.

Figure 5-5 shows a model of the multistep-RIBE. I think that the temperature near the bottom of mesas increased due to the ion irradiation, because the substrate surface and

micro-needles are irradiated directly by the ions. Therefore, the micro-needles are chemically etched. I carried out the following experiment to test this idea. First, I prepared the mesa of InP. At this time, many microneedles appear on the etched bottom surface. Next, I irradiated the Cl ion beam on the sample at an extraction voltage of 400V, this time, the bottom surface of the sample was heated as shown in figure 5-5. Under these etching conditions, the etching behavior is similar to chemical etching. As a result, the microneedles can be disappeared without change of etching profile of mesa.

Figure 5-6 (a) shows an SEM images of the mesa and the cross section of InP after the first RIBE. The ion extraction voltage is 300V. The substrate temperature is 245°C. The etching gas pressure is $1.5x10^{-4}$Torr. The etching time is 8 min. These are typical etching conditions to obtain the vertical etching profile at a relatively low ion extraction voltage. I can see many microneedles of 1μm height. Figure 5-6 (b) shows an SEM image of the mesa and the cross section after the second-step RIBE. The ion extraction voltage is 400V. The initial substrate temperature is 25°C. The etching gas pressure is $1.2x10^{-3}$Torr. The etching time of the multistep RIBE is 18min. At this time, the substrate surface temperature is estimated at to be 250°C. It is clear that the height of the micro-needles can be reduced by the multistep RIBE. The surface roughness is less than 0.3μm. Although the inclination of the upper part is due to the retreat of resist mask, the etched profile of the mesa remains vertically without etching of the sidewall.

Figure 5-7 (a), 5-7(b) and 5-7(c) show the dependence of etching pressure for the multistep-RIBE. Figures 5-7 (a), 5-7(b) and 5-7(c) show the SEM cross section images with a gas pressure $8x10^{-4}$Torr, $1.2x10^{-3}$Torr, $1.6x10^{-3}$Torr. The ion extraction voltage is 400V, the initial temperature is 25°C and the etching time is 18min. The initial temperature is about 25°C. These etching conditions are commonly used. I can see the height of micro-needles is minimized with a pressure of 1.2 $x10^{-3}$Torr. Figure 5-7 (d) shows relation between the roughness and the gas pressure. In this graph, I can see the micro-needle height is minimized at a gas pressure of 1 to $1.2x10^{-3}$Torr. If the wafer is etched under a low gas pressure etching condition, the microneedles remain on the surface. Because that etching mechanism is IBE-like. Therefore, the obtained result by the multistep RIBE is well understandable.

Figures 5-8 (a), 5-8(b) and 5-8(c) show the dependence of the etching time for the multistep-RIBE. Fig. 5-8 (a) is an SEM cross section image with an etching time of 10min, the etching time of Fig. 5-8 (b) is 18min, the etching time of Fig. 5-8 (c) is 30min. The ion extraction voltage is 400V, the initial temperature is 25°C and the gas pressure is 1.2×10^{-3}Torr. I can see the micro-needle height reduces with an increase of etching time, and is minimized at 30min. Figure 5-8 (d) shows the summarized result for various etching time. In this graph, I can also see the micro-needle height is reduced with an increase of etching time. Especially, the average roughness is estimated to about 110Å with an etching time of 30min by measurement with a Dektak. I think that the decrease in the height of microneedles at the multistep etching is derived from the temperature increase due to ion irradiation.

5. 6 Summary

I have carried out in-situ measurement of the sample temperature during RIBE by using a radiation thermometer for the first time.

(1) It was found that the surface temperature is increased by the ion irradiation.

(2) The surface temperature was increased by about 250K with an ion extraction voltage of 400V for 15 min.

(3) Also, I have proposed multistep RIBE for the improvement of etching profiles.

(4) I found that the origin of the side-etching near the bottom of the mesa is the rise of the sample surface temperature due to the ion irradiation.

(5) I have proposed a novel multistep RIBE process for smoothing of micro-needles on etched surface of InP substrate. I found the micro-needles on the etched surface are reduced by the multistep RIBE without changing etched profile of mesas. The ion extraction voltage of all the processes is less than 400V. The micro-needle height is minimized with a gas pressure of 1 $\sim$ 1.2×10^{-3}Torr and reduces with the increase of etching time. The minimum average roughness is about 110Å.

References

[1] K. Asakawa and S. Sugata, "GaAs and AlGaAs anisotropic fine pattern etching using a new reactive ion beam etching system," *J. Vac. Sci. Technol.* B3, pp. 402-405, 1985.

[2] E. M. Clausen, A. von Lehmen, C. Chang-Hasnain, J. P. Harbison and L. T. Florez, "Improved Threshold Characteristics of Air-post Vertical-Cavity Surface-Emitting Laser Using Unique Etching Process," *Electron. Lett.* 27, 2243-2245, 1991.

[3] T. Tezuka, S. Nunoue, H. Yoshida and T. Noda, "Spontaneous Emission Enhancement in Pillar-Type Microcavities," *Jpn. J. Appl. Phys.* 32, pp. L54-L57, 1993.

[4] T. Tadokoro, F. Koyama and K. Iga, "Classification of Etching Mechanism in Reactive Ion Beam Etch," *J. Vac. Sci. Technol.* B7, pp. 1111-1114, 1989.

[5] T. Yoshikawa S. Kohmoto, M. Ozaki, N. Hamao, Y. Sugimoto, M. Sugimoto and K. Asakawa, "Smooth and Vertical InP Reactive Ion Beam Etching with Cl_2 ECR Plasma," *Jpn. J. Appl. Phys.* 31, 1992, pp. L655-657, 1992.

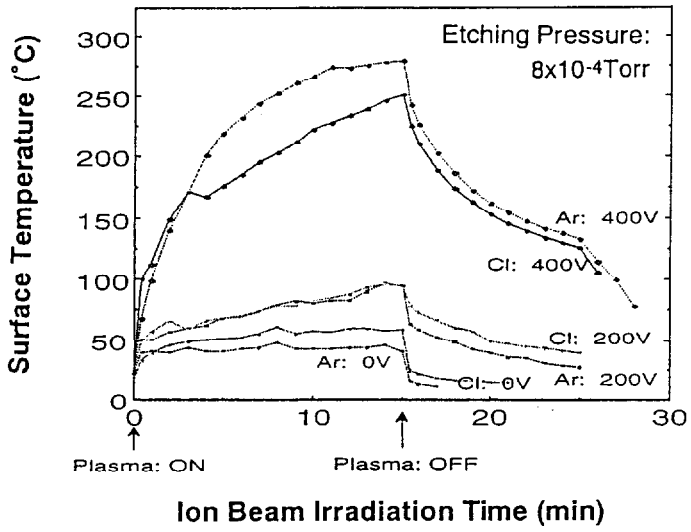

Fig. 5-1 Relationship between ion irradiation time and surface temperature for different ion extraction voltage.

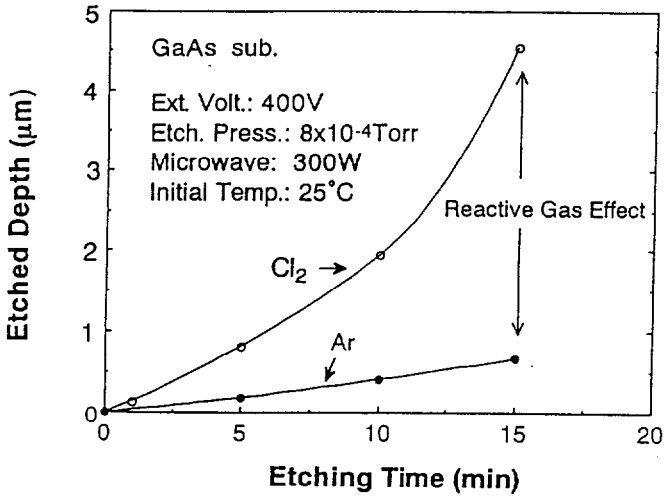

Fig. 5-2 Relationship between etching time and etched depth for GaAs substrate.

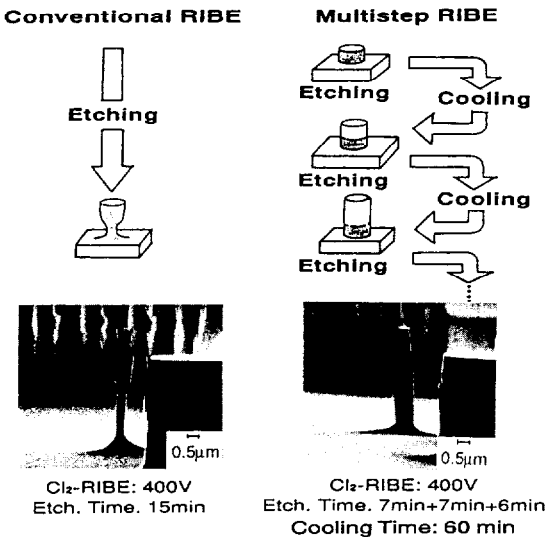

Fig. 5-3 Concept of multistep RIBE and SEM images of etching profiles obtained by conventional RIBE and multistep RIBE.

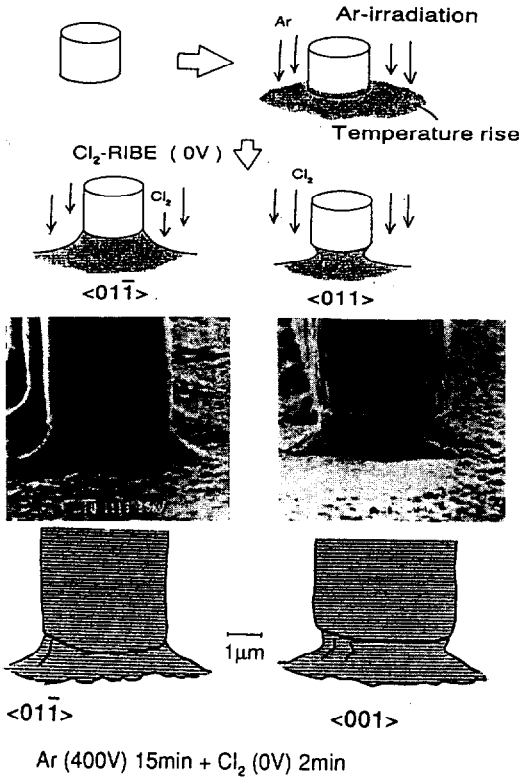

Fig. 5-4 Model of the origin of side-etching near the bottom of a mesa and the experimented result.

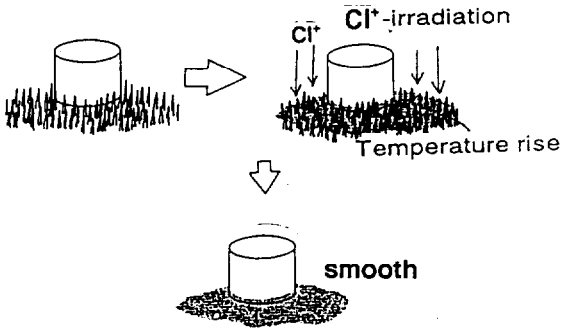

Fig. 5-5 Model of the multistep-RIBE.

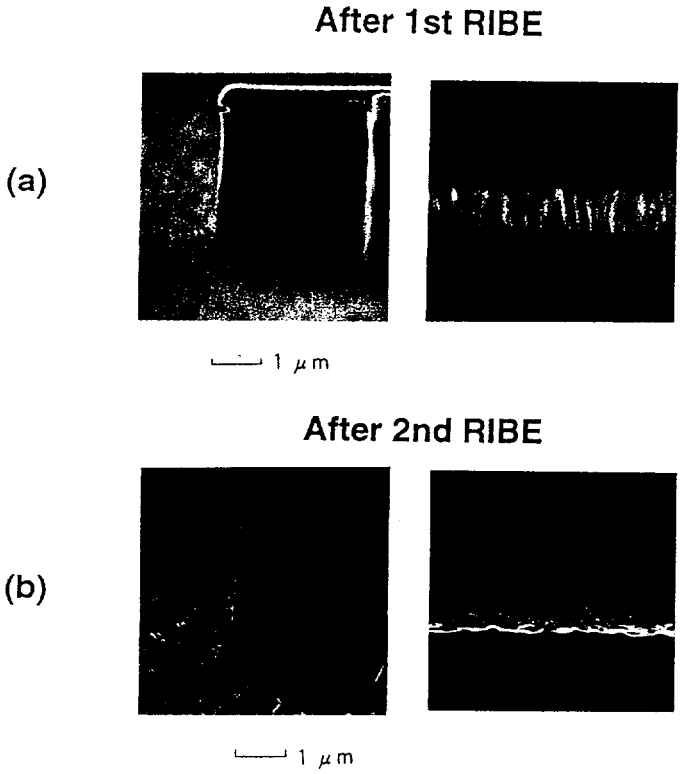

Fig. 5-6 SEM images of mesa and cross section of InP after first step and second step RIBE. (a) Ion extraction voltage: 300V. Substrate temperature: 245°C. Etching Pressure: 1.5×10^{-4}Torr. Etching time: 8 min. (b) Ion extraction voltage: 400V. Initial substrate temperature: 25°C. Etching Pressure: 1.2×10^{-3}Torr. Etching time of multistep RIBE: 18min.

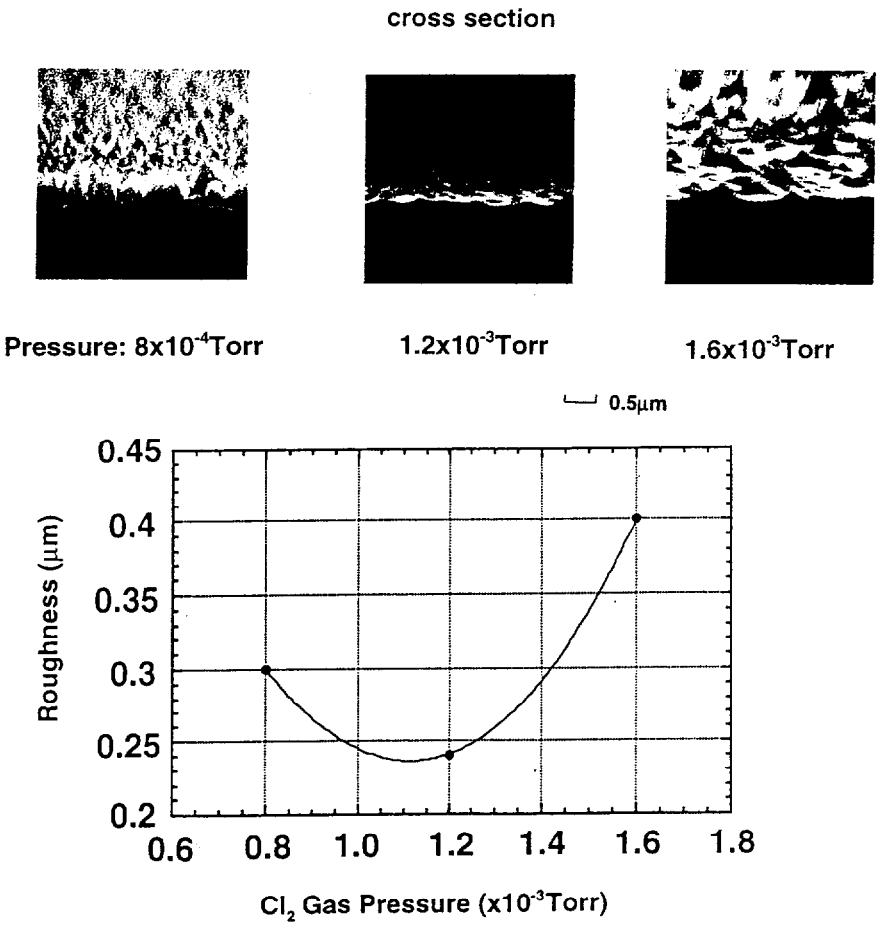

Fig. 5-7 The etching pressure dependence for multistep-RIBE. (a) Gas pressure: 8×10^{-4}Torr, (b) 1.2×10^{-3}Torr, (c) 1.6×10^{-3}Torr. Ion extraction voltage: 400V, initial temperature: 25°C, etching time: 18min. Initial temperature: about 25°C. (d) a graph arranged above SEM images.

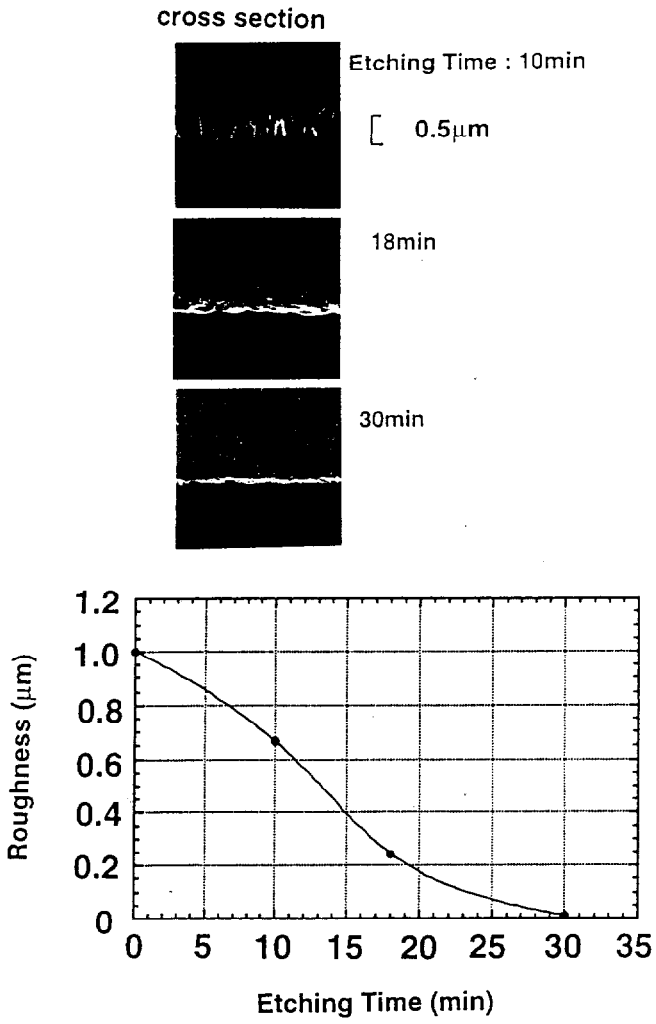

Fig. 5-8 The etching time dependence for multistep-RIBE. (a) Etching time: 10min, (b) 18min, (c) 30min. Ion extraction voltage: 400V, initial temperature: 25°C, gas pressure: 1.2×10^{-3}Torr. (d) a graph arranged above SEM images.

Chapter 6 Plasma Characterization in Chlorine-Based Reactive Ion Beam Etching and Chemically Assisted Ion Beam Etching

6.1 Introduction

Dry etching processes such as reactive ion beam etching (RIBE) and reactive ion etching (RIE) have been widely used for the fabrication of optoelectronic semiconductor devices and VLSI circuits. Plasma chemical processes involving plasma assisted etching are generally rather complex and their etching mechanisms are not fully understood. For a better understanding and to obtain better etching performances of RIBE and chemically assisted ion beam etching (CAIBE)[1], it is helpful to perform analytical studies of ion energy and radical density in plasma.

Until now, many studies on the chemical reactions near the substrate surface and plasma characteristics during dry etching of silicon and related materials have been reported. However, the chemical reactions and plasma characteristics have not yet been fully clarified in the III-V compound semiconductor dry etching process. However I ought to use these dry etching techniques for the micro-fabrication of optoelectronic devices such as etched-mirror semiconductor lasers and microcavity surface emitting lasers[2-3]. In these devices, the vertical etching profile and smooth etched sidewall are required, because the etched sidewall is used as a part of microcavity resonators. In GaAs and related materials, the vertical profile and smooth etched sidewall can be obtained by Cl_2-based RIBE[4]. However, it is difficult to obtain the vertical profile and smooth etched sidewalls in InP and related materials. Yoshikawa *et al.* [5] and Youtsey *et al.* [6] demonstrated good etching profiles of InP etched by chlorine-based RIBE and CAIBE, respectively. However, the plasma characteristics have not been reported in these papers.

In this chapter, I describe the characterization of the chlorine plasma in RIBE and CAIBE systems using a quadrupole mass spectrometer (QMS) with an energy analyzer. The analysis of the chlorine ion energy and its radical density is discussed in the RIBE and CAIBE systems .

6.2 Experimental Setup

Figure 6-1 shows a schematic diagram of an ECR etching system used in this experiment. In CAIBE, neutral Cl_2 gas is supplied from a quartz nozzle in front of the sample holder. The sample holder rotating at 10 rpm is covered perfectly with the Cl_2 jet. I can use this system either for RIBE or CAIBE by changing the Cl_2 gas port.

I used a QMS (Balzers: PPM 421) for the measurement of the plasma characteristics. Figure 6-2 shows the schematic diagram of the QMS. This instrument is the differentially pumped and has an integrated energy analyzer. The mass and the energy of positive and negative ions can be analyzed. Neutral species such as radicals from a plasma or residual gas are ionized by an integrated electron impact ion source and are then detected. For ion sampling with minimum plasma disturbance, the electrically insulated extraction hood can be set to the desired voltage by an external power supply. Ions are sampled through an orifice with a diameter of D=0.1mm in the extraction hood and focused on the entrance of the energy analyzer (CMA: cylindrical mirror analyzer) by an ion optical system in the QMS. In our process chamber, the QMS is set perpendicular to the ion flux. Hence I cannot always detect all the particles, which move perpendicular to the QMS. However, I can detect some particles due to isotropic movements and scattering. In this setting of the QMS, it is fully possible to qualitatively analyze the plasma characteristics, although it is difficult to obtain the absolute density of particles.

6. 3 Measurement of Chlorine Ion Energy in RIBE and CAIBE

In this section, I will describe the following measurements; (1) the energy distribution of Cl^+ from the ECR plasma without an applied voltage, (2) the energy distribution of Cl^+ in the RIBE process, (3) the energy distribution of neutral Cl_2 in the CAIBE process, and (4) the energy distribution of Cl^+ in the CAIBE process.

I used the QMS described above to measure the positive ion energy distribution. For this measurement, the ionizer used as an ion source for neutral particles was turned "off." Therefore, I could obtain only the signal for the ions. Prior to performing these measurements of energy distribution, I measured the energy distributions of Cl_2 and Cl in the process

chamber, and confirmed that these energies were ~0 eV. I also measured Cl^+ energy distribution from the ECR ion source. The ion energy was several tens eV.

Figure 6-3 shows the energy distribution of Cl^+ in the RIBE process. The process gas pressure is 8×10^{-4} Torr and the ion extraction voltage is 400 V. In this figure, I can observe that the energy peaks are at about 20 eV and 400 eV, which correspond to those in the ECR plasma and the ion extraction voltage, respectively. The sharp energy peak of 400 eV shows that the energy of an extracted ion beam is highly uniform. The broad energy peak of about 20 eV may be due to the leakage of the ions generated in the ECR ion source. Hence it can be assumed that the ion energy, contributing to etching, is well determined by the extraction voltage in the RIBE process.

Figure 6-4 shows the energy distribution of neutral Cl_2 in the CAIBE process at plasma "on" and "off." The Ar^+ extraction voltage is 400 V in plasma "on". The Cl_2 flow rate is 2 sccm. The total process gas pressure is 8×10^{-4} Torr. The peak of neutral Cl_2 can be observed in plasma "off". However the peak intensity decreases in plasma "on." Hence, it is assumed that neutral Cl_2 is present in small amounts in the CAIBE process.

Figures 6-5 (a) - 6-5 (e) show the energy distributions of Cl^+ in the CAIBE process. The Cl_2 flow rate is 2 sccm. The total process gas pressure is 8×10^{-4} Torr. Figure 6-5 (a) shows the energy distribution of Cl^+ in the CAIBE process at Ar^+ extraction voltage of 0 V. In this figure, no remarkable energy peak is observed, except for a small peak near 0 eV. Figures 6-5 (b) - 6-5 (e) show the energy distributions of Cl^+ for various Ar^+ extraction voltages between 200 eV and 500 eV. In these figures, it is clear that the Cl^+ energy peaks appear in the energy range of 50-70 eV. It is also observed that these Cl^+ energy peaks increase with an increase of Ar^+ energy. These results show that the neutral Cl_2 is ionized by Ar^+ in the CAIBE process. The white light radiation from Cl_2 gas which is provided from the nozzle can be observed in the CAIBE process. I deduced that this radiation is due to the ionization of Cl_2 gas.

6. 4 Measurement of Radical or Excited State Molecular Density in Chlorine Plasma

It is well-known that ions and radicals play important roles in dry etching processes. However, there have been few reports on the density of radicals in the chlorine-based CAIBE process[6]. In this section, the measurement of chlorine radicals in the RIBE and CAIBE systems are discussed.

I used the same QMS, used in § 6. 3, for the measurement of chlorine radicals. This method of measurement is well-known as the appearance mass spectrometry (AMS) method[7]. The problem, in using this measurement, for the mass spectrometric detection of radicals, is the difficulty in distinguishing between the direct ionization of the free radical and the dissociative ionization of the parent molecule. The appearance potential technique utilizes the several eV difference in the threshold energies of the electron impact ionization of the processes to be separated. For this purpose the mass spectrometer output signal is recorded as a function of the electron energy in the electron impact ion source of the PPM421. The data recorded with the plasma "on" show a much higher intensity at electron energies below the thresholds for dissociative ionization. This additional intensity results from the direct ionization of free radicals created in the plasma. Thus the signal detected between the thresholds for direct ionization of radicals and the threshold for dissociative ionization of the parent molecules is a measure of the radical density in the plasmas.

Figures 6-6 (a), 6-6 (b) and 6-6 (c) show the semilogarithmic plot of the QMS output for Cl_2^+ (m/e=70) and Cl^+ (m/e=35) as a function of the electron beam energy at various Cl_2 pressures in the RIBE process. The Cl_2 flow rate of 2 sccm and the ion extraction voltage of 400 V are constant. It is found that the QMS output signals of Cl_2^+ are larger than those of Cl^+. It is deduced that these signals for Cl_2^+ correspond to ground state or excited state parent molecules. Also, I could not observe the QMS signals for Cl^+ between plasma "on" and "off" at 8×10^{-4} Torr and 1×10^{-4} Torr. However, I can observe the QMS signals for Cl^+ between plasma "on" and "off" at 1×10^{-3} Torr. Therefore, I believe that the Cl radical density increases with an increase of the Cl_2 pressure and there exist few Cl radicals in the present gas pressure range.

Figure 6-7 shows the semilogarithmic plot of the QMS output for Cl_2^+ as a function of the electron beam energy in the CAIBE process. The difference of QMS output signals

between plasma "on" and "off" is negligible. This result shows that the excited state Cl_2 density is lower than the detection limit of this measurement. I also measured the QMS output for Cl^+ as a function of the electron beam energy in the CAIBE process. However, I could not detect any noticeable signal due to weak intensity. Therefore, the effect of the Cl radical might be negligible. Taking into account the result of the ionization of chlorine gas in § 6. 3, it is considered that Cl^+ and excited state Cl_2 in addition to Cl_2 molecules exist in the CAIBE process plasma.

6. 5 Comparison Between RIBE and CAIBE
- Effect on Etching Profile and Sidewall Roughness -

As shown in sections 6. 3 and 6. 4, the ion energy and the radical density of chlorine are clearly different between in RIBE and in CAIBE processes. In this section, the etching profile and etched sidewall roughness are compared between RIBE and CAIBE. The samples prepared here were InP substrates with an electron beam resist mask SAL 601 patterned directly by an electron beam lithography system (ERIONIX: ELS6600) to avoid the mask edge fluctuations. The flow rate of Cl_2 and the substrate temperature were constant at 2 sccm and 250 ℃ in both RIBE and CAIBE, respectively. The extraction voltage of Cl_2 in RIBE and Ar in CAIBE are 400 V. The total process gas pressure is 1×10^{-4}Torr in RIBE and 8×10^{-4}Torr by adding to Ar in CAIBE. Figure 6-8 show scanning electron microscope (SEM) images of InP etched by RIBE and CAIBE. We can see vertical etching profiles in both RIBE and CAIBE. Both etched bottom surfaces are covered with a lot of projections like needles. These projections are originated from micromasks of In. I have already reported how to remove these projections by mutistep- RIBE described in chapter 5.

The sidewall roughness is measured by an electron probe surface roughness analyzer (ELIONIX: ERA-4000). This instrument has four secondary electron detectors which are set facing each other. We can detect the distribution of secondary electron intensity corresponding to the surface inclination of roughness. The surface inclination of roughness at the electron beam incident point can be found quantitatively from the intensity of the output signals of the four detectors. The roughness profile is obtained by the scanning electron beam in the

xy-plane. This electron beam energy is low enough for high resolution measurements. The detail of this instrument has been described in chapter 4. Figure 6-9 shows the three-dimensional plot of the sidewall roughness of etched samples. The measured area is 3μm in the x direction by 4μm in the y direction. The average of peak to peak roughness of the etched sidewall is 11nm in CAIBE, and 14nm in RIBE, respectively. In this measurement, the vertical stripe on etched sidewall of the CAIBE sample is not more remarkable than that of RIBE. It may be due to lower chlorine radical densities and lower chlorine ion energy in CAIBE.

6. 6 Discussions

I have presented the comparison of the chlorine radical and excited state Cl_2 density and energy distribution between the RIBE and CAIBE process. The chlorine radical and ground state or excited state Cl_2 is less in the CAIBE process than that in the RIBE process and the chlorine ion energy in the CAIBE process is smaller than that in the RIBE process. I consider that the difference originates from the fact that the ionized position in the process chamber is different between the CAIBE and RIBE systems. The ionization position in the CAIBE system is in Cl_2 gas flow, just in front of the sample. On the other hand, the position in the RIBE system is in the ECR ion source. In other words, the ionization of chlorine in the CAIBE process is due to the collision between Cl_2 and Ar^+, while the ionization of chlorine in the RIBE process is due to electron cyclotron resonance. Accordingly, I think an etching model of CAIBE as follows. In the previous CAIBE model, it was considered that the Ar^+-ion beam etching (IBE) process was assisted by neutral Cl_2 gas. My new model adds the existence of Cl^+ ionized by Ar^+. The effect of Cl^+ on etching is not clear in the plasma characterization. It is important for a better understanding of the plasma processing to clarify the remaining issues, such as the process gas diffusion. I believe that, by optimizing the etching conditions, the CAIBE and RIBE systems are both useful as dry etching techniques for various semiconductor materials.

6. 7 Summary

I have clarified the aspects of ion energy and radical density of chlorine-based RIBE and CAIBE systems. It is observed that neutral Cl_2 is ionized by Ar^+ in the CAIBE process, and the Cl^+ energy peak appears in the energy range of 50-70 eV and this Cl^+ energy peak increases with an increase of Ar^+ energy. I observed that the excited state chlorine molecule in the CAIBE process was lower than that in the RIBE process. I compared the etching profile and etched sidewall roughness between RIBE and CAIBE. The RIBE and CAIBE process will become increasingly useful as dry etching technique with a greater understanding of the plasma characteristics.

References

[1] M. Hagberg, B. Jonsson and A. G. Larsson, "Investigation of chemically assisted ion beam etching for the fabrication of vertical, ultrahigh quality facets in GaAs," *J. Vac. Sci. & Technol.* B12, pp. 555-566, 1994.

[2] K. Iga and B. Miller, "Chemically Etched-Mirror GaInAsP/InP Lasers," *IEEEJ. Quantum Electron,* 18, pp. 22-29, 1982.

[3] T. Mukaihara, Y. Hayashi, N. Hatori, N. Ohnoki, A. Matsutani, F. Koyma, K. Iga, "Low-threshold Mesa-Etched Vertical-Cavity InGaAs/GaAs Surface-Emitting Lasers Grown by MOCVD," *Electron. Lett.,* vol. 31, pp. 647-648, 1995.

[4] K. Asakawa and S. Sugata, "GaAs and AlGaAs anisotropic fine pattern etching using a new reactive ion beam etching system," *J. Vac. Sci. & Technol,.* B3, pp. 402-405, 1985.

[5] T. Yoshikawa, S. Kohmoto, M. Anan, N. Hamao, M. Baba, N. Takado, Y. Sugimoto, M. Sugimoto and K. Asakawa," Chlorine-based Smooth Reactive Ion Beam Etching of Indium-Containing III-V Compound Semiconductor," *Jpn. J. Appl. Phys.*, vol. 31, pp. 4381-4386, 1992.

[6] C. Youtsey, R. Grundbacher, R. Panepucci, I. Adesida and C. Caneau, "Characterization of chemically assisted ion beam etching of InP," *J. Vac. Sci. & Technol.,* B12, pp. 3317-3321, 1994.

[7] H. Sugai and H. Toyoda, "Appearance mass spectrometry of neutral radicals in radio frequency plasmas," *J. Vac. Sci. & Technol.* A10, pp. 1193-1200, 1992.

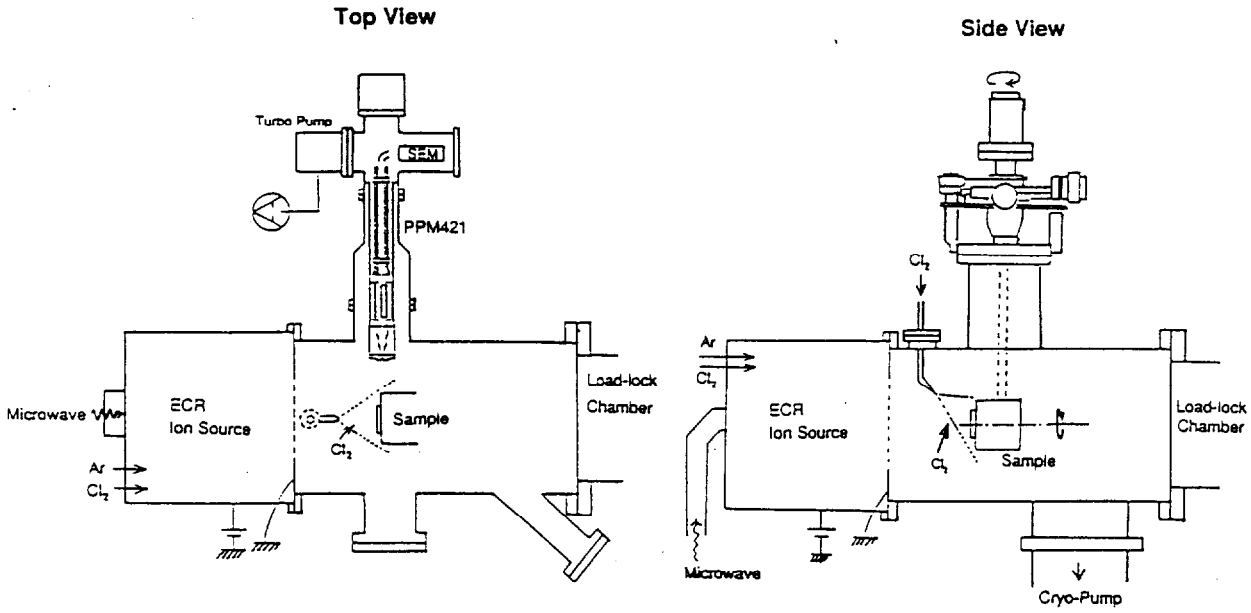

Fig. 6-1 Schematic diagram of an ultra-high vacuum ECR etching system.

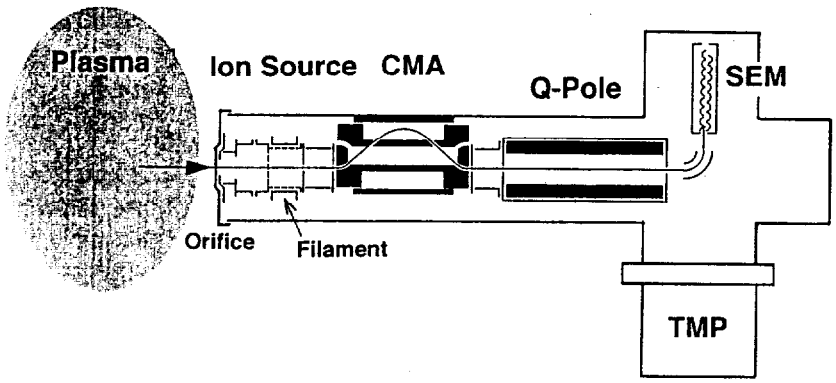

Fig. 6-2 Schematic diagram of the QMS.

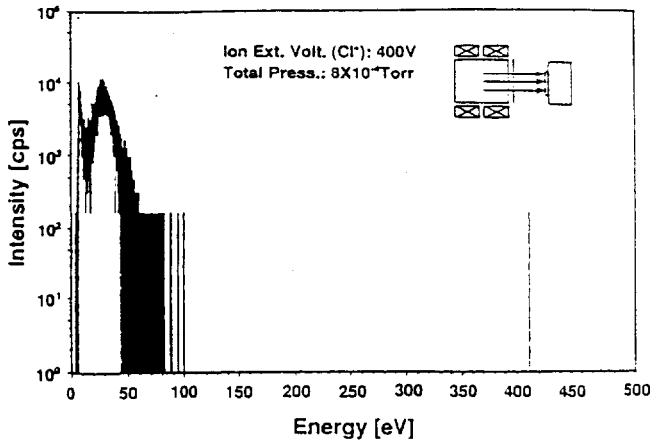

Fig. 6-3 Energy distribution of Cl^+ in the RIBE process. The process gas pressure is 8×10^{-4} Torr and the ion extraction voltage is 400 V. The microwave power is 300 W.

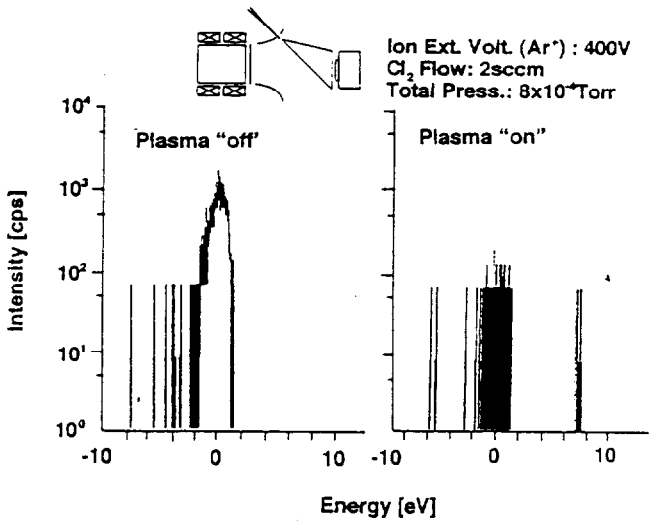

Fig. 6-4 Energy distribution of neutral Cl_2 in the CAIBE process. The Ar^+ extraction voltage is 400 V and the Cl_2 flow rate is 2 sccm. The total process gas pressure is 8×10^{-4} Torr. The microwave power is 300 W.

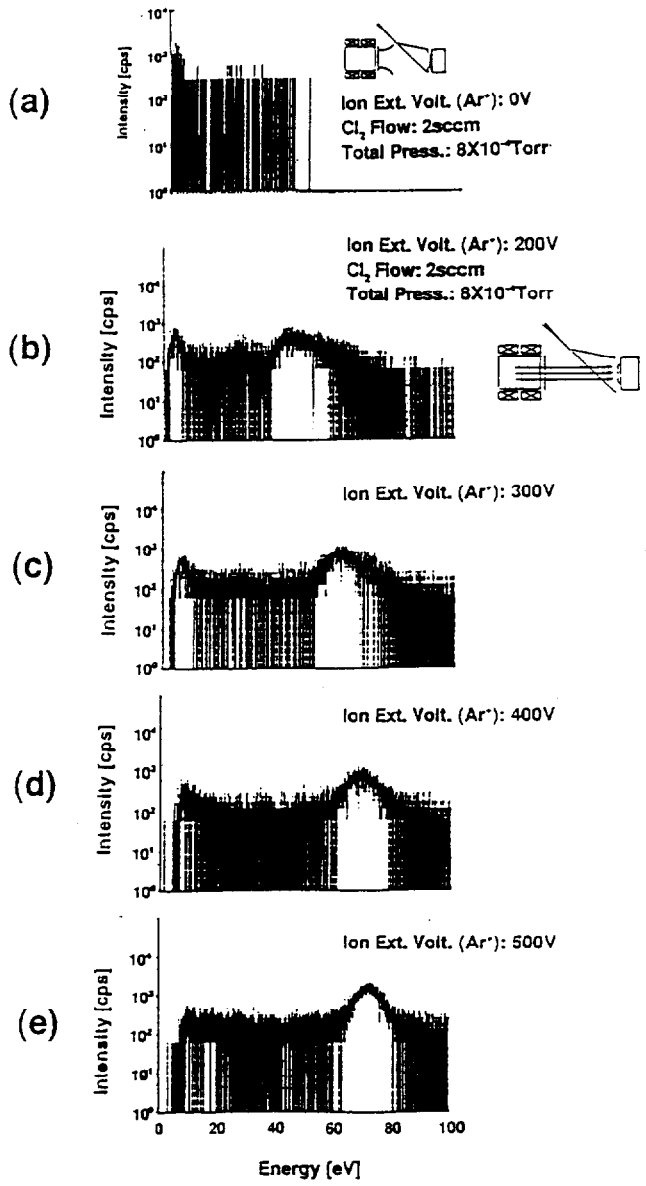

Fig. 6-5 Energy distributions of Cl^+ for Ar^+ energy of 0-500 eV in the CAIBE process. The Cl_2 flow rate is 2 sccm. The total process gas pressure is 8×10^{-4} Torr. The microwave power is 300 W. The ion extraction energy of Ar^+ energy is (a) 0 eV, (b) 200 eV, (c) 300 eV, (d) 400 eV and (e) 500 eV.

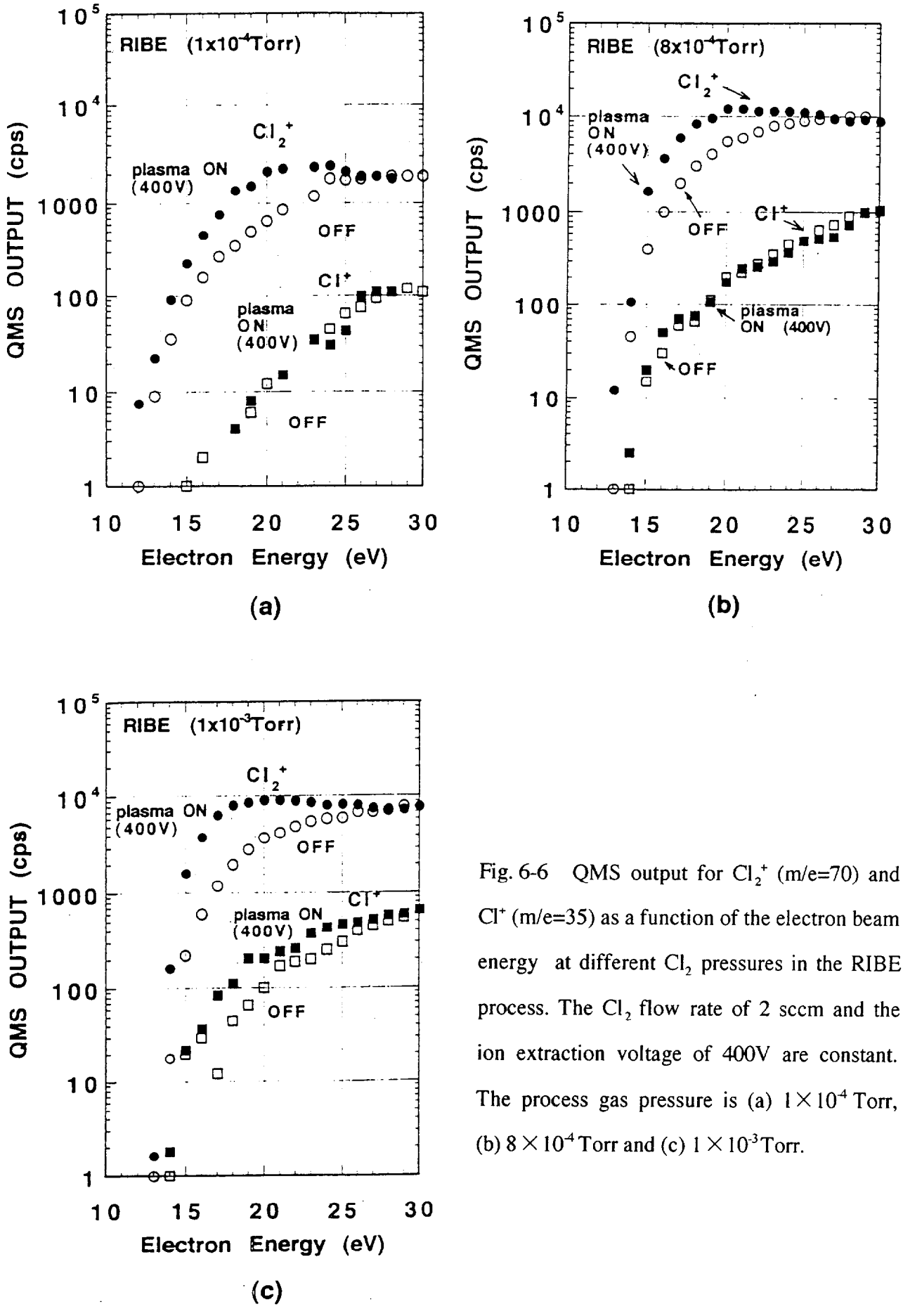

Fig. 6-6 QMS output for Cl_2^+ (m/e=70) and Cl^+ (m/e=35) as a function of the electron beam energy at different Cl_2 pressures in the RIBE process. The Cl_2 flow rate of 2 sccm and the ion extraction voltage of 400V are constant. The process gas pressure is (a) 1×10^{-4} Torr, (b) 8×10^{-4} Torr and (c) 1×10^{-3} Torr.

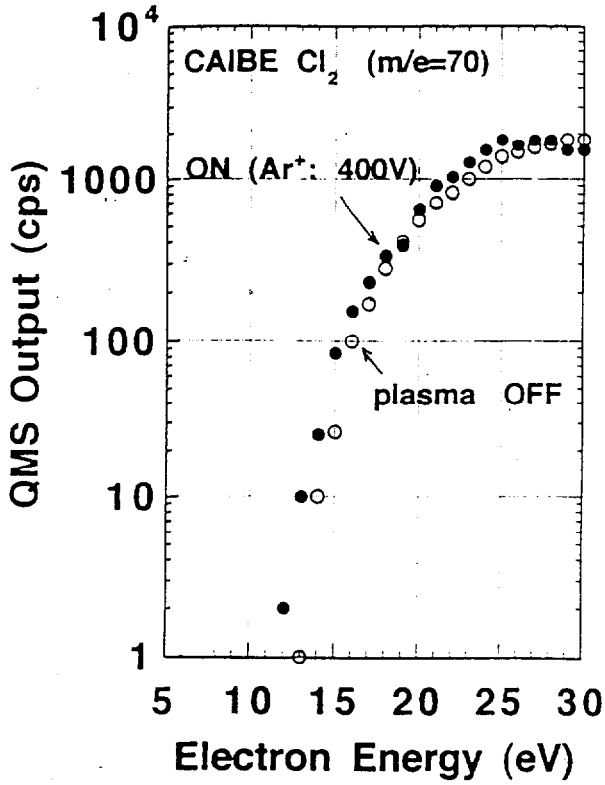

Fig. 6-7 QMS output for Cl_2^+ as a function of the electron beam energy, in the CAIBE process. The Cl_2 flow rate of 2 sccm and the Ar^+ ion extraction voltage of 400 V are constant. The process gas pressure is 1×10^{-4}Torr.

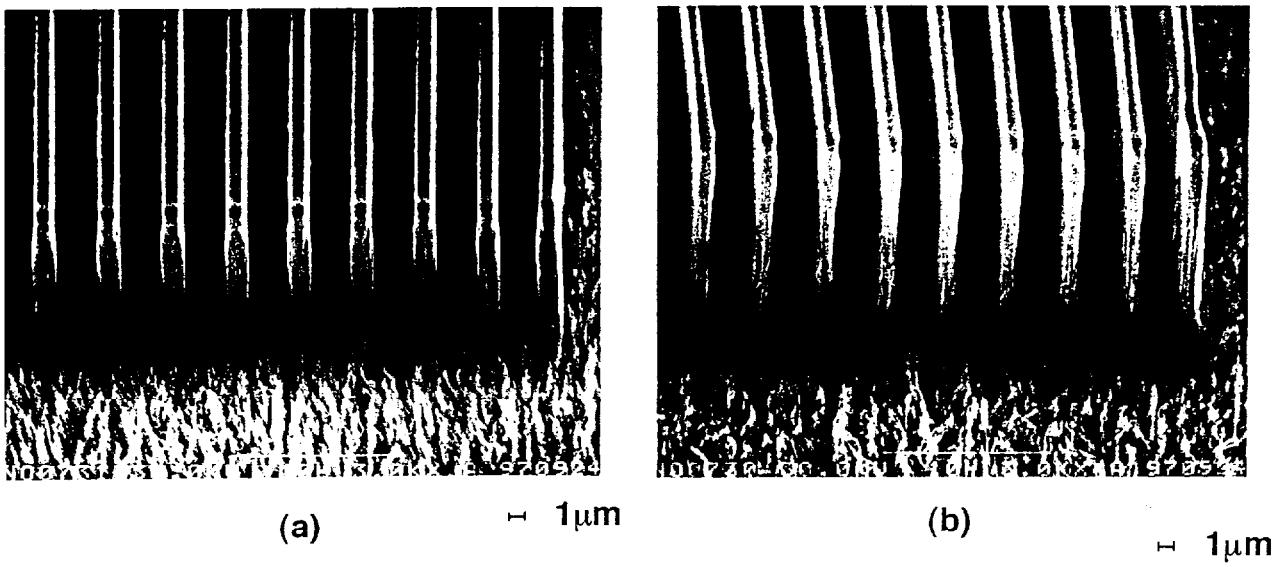

Fig. 6-8

SEM images of InP etched by (a) RIBE and (b) CAIBE. The flow rate of Cl_2 and the substrate temperature kept constant at 2sccm and 250℃. The extraction voltage of Cl_2 in RIBE and Ar^+ in CAIBE are 400V. The total process gas pressure is 1×10^{-4}Torr in RIBE and 8×10^{-4}Torr by adding to Ar in CAIBE.

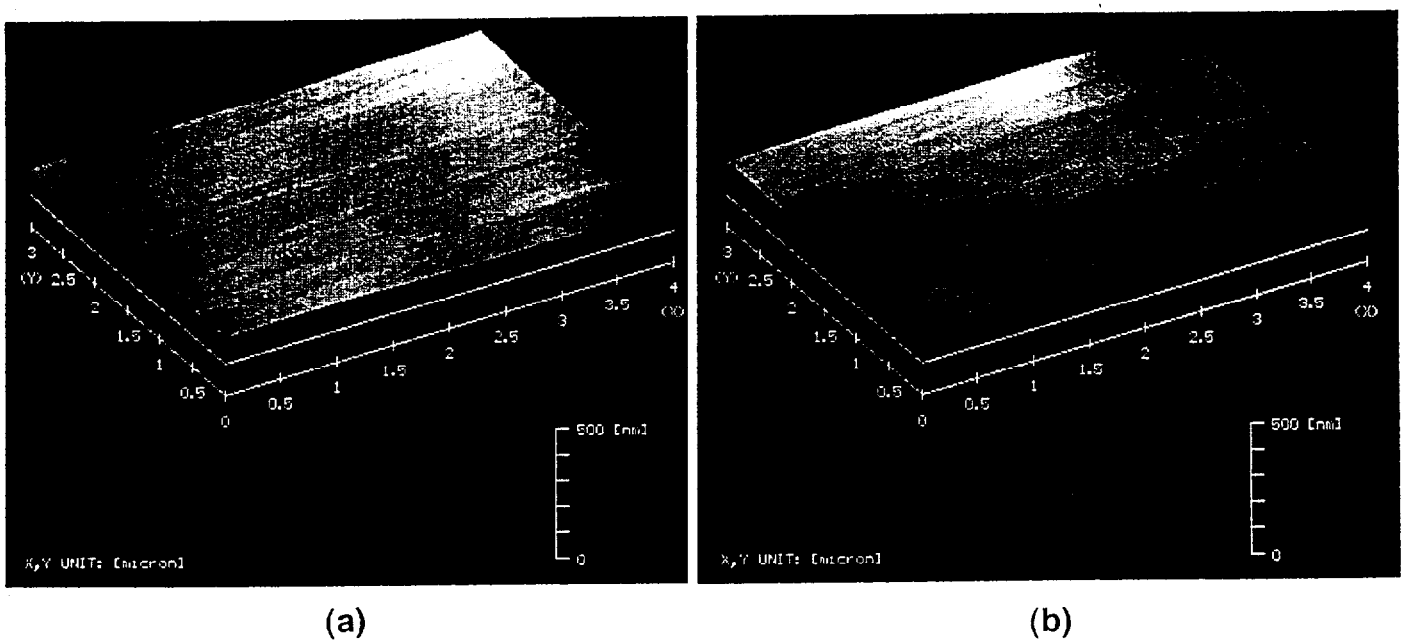

Fig. 6-9

3-dimensional plot of sidewall roughness of etched sample. (a) RIBE, (b) CAIBE.

Chapter 7 C_{60} Resist Mask of Electron Beam Lithography for Chlorine-based Reactive Ion Beam Etching

7. 1 Introduction

Dry etching process is as an effective microfabrication technique to form micro-optical devices such as VCSELs, etched facet lasers and nanoscale quantum devices. In these applications, the resist material for dry-etching process is an important issue. Electron beam (e-beam) lithography is a suitable technique for micro- or nano-scale patterning. The resolution of nanoscale patterns is limited by the molecular size of resist material. In this point, some resist having a very small molecular size is desirable. The size of fullerene such as C_{60} is known to be small. If the C_{60} can be used as an electron beam resist, it may be useful for nanoscale patterning. Up to now, two approaches using C_{60} as a resist material have been reported. Ishii *et al.* have proposed a nanocomposite resist system that incorporates C_{60} molecules into a conventional resist material[1, 2]. They obtained an enhancement by 7 % in etching resistance at 5 wt% content of C_{60} in ZEP resist for Cl_2-ECR etching. This process is suitable to avoid the collapse of high aspect ratio patterns. Tada *et al.* have reported that e-beam irradiation also reduces the dissolution rate of C_{60} films in organic solvents[3]. They have shown the properties of C_{60} as a negative-type e-beam resist and demonstrated the performance of this resist by defining nanoscale patterns in Si etching using fluorine compound gas. However, the properties of C_{60} film as an e-beam resist in dry etching for GaAs and InP using chlorine gas has not been clarified yet.

In this chapter, the properties of C_{60} as an e-beam resist mask in chlorine based reactive ion beam etching (RIBE) is described.

7. 2 Sensitivity of C_{60} Film for Electron Beam

In this experiment, I have used an electron beam lithography system (ERIONIX Inc.: ELS3300 and ELS6600) and a high-vacuum RIBE system. C_{60} films were evaporated on GaAs and InP substrates by the sublimation of C_{60} powders in a vacuum chamber. Figure 7-1 shows the response curve of the C_{60} film to e-beam exposure. The e-beam acceleration

voltage is 50 kV. The vertical and horizontal axis shows the thickness after development in monochlorobenzene (MCB) for 15 sec and the exposure dose of e-beam, respectively. The sensitivity as a negative type resist was $\sim$25mC/cm^2 for MCB. This sensitivity is $\sim$1/4000 for conventional novolac-based resist SAL-601ER7 (Shipley) and $\sim$1/2 of that reported by Tada *et al*. However, it is would be enough for direct patterning in a very small region.

7. 3 Etching Properties of C_{60} Film in Cl_2-RIBE

Figure 7-2 shows the etching rate for C_{60}, InP and GaAs against an ion extraction voltage in Cl_2-RIBE. The etching pressure was 8 x 10^{-4} Torr. The substrate was not heated. In Fig. 7-2, I can see that the etching rate of C_{60} and GaAs is almost proportional to the ion extraction voltage V, and that of InP is proportional to $V^{5/2}$. The C_{60} film shows a similar etching characteristic as GaAs in Cl_2-RIBE.

Figure 7-3 shows the etching rate ratio of C_{60} film for GaAs and InP in the same etching condition shown in Fig. 7-2. The maximum etch rate ratio of C_{60} for GaAs and InP were 20 and 5, respectively. Therefore, the C_{60} film can be used as material of a dry-etching mask.

Figure 7-4 shows the etching rate for C_{60}, InP and GaAs against gas pressure in Cl_2-RIBE. The maximum etching rate ratio is obtained at 8×10^{-4} Torr for both GaAs and InP. The ion extraction voltage was 400 V and the substrate was not heated. In Fig. 7-4, I can see that the etching rate of C_{60} film decreases above at 1 mTorr, while those of InP and GaAs are almost constant between 0.4 mTorr and 1.2 mTorr. In addition , the etch rate ratio of C_{60} film for GaAs and InP between 0.4 mTorr and 0.8 mTorr were 20 and 5, respectively.

I fabricated micropillars in GaAs with the C_{60} mask. The thickness of the C_{60} film was about 3600 Å. The dot patterns were formed by a 20-keV e-beam. Figure 7-5 shows the scanning electron microscope (SEM) photograph of GaAs micropillars of $< 0.5\mu$m in diameter etched by Cl_2-RIBE. The ion extraction voltage was 400 V. The Cl_2 pressure was 8×10^{-4} Torr. The substrate was not heated. In this photograph, it is found that GaAs pillars of submicrometer diameter were fabricated with good anisotropic etching profiles. Therefore, I think that the C_{60} film is a useful resist material for chlorine based dry-etching processes of

GaAs, InP and related materials.

In addition, the C_{60} mask irradiated by electron beam can be removed by using O_2 plasma. I also confirmed that the C_{60} mask pattern irradiated by electron beam can be developed by sublimating non electron beam irradiating part at 400℃ in vacuum. Therefore, I think that all processes from epitaxy to device fabrication can be carried out in vacuum shown in Fig. 7-6. To perform all processes in vacuum will be important as a clean process and low damage process.

7. 4 Summary

In summary, I have characterized the C_{60} film irradiated with an e-beam as a dry-etching mask for Cl_2-RIBE. The sensitivity as a negative type resist was $\sim$25 mC/cm^2 for MCB. The maximum etch rate ratio of C_{60} for GaAs and InP were 20 and 5, respectively. In addition, I have succeeded in fabricating micropillars in GaAs with the C_{60} mask. The C_{60} film would be one of candidates of a dry-etching mask for nanoscale fabrication of semiconductor by optimizing the lithography condition.

References

[1] T. Ishii, H. Nozawa and T. Tamamura, "Nanocomposite resist system," *Appl. Phys. Lett.*, vol. 70, pp. 1110-1112, 1997.

[2] T. Shibata, T. Ishii, H. Nozawa and T. Tamamura, "High-Aspect-Ratio Nanometer-Pattern Fabrication Using Fullerene-Incorporated Nanocomposite Resist for Dry-Etching Application," *Jpn. J. Appl. Phys.*, vol. 36, pp. 7642-7645, 1997.

[3] T. Tada and T. Kanayama, "Nanolithography Using Fullerene Films as an Electron Beam Resist," *Jpn. J. Appl. Phys.*, vol. 35, L63-L65, 1996.

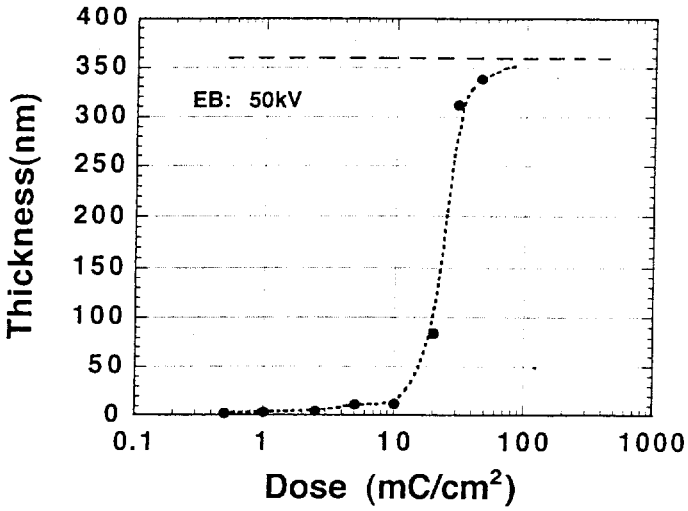

Fig. 7-1 Response curve of the C_{60} film for 50-keV e-beam exposure. The thickness after development in monochlorobenzene (MCB) for 15 sec.

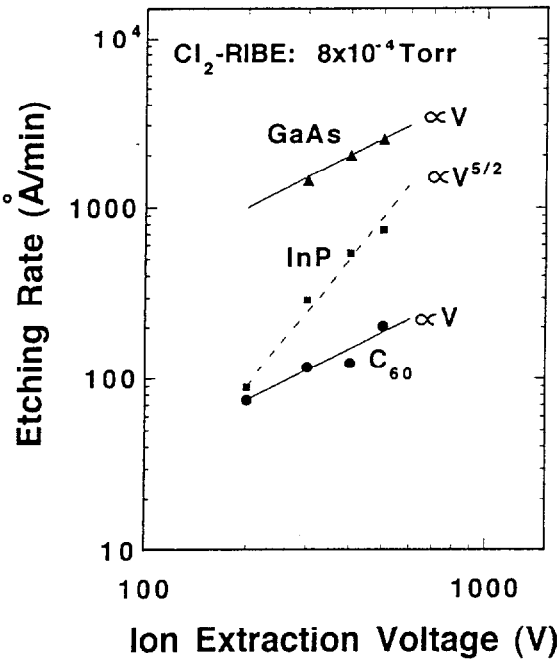

Fig. 7-2 Etching rate for C_{60}, InP and GaAs as a function of Cl_2 ion extraction voltage. Cl_2 gas pressure: 8×10^{-4} Torr.

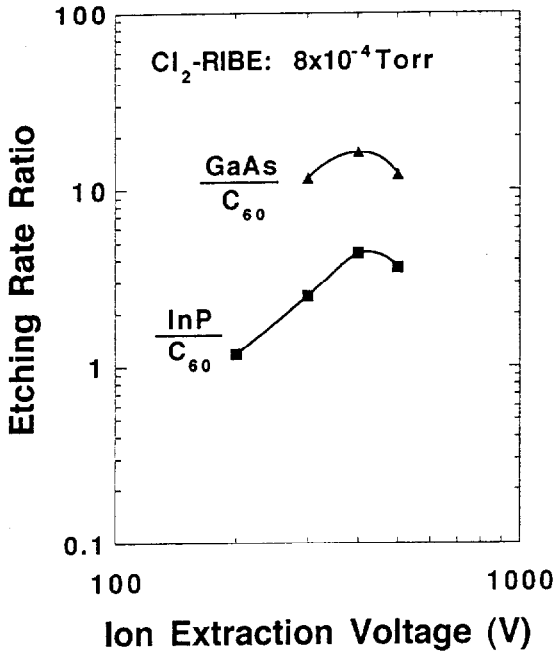

Fig. 7-3 Etching rate ratio of C_{60} for GaAs and InP against different Cl_2 ion extraction voltage.

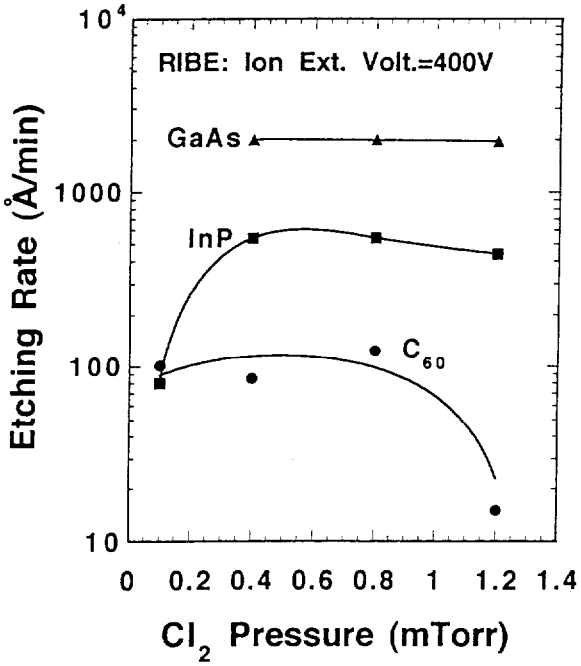

Fig. 7-4 Etching rate for C_{60}, InP and GaAs as a function of Cl_2 gas pressure. The Cl_2 ion extraction voltage: 400 V.

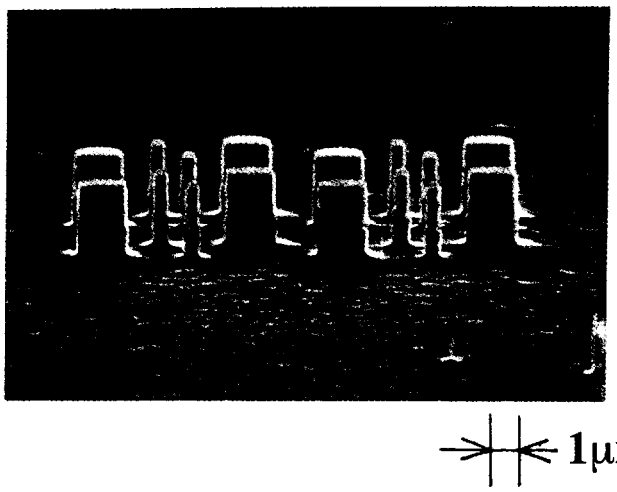

Fig. 7- 5 SEM photograph of the pillars etched by Cl_2-RIBE using C_{60} mask. The substrate is GaAs.

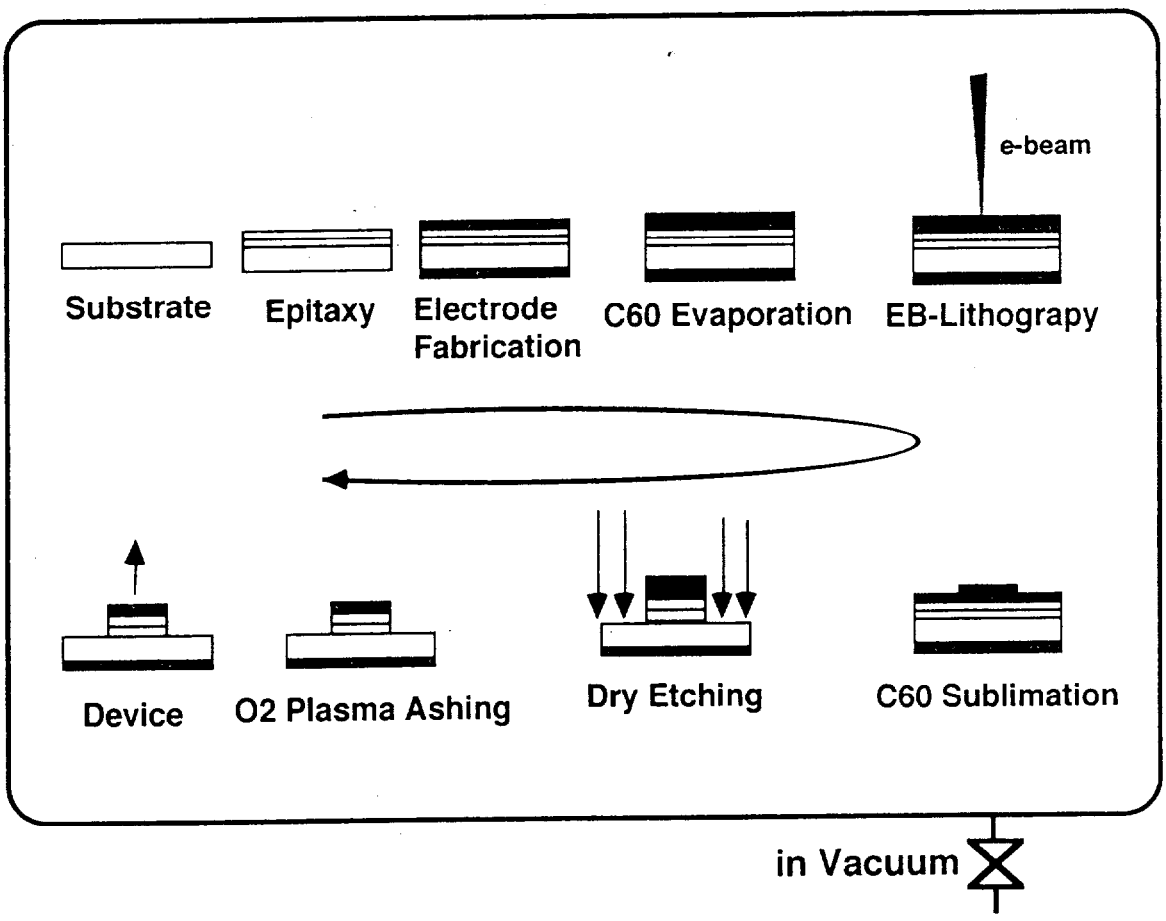

Fig. 7- 6 Device fabrication in vacuum by using e-beam irradiated C_{60} film as an etching mask

Chapter 8 Application of RIBE for Microoptoelectronic Devices

8.1 Introduction

In this chapter, application of RIBE and RIE for microoptoelectronic devices and prospects of dry etching are discussed.

First, I show the etching characteristics of dielectric materials of Si, SiO_2 and TiO_2 for fabrication of SiO_2/TiO_2 multilayer reflector of surface emitting laser. The dependence of the etching rate on the gas pressure and the effect of radicals is discussed. Circular fine patterns of SiO_2/TiO_2 multilayer $5\mu m$ in diameter is demonstrated. Secondary, I show that some lasing characteristics of index-guided InGaAs/GaAlAs VCSELs and the fabrication of VCSEL array with a native oxide confinement structure and some example for micro-optoelectronic devices fabricated by using Cl_2-RIBE technique.

8. 2 Microfabrication of SiO_2/TiO_2 Multilayer Reflector for Surface Emitting Lasers by Reactive Ion Etching (RIE)

Ultralow threshold operation of a surface emitting laser is expected by introducing a microcavity structure. In order to realize such a microcavity laser, fabrication of a highly reflective mirror is one of the key technologies. For this purpose, a dielectric multilayer reflector consisting of SiO_2/TiO_2 or Si/SiO_2 is used. In order to control the transverse mode of the microcavity laser as well as to inject current into the active layer, fabrication of a very small dielectric multilayer reflector is needed[1]. Also, a steep and smooth etching profile is required for highly reflective micromirror by eliminating diffraction and scattering losses in dielectric multilayers. In a wet chemical etching or plasma etching process, the etching shape is not necessarily smooth and steep because the etching rates of TiO_2 and Si are different from that of SiO_2. On the other hand, the etching shape in reactive ion etching is expected to be smooth and steep because of oriented etching by ion. Therefore, the reactive ion etching process is suitable for making a tiny structure of dielectric materials. The RIE has been widely used for the microfabrication process of semiconductor and dielectric materials, but its etching characteristics for multilayered dielectric materials have not been investigated in

detail. We have introduced a reactive ion etching (RIE) system to fabricate a micromultilayer reflector a few microns in diameter for surface emitting lasers. In this section, the etching characteristics of dielectric materials of Si, SiO_2 and TiO_2 are clarified. The dependence of the etching rate on the gas pressure and the effect of radicals have been discussed. Circular fine patterns of SiO_2/TiO_2 multilayer 5 μm in diameter were fabricated.

The RIE system has parallel planar electrodes as described in chapter 2. I used two kinds of materials for the etching table, i.e., Teflon (C_nF_{2n}) and quartz in this experiment. Dielectric films of Si, SiO_2 and TiO_2 are prepared by an electron beam evaporator.

Figure 8-1 shows the effect of the materials of an etching table on the etching rate of dielectric materials. It is obvious that the etching rate of Si decreases; however, the etching rate of SiO_2 and TiO_2 increases by replacing the quartz table by a Teflon table. The effect of the Teflon table refers to the absorption of free fluorine radicals generated by released C_nF_{2n} gas[2]. Generally, the oxides are etched by ion and Si is etched by radicals[3]. The result of the experiment clearly shows the effect of Teflon.

Figure 8-2 shows the relation between the etching rate and the etching pressure. It is obvious that Si has a different tendency from the oxides, SiO_2 and TiO_2. At the pressure of 0.1 Torr, the etching rates of the oxides become minimum and that of Si becomes maximum. This result indicates that the etching by free fluorine radicals is more active than by ions at 0.1Torr, since Si is etched by fluorine radicals, as shown in Fig. 9-1.

A 7-pair multilayer reflector consisting of quarter-wavelength layers of TiO_2 (880Å) and SiO_2 (1500Å) was prepared on a GaAs substrate by means of an electron beam evaporator. After Cr was evaporated on this multilayer, a circular mask pattern of Cr with a diameter of 5 μm was formed by a standard photolithographic process and etching by HCl. The thickness of Cr was 2000Å. The sample was etched by the RIE with a pressure of 0.12Torr and an rf power of 100W. In this condition, the GaAs substrate is slightly etched with the etch rate of 25Å per minute. The etching rate of Cr is 20Å/min. The etch rate ratio of Cr and the multilayer is about 60.

Figure 8-3 shows an SEM photograph of the etched sample of a dielectric multilayer by RIE. The total etching time of the multi-layer corresponds to the sum of that of each layer.

Five-micron-diameter circular array patterns were formed with good uniformity. The steep vertical shape can be obtained. The polarization controlled surface emitting laser using micro dielectric multilayer reflector was fabricated by RIE in 1991 as shown in Fig. 8-4[4].

8. 3 Application to Surface Emitting Lasers

The low-threshold mesa-etched vertical-cavity InGaAs/GaAs surface-emitting lasers was fabricated in 1995 (Fig. 8-5) [8]. Low threshold current of 0.33, 0.5 and 1.2mA were obtained for the 6, 10 and 20μm diameter devices. Figure 8-6 shows a schematic diagram of a fabricated InGaAs/GaAlAs VCSEL with an oxide confinement structure. The epitaxial layer was grown by low-pressure MOCVD at 700°C on a GaAs (100) substrate. The active region consists of three 80Å thick strained $In_{0.2}Ga_{0.8}As$ quantum wells sandwiched by 100Å thick GaAs barriers. The active region is sandwiched by $Al_{0.4}Ga_{0.6}As$ layer which form separate confinement heterostructure(SCH) for the vertical carrier confinement. Both the GaAs/AlAs DBR's consisting of periodic quarter wavelength (1/4) stacks provide high reflective mirrors, resulting in low threshold current density. The top (Zn-doped) mirror has 20 periods with 180Å linearly-graded layers at GaAs/AlAs heterojunctions for low series resistances. The bottom (Se-doped) mirror with GaAs/AlAs abrupt interfaces has 22.5 periods. This device has been introduced modulation doping with high and low carrier concentrations of $3x10^{18}cm^{-3}$ in AlAs and $1x10^{18}cm^{-3}$ in GaAs layers at both side mirrors, respectively. Circular mesas with 20 and 40μm ϕ active region diameters were formed by Cl_2 based RIBE. The employed process for oxidizing AlAs layers of DBR is shown as follows. After RIBE process, the sample were annealed at 400°C in nitrogen gas ambient bubbled through 80°C water. The generated light propagates along an index-guide that consists of GaAs/AlAs DBR core and a GaAs/Al_xO_y cladding [6].

Fig. 8-7 shows the light output versus current characteristics for several oxidized 20μm ϕ core devices. A threshold current of 70μA was achieved [7]. Because the corresponding threshold current density is as small as $360A/cm^2$, further reduction of threshold current will be expected.

8. 4 Fabrication of VCSEL array using Dry Etching

The advantage of VCSELs is as follows:

(1) A large number of laser chip can be fully monolithically processed.

(2) The probe test can be performed before separation into chip.

(3) A large-scale 2D laser array can be formed, and so on.

In this section, fabrication of VCSEL 2-D array is described.

I have fabricated VCSEL array to realize devices with these advantages. The sample was grown by MOCVD on the n-type GaAs substrate, consisting of one wavelength thick AlGaAs spacer layer with a GaAs single quantum well (SQW), as well as upper and lower DBRs as shown in section 8. 3. The upper and lower DBRs consist of 18 pairs and 22 pairs of AlAs/AlGaAs quarter wave stacks, respectively. Then a circular EB resist mask array was obtained by electron beam lithography. The diameters of the masks were distributed from 5μm to 30μm. A pillar-type microcavity array was fabricated by RIBE.

Next, the AlAs layer of DBR was oxidized as shown in section 8. 3. Then, the oxidized mesas were covered with polyimid and patterned the window for probe contact by conventional photolithography technique. After opening the contact window, p-side and n-side electrode were evaporated, respectively. Next, an electron beam (EB) resist was coated on the upper mesas (p-side). Then, the p-side electrode pads were fabricated by EB lithography and Ar-IBE. The size of each electrode pad is 250μm x 250μm. The pitch of VCSEL is 250μm. The n-side light output holes are fabricated by conventional photolithography technique. Each electrode can be contacted independently by a probe. So that, Each VCSEL can be operated without separating the wafer. Figure 8-8 shows the photograph of p-side and n-side of VCSEL array fabricated as above mentioned. In addition, the micro cavity array of GaInAsP/InP was fabricated by using Cl_2-RIBE technique as shown in Fig. 8-9.

8. 5 Application to Micro-optoelectronic Devices

The RIBE process have contributed to fabrication of many micro-optoelectronic devices. I would like to show some example for micro-optoelectronic devices fabricated by using Cl_2-RIBE technique. The micro-arc-ring (MARC) lasers, which consists of one concave

mirror and two plane mirrors was fabricated in 1994 (Fig. 8-10) [9]. The pulsed threshold was 50mA for 0.98mm GaInAs/GaAs QW devices with the size of 100μm. The reflectivity of the etched reflector was estimated ~74% from the threshold current density. The horizontal short cavity DBR Laser was fabricated in 1994 (Fig. 8-11)[10]. The InGaAs/GaAs strained quantum well lasers with etched micro-corner reflectors was fabricated in 1995 (Fig. 8-12)[11]. The threshold current density was ~800A/cm^2 for 100μm long GaInAs/GaAs QW devices. The reflectivity of a 4μm wide corner reflector could be estimated ~65% from threshold current density. The miniature semiconductor optical power splitter with submicrometer wide aperture was fabricated in 1996 (Fig. 8-13) [12]. This device was a GaInAs/GaAs Fabry-Perot cavity laser including the power splitter inside the laser cavity. A uniform power splitting over 20 output waveguides was obtained with the 100μm long free-space region.

8. 6 Summary

In this chapter, application of RIBE and RIE for microoptoelectronic devices and prospects of dry etching are discussed.

(1) Some etching characteristics of dielectric materials such as SiO_2, TiO_2, and Si were examined for the purpose of micro-fabrication of a multilayer reflector.

(2) As a preliminary experiment, the pressure dependence of the etching rate and the effect of the material of the etching table were clarified.

(3) A tiny circular structure of SiO_2/TiO_2 multilayer reflector with a diameter of 5 μm was fabricated by RIE. By optimizing the etching condition, a microreflector of less than a few microns will be obtained.

(4) I show that some lasing characteristics of index-guided InGaAs/GaAlAs vertical-cavity surface-emitting lasers (VCSELs) with a native oxide confinement structure, which provided a low threshold current of 70mA, are presented.

(5) I fabricated pillar-type microcavity 2-D array VCSEL using oxidized DBR and separated electrodes. The fabricated device can be performed the probe test without separating the wafer.

(6) The ECR Cl2-RIBE technique contributed to fabrication of many micro-optoelectronic

devices, such as MARC laser, horizontal short cavity DBR laser and optical power splitter etc.

References

[1]M. Shimizu, F. koyama and K. Iga, "BPM Analysis for Transverse Mode Stabilization of Surface Emitting Laser," *Dig. 3rd Optoelectronic Conf.,* 13B1-5, pp. 196-197.

[2] S. Matsuo and Y. Takehara, "Preferential SiO2 Etching on Si Substrate by Plasma Reactive Sputter Etching," *Jpn. J. Appl. Phys,.* 16, pp. 175-176.

[3] B. Chapman, "Glow Discharge Process Sputtering and Plasma Etching," *John Wiley & Sons, New York,* 1980.

[4]M. Shimizu, T. Mukaihara, F. Koyama and K. Iga, "Polarization Control for Surface Emitting Lasers," *Electron. Lett.*, vol. 27, no. 12, pp. 1067-1069, 1991.

[5]M. H. MacDougal, H. Zhao, P. D. Dapkus, M. Ziari and W. H. Steier, "Wide-bandwidth distributed Bragg reflectors using oxide/GaAs multilayers," *Electron. Lett.*, vol. 30, pp. 1147-1149, 1994.

[6]Y. Hayshi, T. Mukaihara, N. Hatori, N. Ohnoki, A. Matsutani, F. Koyama and K. Iga, "A record threshold InGaAs/GaAlAs vertical cavity surface emitting laser," in *Conf. Dig. Quantum Optoelectron.*, PDP2, 1995.

[7]T. Mukaihara, Y. Hayashi, N. Hatori, N. Ohnoki, A. Matsutani, F. Koyma, K. Iga, "Low-threshold Mesa-Etched Vertical-Cavity InGaAs/GaAs Surface-Emitting Lasers Grown by MOCVD," *Electron. Lett.,* vol. 31, pp. 647-648, 1995.

[8]T. Tadokoro, F. Koyama and K. Iga, "Comparison of Luminescence from InP Processed by Reactive Ion BeamEtching," *Jpn. J. Appl. Phys,.* 29, pp. 242-243, 1990.

[9]S. Mitsugi, J. Katoh, F, Koyama, A. Matsutani, T. Mukaihara and K. Iga, "Design and Lasing Operation of Micro-Arc-Ring Lasers," *Jpn. J. Appl. Phys.*, vol. 33, pp. 6201-6202, 1994.

[10]M. Hamasaki, T. Baba, A. Yamada, N. Watanabe, A. Matsutani, F. Koyama and K. Iga, "Horizontal Short Cavity DBR Laser by RIBE Technique," *55th Autumn Meeting of Jpn. Soc. Appl. Phys.*, 21p-S-5, 1994.

[11]J. Katoh, F. Koyama, A. Matsutani, T. Mukaihara and K. Iga, "InGaAs/GaAs Strained Quantum Well Lasers with Etched Micro-Corner Reflectors," *1995 Int. Conf. on Solid State Device and Materials, Yokohama,* S-I-10-2, 1995.

[12]K. Suzuki, F. Koyama, A. Matsutani, J. Kato, T. Mukaihara and K. Iga, "Miniature semiconductor optical powere spilitters with submicrometer wide aperture", *Electron. Lett.*, vol. 32, no. 7, pp. 654-655, 1996.

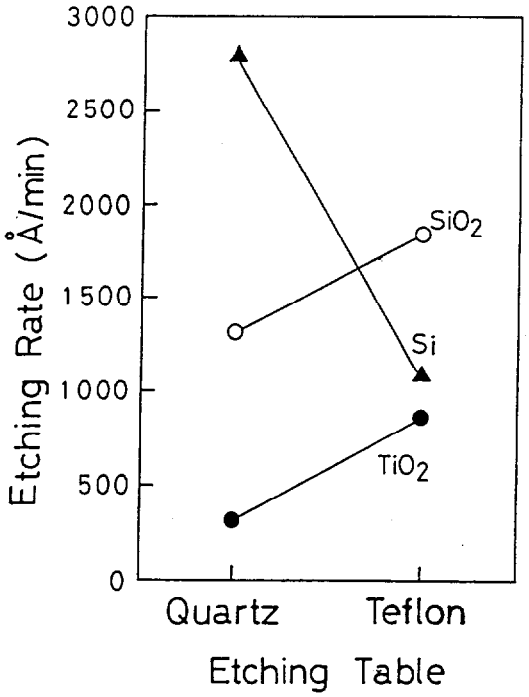

Fig. 8-1 Relation between material of etching table and etching rate. Power: 100W, Etching gas: CF_4, Pressure: 0.12Torr.

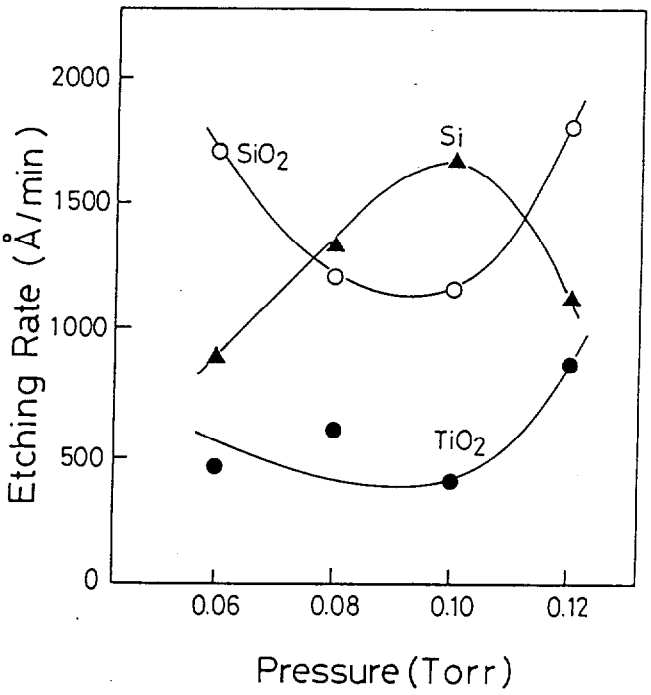

Fig. 8-2 Relation between etching pressure and etching rate of Si, SiO_2, TiO_2. Power: 100W, Etching Table: Teflon, Gas: CF_4.

Fig. 8-3 SEM photograph of SiO_2/TiO_2 (7pair,5 μmϕ) patterns etched by RIE system. Power: 100W, Etching gas: CF_4, Pressure: 0.12Torr.

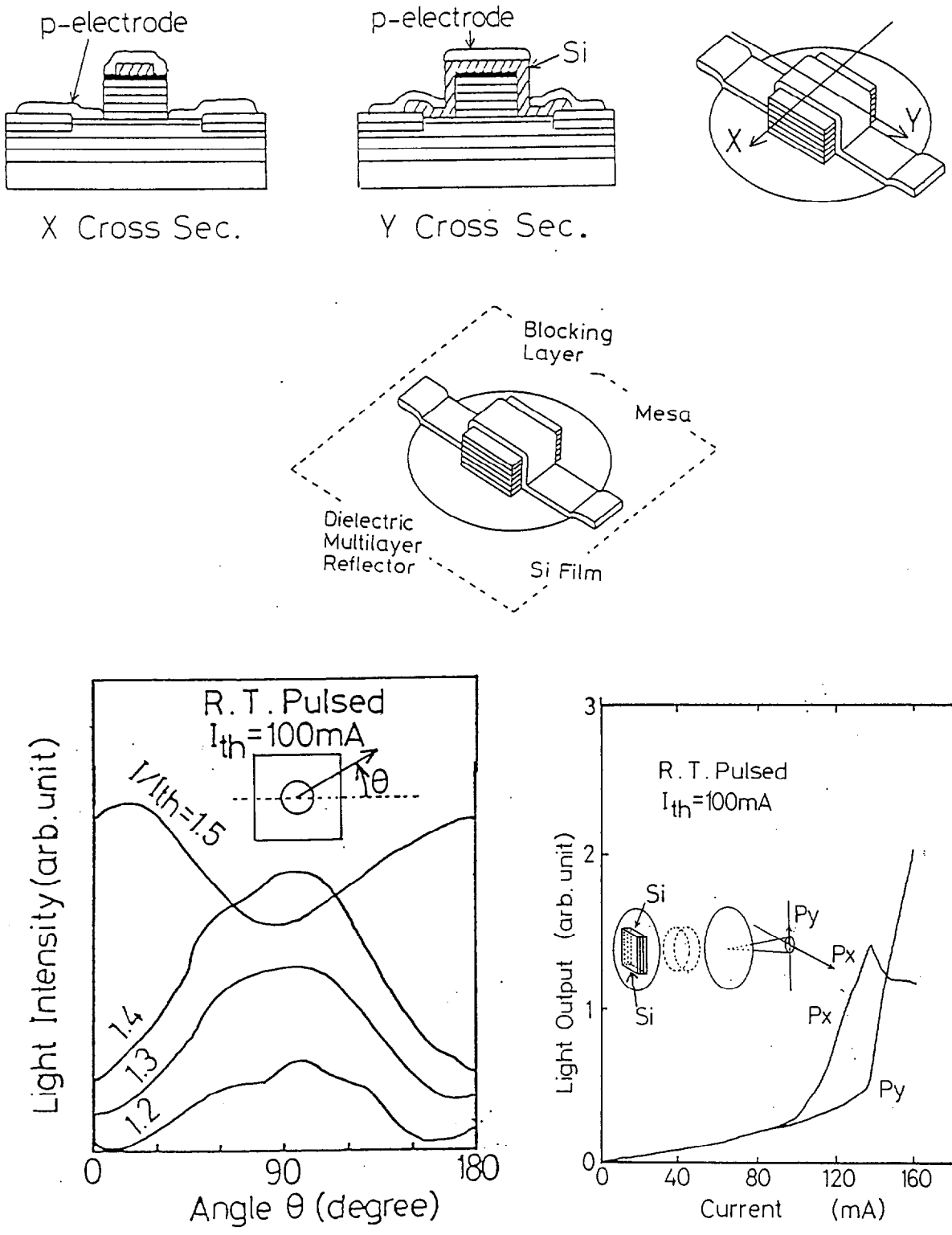

Fig. 8-4 The polarization controlled surface emitting laser using micro dielectric multilayer reflector fabricated by RIE

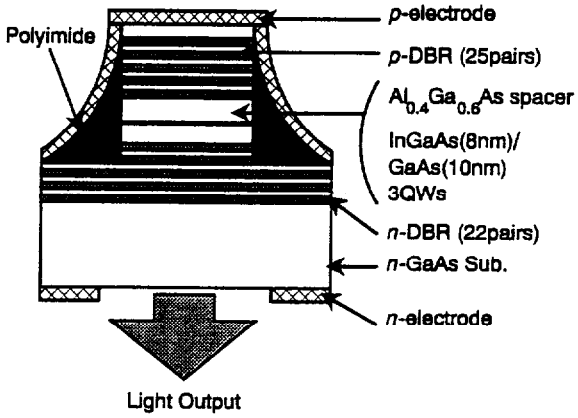

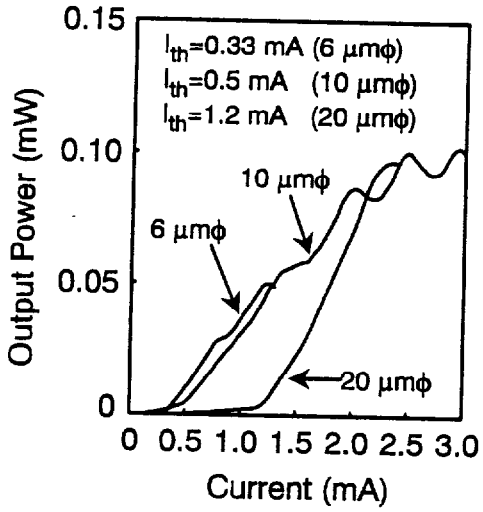

Fig. 8-5 Low-threshold mesa-etched vertical-cavity InGaAs/GaAs surface-emitting lasers.

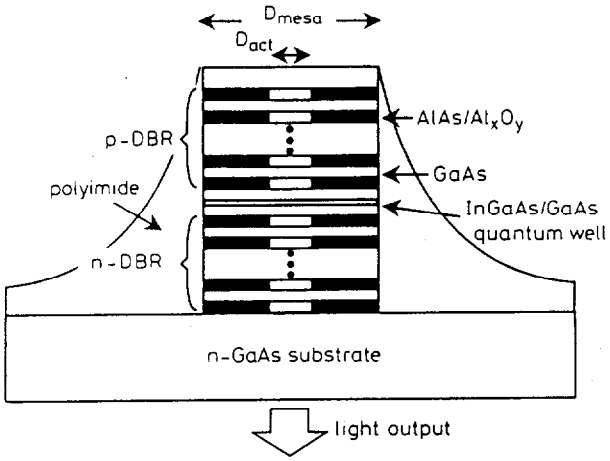

Fig. 8-6 A schematic view of a fabricated InGaAs/GaAlAs VCSEL with a oxide confinement structure.

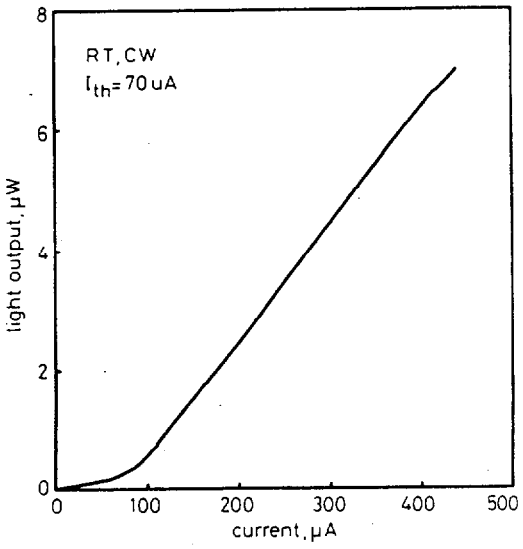

Fig. 8-7 *I-L* characteristics for several oxidized 5μmϕ core devices.

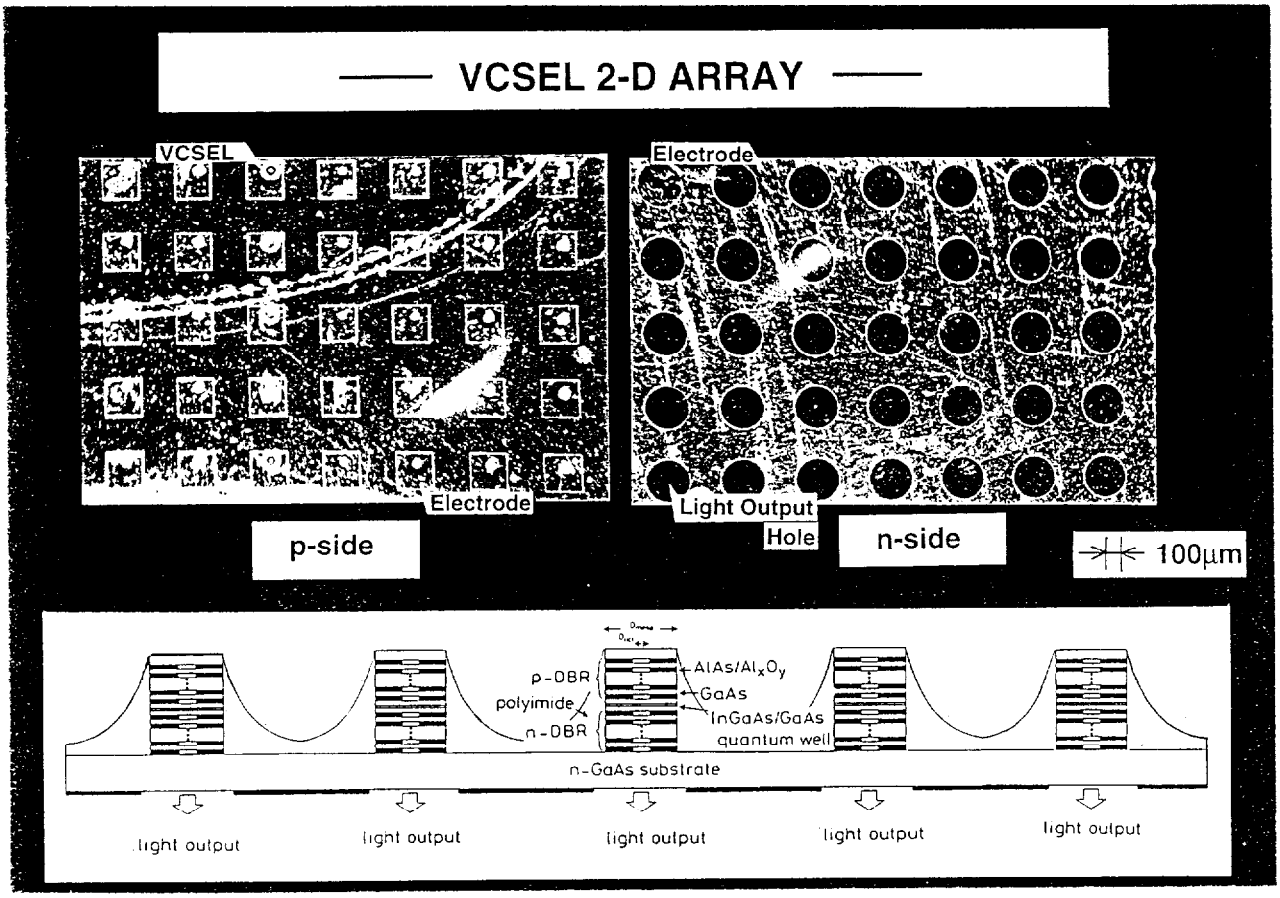

Fig. 8-8 Photograph of p-side and n-side of VCSEL array.

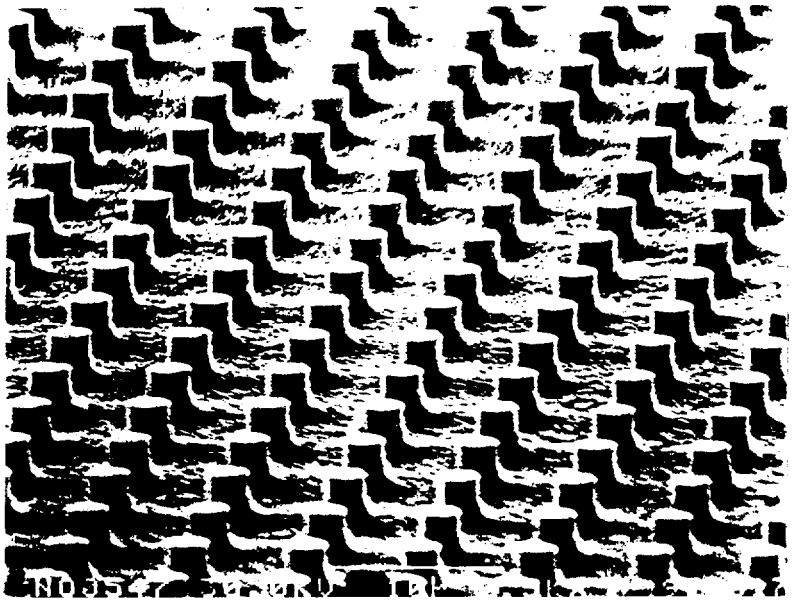

Fig. 8-9 Micro cavity array of GaInAsP/InP was fabricated by using Cl_2-RIBE technique.

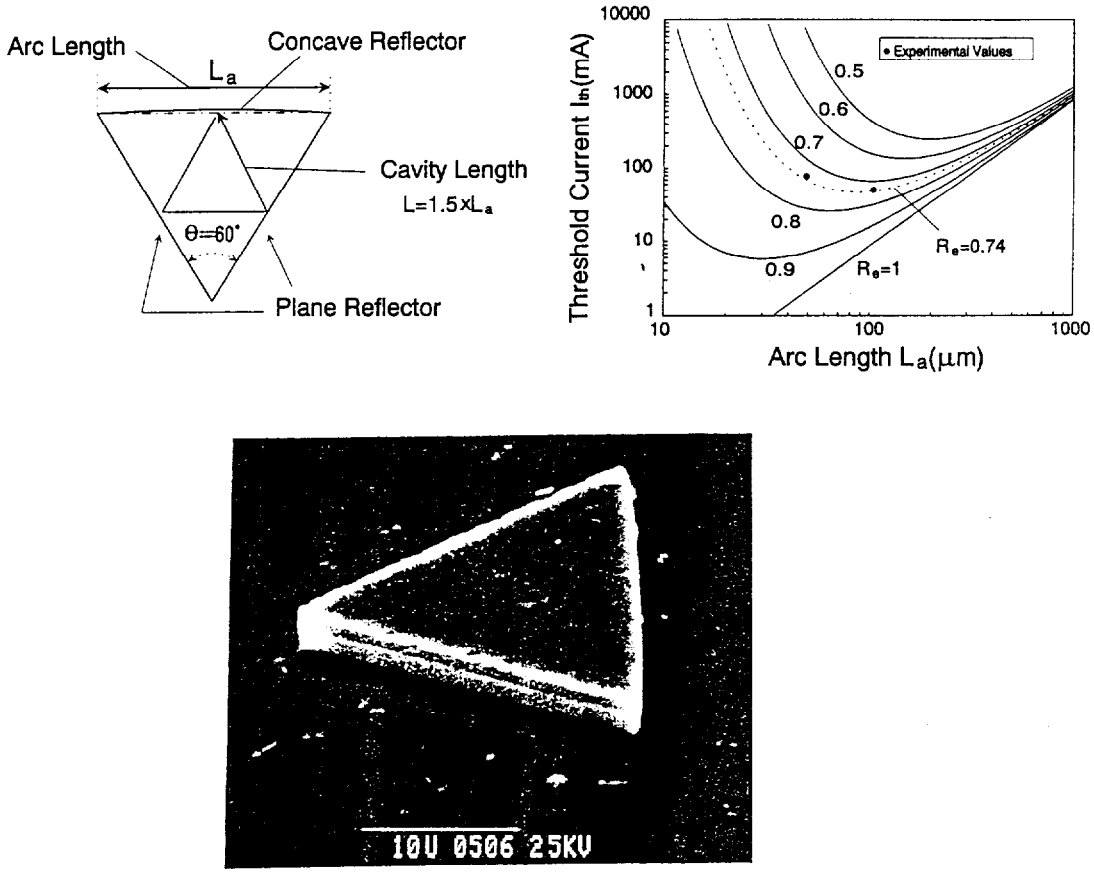

Fig. 8-10 Micro-arc-ring (MARC) lasers, which consists of one concave mirror and two plane mirrors [9].

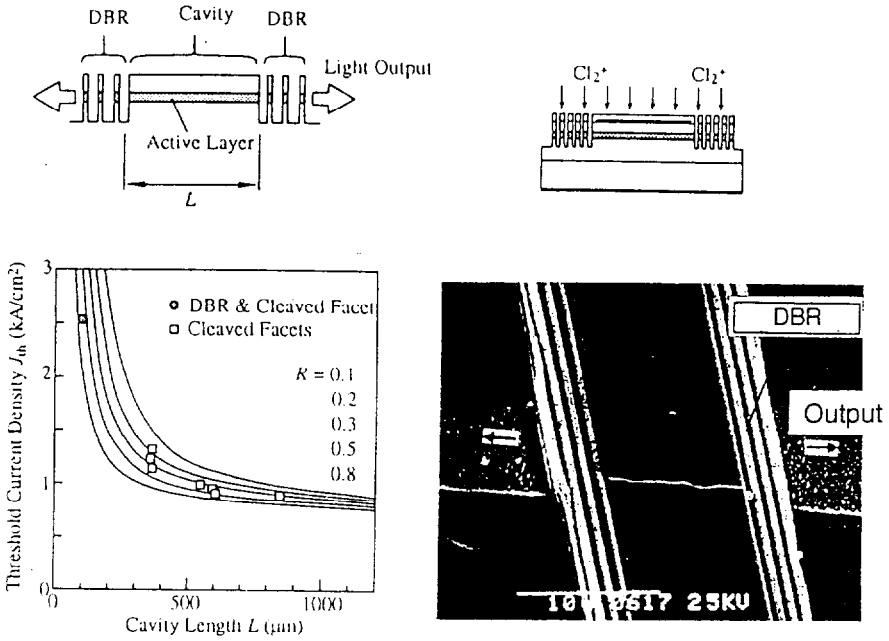

Fig. 8-11 Horizontal short cavity DBR Laser [10].

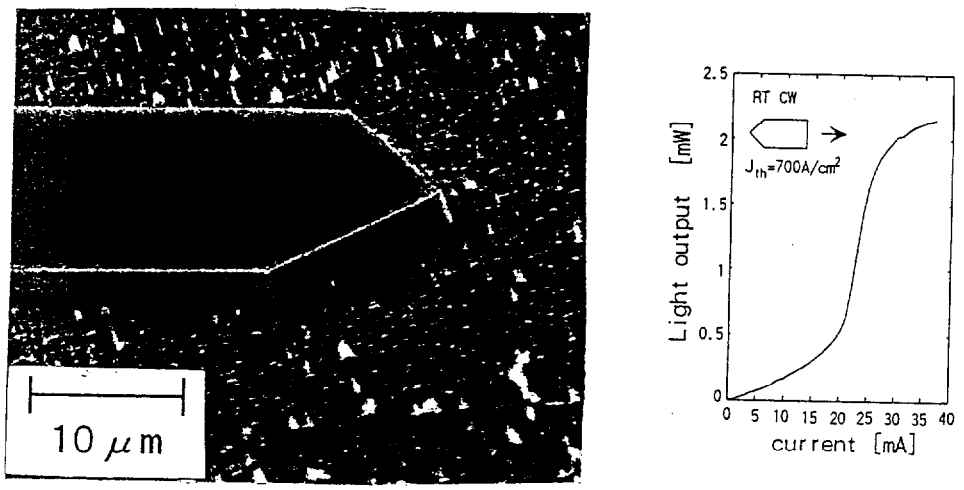

Fig. 8-12 InGaAs/GaAs strained quantum well lasers with etched micro-corner reflectors [11].

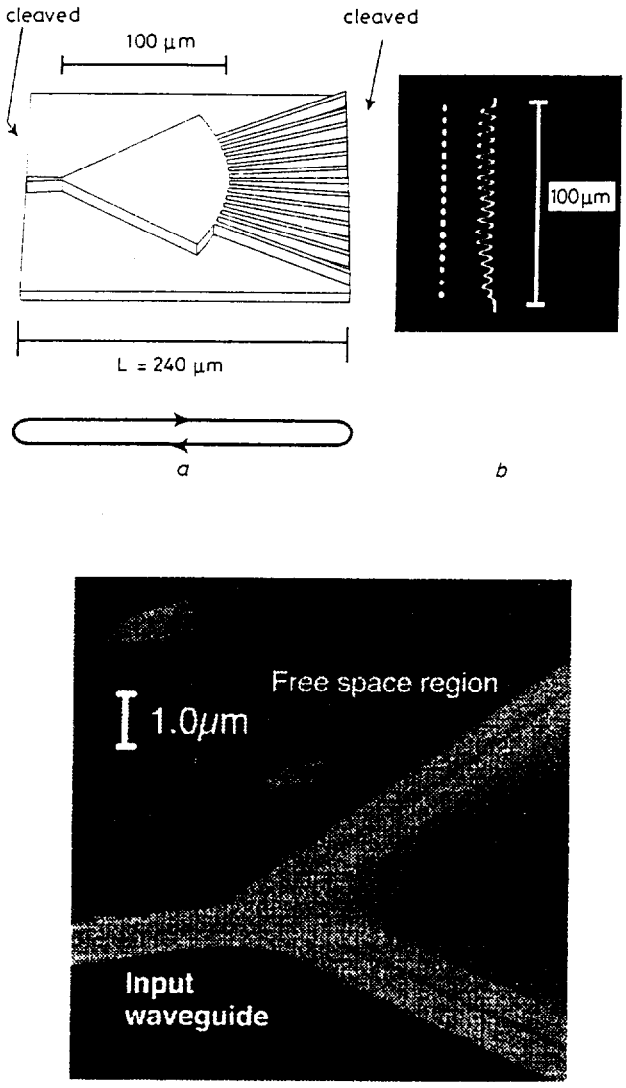

Fig. 8-13 Miniature semiconductor optical power splitter with submicrometer wide aperture [12].

Chapter 9 Conclusion

9.1 Prospects of Dry Etching

In this section, the prospects of dry etching process are discussed. Now, the dry etching technology has some important issues as follows.

(1) Development of large diameter ion source.

(2) Damage-free etching process.

(3) Ultra-fine etching profile control.

I would like to describe my opinion to solve these problems as follows.

(1) Development of large diameter ion source

Recently, the electronics technologies require 0.1μm-rule as precise device fabrications. Also, those require uniformity in device fabrication for 6" wafers. Therefore, large diameter plasma is required as an ion source for dry etching process. Generally speaking, it is difficult to make a large diameter ECR plasma ion source. Because, it is difficult to make an uniform magnetic field in large area. While it is easy to make a large diameter plasma source in conductive coupled plasma (CCP), such as RIE, the induced damage by this technique is larger than that of ECR. In these days, the development for large diameter plasma sources such as inductive coupled plasma (ICP), hericon wave plasma (HWP) and UHF plasma is starting. These new techniques will be expected as a large diameter and high density plasma ion source.

(2) Damage-free etching process

In future, sub half-micron device fabrication process requires damage-free etching or reducing induced damage process by dry etching. It is well-known that the ion energy as small as 20eV does not exert induced damage on semiconductor wafers. Also, in high ion density plasma, the induced damage is very small. Therefore, the future dry etching process for 0.1μm-rule requires the high density plasma ion source and lower ion energy. The ICP and/or HWP are expected as a plasma source to satisfy the requirements above mentioned.

These plasma sources can obtain the plasma density as high as an ECR plasma and the plasma pressure as low as an ECR plasma source. So, the development of these techniques without induced damages is expected in future. Especially, the ICP source is non-magnetic field, and the large diameter plasma can be generated easily.

(3)Ultra-fine etching profile control

The etching profile control is one of the most important issue for dry etching process in sub-half-micron fabrication. The etching profile is often not straight due to charging on etching mask, like SiO_2, photoresist and so on. In ECR plasma source, it is important to obtain uniform the magnetic field. In other words, it is important to reduce the gradient of voltage, and to control the distribution of ion energy. However, only the control of ion energy distribution may not enable perfect profile control. Neutral radical is also contribute to dry etching process. Usually the neutral radical is independent of the applied extraction voltage. And the radical has isotropic trajectory due to only its thermal motion. Therefore, it is important to find a manner to control the radical and ion flux at the same time. In addition, the negative ion will be used extensively for reducing of mask charging.

I believe that, in future, the dry etching technique will be more important process in various fields as described in section 1.

9. 2 Conclusion

In order to establish the dry etching process for the fabrication of micro-structure optoelectronic devices, I have carried out my doctoral study with the following purposes; (1) To establish microfabrication of multilayers for VCSELs, (2) To characterize and to avoid RIE and RIBE induced damage, (3) To evaluate quantitatively etched sidewall roughness and to improve etching profiles, including the investigation of new suitable mask material, (4) To characterize process plasma in RIBE, (5) To apply the RIBE for the fabrication of VCSELs and microstructure optoelectronic devices. The results obtained in this work are summarized as follows:

(1) Microfabrication of multilayers for VCSELs

I have established GaInAsP/InP RIBE dry etching processes for forming microcavity VCSELs. I have examined Cl_2-RIBE for GaInAsP/InP multilayers for the first time, in order to fabricate a microresonator composed of semiconductor multilayers (Chap. 2).

(a) The straight side wall of the GaInAsP/InP multilayer was obtained.

(b) The loading effect derived from the high-density pattern was observed.

(2) Characterization and avoidance of RIBE and RIE induced damage

I investigated the sidewall and bottom surface damage induced by Cl_2-RIBE and RIE (Chap. 3).

(a) The induced damage of processed InP was studied by C-V measurement. The damaged layer thickness was estimated to be $\sim$1000Å.

(b) The ion-incident-angle dependence of the sidewall damage was presented, showing that the sidewall damage was <200Å with an ion extraction voltage of 400V.

(c) I carried out for the first time the depth measurement of the sidewall damage from the direct PL measurement of the etched sidewall of a GaInAsP/InP DH wafer after RIBE. I found that the PL intensity of the etched sidewall decreased considerably. In order to clarify the damage depth of the etched sidewall, I measured the PL intensity with etching the sidewall slowly. The damage depth of the etched sidewall is estimated to be 20-30Å. The sidewall damage is the same in the region of 300V-500V.

(d) In order to eliminate the induced damage, I proposed a novel two-step RIBE.

(e) The bottom surface damage of a wafer induced by RIE was investigated by PL study. The active layer in the DH wafer was not affected by the RIE process. Also, the damage of the cladding layer can be relaxed by post thermal annealing.

(3) Quantitative evaluation of etched sidewall roughness, improvements of etching profile and investigation of novel mask material

The sidewall roughness of InP etched by RIBE was measured using the electron probe surface roughness analyzer for the first time (Chap. 4). I carried out in-situ measurements of the sample temperature during RIBE by using a radiation thermometer for the first time (Chap. 5). I have characterized the C_{60} film irradiated with an e-beam as a dry-etching mask for Cl_2-RIBE (Chap. 7).

(a) The minimum value of the sidewall roughness average was 1nm. The peak to peak roughness was 5.8nm.

(b) I pointed out that ion extraction voltage should be reduced and gas pressure should be increased for a smooth InP etching, while maintaining anisotropic etching profiles.

(c) It was found that the surface temperature is increased by the ion irradiation. The surface temperature was increased by about 250K with an ion extraction voltage of 400V for 15 min. The increase in sample temperature considerably affects on the etching profile.

(d) I have proposed a novel multistep RIBE for the improvement of etching profiles. I found that the origin of the side-etching near the bottom of the mesa is the rise of the sample surface temperature due to the ion irradiation.

(e) The proposed multistep RIBE process is also effective for smoothing of micro-needles on an etched surface of an InP substrate. I found these micro-needles on the etched surface are reduced by the multistep RIBE without changing etched profile of mesas.

(f) The sensitivity of C_{60} as a negative type resist was $\sim$25 mC/cm^2 for MCB. The maximum etch rate ratio of C_{60} for GaAs and InP were 20 and 5, respectively. In addition, I have succeeded in fabricating micropillars in GaAs with the C_{60} mask. I proposed that the total device fabrication processes from epitaxy to device fabrications can be completed in

vacuum using the C_{60} mask.

(4) Plasma Characterization in RIBE

I have clarified the aspects of ion energy and radical density of chlorine-based RIBE and CAIBE systems (Chap. 6). I observed that neutral Cl_2 is ionized by Ar^+ in the CAIBE process, and the Cl^+ energy peak appears in the energy range of 50-70 eV and this Cl^+ energy peak increases with an increase of Ar^+ energy. I also observed that the number of excited state chlorine molecules in the CAIBE process was smaller than that in the RIBE process.

(5) Application to VCSELs or microstructure optoelectronic devices

Applications of RIBE for microoptoelectronic devices and prospects of dry etching are discussed (Chap. 8). We realized record low threshold index-guided InGaAs/GaAlAs VCSELs with a native oxide confinement structure by using the established etching technique. In addition, I fabricated VCSEL 2-D array with independent electrodes.

To conclude this study, I believe that, in future, the dry etching technique will be more important process in various fields. The result of this study will contribute to the development of future optoelectronic devices.

Acknowledgments

I would like to gratefully acknowledge Professor K. Iga and Associate Professor F. Koyama, the advisor of my work at Tokyo Institute of Technology, for their general guidance and support.

I would like to acknowledge Prof. S. Arai, Prof. J. Hanna, Prof. H. Munekata, Associate Prof. K. Tsutsui for their advice and suggestions to this work.

I wish to acknowledge Prof. Emeritus Y. Suematsu of Tokyo Institute of Technology, Prof. Y. Kokubun, Associate Professor T. Baba of Yokohama National University, Associate Prof. K. Moriki of Musashi Institute of Technology, Prof. H. Kawanishi, Lecturer T. Honda of Kohgakuin University, Prof. K. Kishino of Sohia University, Prof. T. Kambayashi of Nagaoka Institute of Technology, Prof. M. Asada and Associate Prof. Y. Miyamoto of Tokyo Institute of Technology for their technical advice and suggestion.

I gratefully appreciate Mr. Sakaguchi, Lecturer T. Miyamoto for their helpful advice and discussions and technical support. I also appreciate Ms. F. Matsunaga, research member of Iga and Koyama group and faculty members of P&I laboratory for their hospitality and assistance.

List of Publications and Presentations

A. Papers

(1) A. Matsutani, F. Koyama and K. Iga, "Microfabrication of Dielectric Multilayer Reflector by Reactive Ion Etching and Characterization of Induced Wafer Damage," *Jpn. J. Appl. Phys.*, vol.30, pp. 428-429, 1991.

(1)' A. Matsutani, F. Koyama and K. Iga, "Micro-Fabrication of Dielectric Multilayer Reflector by Reactive Ion Etching," *Bulletin of Research Laboratory of Machinery and Electronics (T. I. T.)*, No. 65, pp. 9-12, 1990.

(2) A. Matsutani, F. Koyama and K. Iga, "Reactive Ion Beam Etch of GaInAsP/InP Multilayer and Removal of Damage Layer by Two Step RIBE," *Jpn. J. Appl. Phys.*, vol. 30, pp. 2123-2126, 1991.

(3) A. Matsutani, F. Koyama and K. Iga, "Characterization of Sidewall Damage Induced by Reactive Ion Beam Etching," *Jpn. J. Appl. Phys.*, vol. 31, pp. 1541-1544, 1992.

(4) S. Mitsugi, J. Katoh, F, Koyama, A. Matsutani, T. Mukaihara and K. Iga, "Design and Lasing Operation of Micro-Arc-Ring Lasers," *Jpn. J. Appl. Phys.*, vol. 33, pp. 6201-6202, 1994.

(5) A. Matsutani, F. Koyama and K. Iga, "Measurement of Sidewall Roughness of InP Etched by Reactive Ion Beam Etching," *Jpn. J. Appl. Phys.*, vol. 33, pp. 6737-6738, 1994.

(6) A. Matsutani, F. Koyama and K. Iga, "Three-Dimensional Electron Probe Roughness Analysis of InP Sidewall Processed by Reactive Ion Beam Etching," *Appl. Phys. Lett..*, vol. 66, pp. 64-66, 1995.

(7) S. Mitsugi, F. Koyama, J. Katoh, A. Matsutani, T. Mukaihara and K. Iga, "GaInAs/GaAs Micro-Arc Ring Semiconductor Laser," *Jpn. J. Appl. Phys.* vol. 34, pp. 1265-1269, 1995.

(8) A. Matsutani, F. Koyama and K. Iga, "Surface Temperature Increase in Reactive Ion Beam
Etch and Improvement of Profiles by Multistep Etching," *Jpn. J. Appl. Phys.*, vol. 34, pp. 2053-2054, 1995.

(9) Y. Hayashi, T. Mukaihara, N. Hatori, N. Ohnoki, A. Matsutani, F. Koyma, K. Iga, "Record Low Threshold Index-Guided InGaAs/GaAlAs Vertical-Cavity Surface-Emitting Laser with a Native Oxide Confinement Structure," *Electron. Lett.*, vol. 31, pp.560-562, 1995.

(10) T. Mukaihara, Y. Hayashi, N. Hatori, N. Ohnoki, A. Matsutani, F. Koyma, K. Iga, "Low-threshold Mesa-Etched Vertical-Cavity InGaAs/GaAs Surface-Emitting Lasers Grown by MOCVD," *Electron. Lett.*, vol. 31, pp. 647-648, 1995.

(11) Y. Hayashi, T. Mukaihara, N. Hatori, N. Ohnoki, A. Matsutani, F. Koyma, K. Iga, "Low-threshold Mesa-Etched Vertical-Cavity InGaAs/GaAs Surface-Emitting Lasers Grown by MOCVD," *IEEE Photon. Technol.. Lett.*, vol. 7, pp. 1234-1236, 1995.

(12) K. Suzuki, F. Koyama, A. Matsutani, J. Kato, T. Mukaihara and K. Iga, "Miniature

semiconductor optical powere spilitters with submicrometer wide aperture", *Electron. Lett.*, vol. 32, no. 7, pp. 654-655, 1996.

(13) T. Mukaihara, N. Hatori, N. Ohnoki, A. Mizutani, A. Matsutani, F. Koyama and K. Iga, "Fabrication Processes for low threshold InGaAs vertical-cavity surface emitting laseres", *Physica B*, no. 227, pp. 400-403, 1996.

(14) N. Hatori, T. Mukaihara, M. Abe, N. Ohnoki, A. Mizutani, A. Matsutani, F. Koyama and K. Iga, "Characterization of residual stress in active region due to AlAs Native oxide of vertical-cavity surface emitting laseres", *Jpn. J. Appl. Phys.*, vol. 35, no.12A, pp. 6108-6109, 1996.

(15) K. Saotome, A. Matsutani, T. Shirasawa, M. Mori, T. Honda, T.Sakaguchi, F. Koyama, and K. Iga, "Reactive ion beam etching of GaN grown by MOVPE," *Mat. Res. Soc. Symp. Proc.* vol.449, pp.1029-1033,1997.

(16) N. Hatori, T. Mukaihara, N. Ohnoki, A. Mizutani, M. Abe, A. Matsutani, F. Koyama, and K. Iga, "InGaAs/GaAs vertical-cavity surface-emitting lasers with AlAs selective oxide layers," *IEICE C-I*, vol. J80-C-I, no. 9, pp. 407-413, September 1997.

(17) A. Matsutani, F. Koyama and K. Iga, "Plasma Characterization in Chlorine-Based Reactive Ion Beam Etching and Chemically Assisted Ion Beam Etching," *Jpn. J. Appl. Phys.*, vol. 37, pp. 2747-2751, 1998.

(18) A. Matsutani, F. Koyama and K. Iga, "C_{60} Resist Mask of Electron Beam Lithography for Chlorine-Based Reactive Ion Beam Etching," *Jpn. J. Appl. Phys.*, vol. 37, pp.4211-4212, 1998.

B. International Conferences

(1) A. Matsutani, F. Koyama and K. Iga, "Micro Dry Etching Process for Vertical Surface Emitting Lasers," *Second International Meeting Advanced Processing and Characterization Technologies (APCT'91)* , T2, Florida, 1991.

(2) K. Iga, F. Koyama and A. Matsutani, "RIBE and RIE for Micro-Cavity Surface Emitting Lasers - Technology & Damage," *LEOS'91 Summer Topical Meetings, Newport Beach, CA* , ThC. 1, 1991

(3) A. Matsutani, F. Koyama and K. Iga, "Measurement of Sidewall Roughness of InP Etched by Reactive Ion Beam Etching," *LEOS'94 Summer Topical Meetings, Lake Tahoe, NV*, T1. 3, 1994.

(4) S. Mitsugi, J. Katoh, F. Koyama, A. Matsutani, T. Mukaihara and K. Iga, "GaInAs/GaAs Micro-Arc Ring Semiconductor Laser," *1994 Int. Conf. on Solid State Device and Materials, Yokohama,* S-I-10-2, 1994.

(5) F. Koyama, S. Mitsugi, J. Katoh, A. Matsutani, K. Suzuki and K. Iga, "RIBE Micro-Fabrication of Semiconductor Photonic Devices for Micro-Photonic Integrated Circuits," *IEEE Laser and Electro-Optics 94, Boston, I-O-5.2,* 1994.

(6) Y. Hayashi, T. Mukaihara, N. Hatori, N. Ohnoki, A. Matsutani, F. Koyama, and K. Iga, "A record low threshold InGaAs/GaAlAs vertical-cavity surface-emitting laser," *Quantum Optoelectronics Conference*, No. PDP2, *Dana Point*, March 1995.

(7) T. Mukaihara, Y. Hayashi, N. Hatori, N. Ohnoki, A. Matsutani, F. Koyama and K. Iga,

"0.33mA threshold InGaAs/GaAs Vertical-Cavity Surface-Emitting Laser Grown by MOCVD," *CLEO*, 1995.

(8) F. Koyama, K. Suzuki, A. Matsutani, J. Kato, T. Mukaihara and K. Iga, "Active semiconductor power splitters with sub-micron wide input aperture," *Proc. of 10th International Conference on Integrated Optics and Optical Fiber Communication,* No. ThD2-5, pp. 106-107, June 1995.

(9) J. Katoh, F. Koyama, A. Matsutani, T. Mukaihara and K. Iga, "InGaAs/GaAs Strained Quantum Well Lasers with Etched Micro-Corner Reflectors," *1995 Int. Conf. on Solid State Device and Materials, Yokohama,* S-I-10-2, 1995.

(10) A. Matsutani, F. Koyama and K. Iga, "Suppression of Side-Etch and Smoothing of Micro-Needle on Etched Surface by Multistep RIBE," *LEOS'95 Annual Meeting, San Francisco, CA*, OMP 5. 2, 1995.

(11) F. Koyama, A. Matsutani and K. Iga, "Etched Facet Semiconductor Resonators Fabricated by Reactive Ion Beam Etching for Micro-Photonic Integrated Circuits," *LEOS'95 Annual Meeting, Sanfrancisco, CA*, OMP 5. 3, 1995.

(12) T, Mukahihara, N. Hatori, N. Ohnoki, A. Mizutani, M.Abe, A. Matsutani, F. Koyama and K. Iga, "Fabrication process for low threshold InGaAs vertical-cavity surface emitting lasers," *The Third International Symposium on New Phenomena in Mesoscopic Structures,* No. P16, 1995.

(13) K. Saotome, A. Matsutani, T. Honda, F. Koyama and K. Iga,"Estimation of etched reflectivity of GaN-based semicnductor lasers", *The International Symposium on Blue Laser and Light Emitting Diodes*, We-P26, March 1996.

(14) K. Saotome, A. Matsutani, T. Shirasawa, M. Mori, T. Sakaguchi, T. Honda, F. Koyama and K. Iga," Reactive ion beam etching of GaN grown by MOCVD on sapphire (0001)", *15 Electronic Materials Symposium*, C-15, pp. 61-62, 1996.

(15) S. Mitsui, F. Koyama, A. Matsutani, T. Miyamoto and K. Iga,"A design of polygonal micro-ring cavities for photonic integrated circuits", *Proceedings of IEEE Lasers and Electro-Optics Society Annual Meeting*, Boston, WR4, 1996.

(16) M. Takahashi, N. Egami, A. Mizutani, A. Matsutani, F. Koyama, and K. Iga, T. Nakanishi, and M.Nakayama,"Vertical-cavity surface-emitting lasers grown on GaAs(311)A substrates for a wide temperature range of polarization control,"*OSA TOPS (Trends in Optics and Photonics) ,15 Advances in Vertical Cavity Surface Emitting Lasers*, 2-9, 1997.

(17) M. Takahashi, N. Egami, A. Mizutani, A. Matsutani, F. Koyama, and K. Iga, "Dynamically stable polarization characteristics of oxide-confinementvertical-cavity surface-emitting lasers grown on GaAs(311)A substrate,"*IEEE 1997 Summer Topical Meetings (Montreal, Canada)*, 35-36, 1997.

C. Domestic Conferences

(1) A. Matsutani, F. Koyama and K. Iga, "Micro-fabrication of SiO_2/TiO_2 Multi-layer Reflector for Surface Emitting Laser by RIE," *51st Autumn Meeting of Jpn. Soc. Appl. Phys.*, 28p-ZK-8, 1990.

(2) A. Matsutani, F. Koyama and K. Iga, "Cl_2-RIBE of GaInAsP/InP Semiconductor Multilayer for Surface Emitting Laser," *38th Spring Meeting of Jpn. Soc. Appl. Phys.*, 31p-K-4, 1991.

(3) A. Matsutani, F. Koyama and K. Iga, "Incidence Ion Beam Angle Dependence of Cl_2-RIBE Induced Damage," *52nd Autumn Meeting of Jpn. Soc. Appl. Phys.*, 11p-H-12, 1991.

(4) A. Matsutani, F. Koyama and K. Iga, "Characterization on Damage of GaInAsP/InP Sidewall Etched by RIBE," *39th Spring Meeting of Jpn. Soc Appl. Phys.*, 29a-S-4, 1992.

(5) A. Matsutani, F. Koyama and K. Iga, "Micro-Mesa Etch by RIBE Using EB Written Masks," *53rd Autumn Meeting of Jpn. Soc. Appl. Phys..*, 18p-ZA-4, 1992.

(6) H. Katoh, H. Kuroda, A. Takeuchi, K. Moriki, A. Matsutani, T. Sakaguchi and K. Iga, "Optical Beam Scanner Composed of Narrow Spaced AlGaAs/GaAs-Waveguide Array," *53rd Autumn Meeting of Jpn. Soc. Appl. Phys..*, 1993.

(7) H. Kuroda, H. Katoh, Y. Ryu, K. Moriki, A. Matsutani, T. Sakaguchi and K. Iga, "Optical Multi-branching Device Using Diffraction in 2-D Polymer Waveguide," *53rd Autumn Meeting of Jpn. Soc. Appl. Phys..*, 1993.

(8) A. Matsutani, F. Koyama and K. Iga, "Sidewall Roughness Analysis of InP Etched by RIBE," *41st Spring Meeting of Jpn. Soc. Appl. Phys..*, 30a-V-11, 1994.

(9) S. Mitsugi, J. Katoh, A. Matsutani, T. Miyamoto, T. Mukaihara, F. Koyama and K. Iga, "Size Reduction of Micro-arc Ring Laser," *41st Spring Meeting of Jpn. Soc. Appl. Phys..*, 31a-K-4, 1994.

(10) H. Kuroda, T. Nishimura, Y. Ryu, K. Moriki, A. Matsutani, T. Sakaguchi and K. Iga, "Optical Multi-branching Device Using Diffraction in 2-D Polymer Waveguide (II)," *41st Spring Meeting of Jpn. Soc. Appl. Phys..*, 30p-G-11, 1994

(11) Y. Ryu, K. Segawa, H. Kuroda, K. Moriki, A. Matsutani, T. Sakaguchi and K. Iga, "Optical Waveguide Array Scanner Using AlGaAs/GaAs MQW Structure," *41st Spring Meeting of Jpn. Soc. Appl. Phys.*, 31p-G-2, 1994.

(12) T. Baba, M. Hamasaki, A. Matsutani and K. Iga, "Fabrication of InGaAs/AlGaAs Rectangular Disk Laser," *41st Spring Meeting of Jpn. Soc. Appl. Phys..*, 31a-K-5, 1994.

(13) A. Matsutani, F. Koyama and K. Iga, "Measurement of Temperature Increase due to Ion Irradiating and Improvement of Etching Profile by Repeated RIBE," *55th Autumn Meeting of Jpn. Soc. Appl. Phys..*, 20p-V-4, 1994.

(14) J. Katoh, F. Koyama, A. Matsutani, T. Mukaihara and K. Iga, "GaInAs/GaAs Strained Quantum Well Short Cavity Lasers with Micro-corner Reflectors," *55th Autumn Meeting of Jpn. Soc. Appl. Phys.*, 21p-S-4, 1994.

(15) M. Hamasaki, T. Baba, A. Yamada, N. Watanabe, A. Matsutani, F. Koyama and K. Iga, "Horizontal Short Cavity DBR Laser by RIBE Technique," *55th Autumn Meeting of Jpn. Soc. Appl. Phys.*, 21p-S-5, 1994.

(16) K. Suzuki, F. Koyama, J. Katoh, A. Matsutani and K. Iga, "Semiconductor Optical

Power Splitters with Submicron Apertures," *Autumn Nat'l Conv. Rec. IEICE of Jpn.*, C-182, 1994.

(17) K. Suzuki, F. Koyama, J. Katoh, A. Matsutani and K. Iga, "Semiconductor Optical Power Splitters with Submicron Apertures," *42nd Spring Meeting of Jpn. Soc. Appl. Phys..*, 31a-K-5, 1995.

(18) T. Mukaihara, Y. Hayashi, N. Hatori, N. Ohnoki, A. Matsutani, F. Koyama and K. Iga, "Low Threshold Operation of InGaAs/GaAs VCSELs Grown by MOCVD," *Spring Nat'l Conv. Rec. IEICE of Jpn.*, C-362, 1995.

(19) A. Matsutani, F. Koyama and K. Iga, "Depression of Micro-projection on Etched Surface by 2step-Reactive Ion Beam Etch," *56th Autumn Meeting of Jpn. Soc. Appl. Phys..*, 28p-ZB-12, 1995.

(20) S. Mitsugi, A. Matsutani, T. Miyamoto, Y. Kurita, T. Takada, F. Koyama and K. Iga, "1.55μm GaInAsP/InP Micro-arc Ring Cavity Semiconductor Lasers," *56th Autumn Meeting of Jpn. Soc. Appl. Phys..*, 28a-ZA-8, 1995.

(21) M. Hamasaki, P. Kaewplung, T. Baba, A. Matsutani, F. Koyama and K. Iga, "Fabrication of 1.55μm GaInAsP/InP Horizontal Short Cavity DBR Lasers," *56th Autumn Meeting of Jpn. Soc. Appl. Phys..*, 28a-ZA-10, 1995.

(22) T. Mukaihara, N. Hatori, N. Ohnoki, A. Matsutani, F. Koyama and K. Iga, "Threshold reduction of InGaAs/GaAs vertical-cavity surface-emitting lasers," *Fall Nat'l Conv. Rec. IEICE of Jpn.*, SC-2-6, 1995.

(23) A. Matsutani, T. Honda, T. Sakaguchi, K. Saotome, F. Koyama and K. Iga, "ECR-Reactive ion Beam Etching of GaN using Cl_2," *43rd Spring Meeting of Jpn. Soc. Appl. Phys..*, 27p-M-19, 1996.

(24) M. Abe, T. Mukaihara, N. Hatori, N. Ohnoki, A. Matsutani, F. Koyama and K. Iga, "Characterization for stress due to AlAs oxidation process in vertical-cavity surface emitting lasers," *43rd Spring Meeting of Jpn. Soc. Appl. Phys..*, 26p-C-2, 1996.

(25) S. Mitsugi, A. Matsutani, T. Miyamoto, T. Takada, F. Koyama and K. Iga, "Fabrication of 1.55μm GaInAsP/InP micro-arc ring lasers formed by CH4/H2 RIE," *43rd Spring Meeting of Jpn. Soc. Appl. Phys..*, 26p-C-11, 1996.

(26) K. Saotome, A. Matsutani, T. Honda, T. Sakaguchi, F. Koyama and K. Iga, "PL-characterization of GaN film etched by photo-assisted wet etching," *57th Autumn Meeting of Jpn. Soc. Appl. Phys.*, 9a-C-11, 1996.

(27) K. Saotome, T. Honda, A. Matsutani, T. Shirasawa, N. Mochida, M. Mori, A. Inoue, T. Sakaguchi, F. Koyama and K. Iga, "Micro-fabrication by ECR-RIBE for GaN-based surface emitting lasers,"*44th Spring Meeting of Jpn. Soc. Appl. Phys.*, 31a-K-7, 1997.

(28) A. Matsutani, F. Koyama and K. Iga, "Ionization of Reactive Gas in CAIBE," *44th Spring Meeting of Jpn. Soc. Appl. Phys.*, 30p-ZD-19, 1997.

(29) A. Matsutani, F. Koyama and K. Iga, "Measurement of chlorine radicals in CAIBE and RIBE systems," *58th Autumn Meeting of Jpn. Soc. Appl. Phys.*, 4a-A-9, 1997.

(30) A. Matsutani, F. Koyama and K. Iga, "Cl_2-RIBE for GaAs and InP using Fullerene Film

as an ElectroBeam Resist," *45th Spring Meeting of Jpn. Soc. Appl. Phys.*, 30p-Q-1, 1998.

D. Technical Meetings and Symposia

(1) A. Matsutani, F. Koyama and K. Iga, "Reactive Ion Beam Etch of GaInAsP/InP Heterostructure and Characterization of Induced Damage," *Technical Report of IEICE, OQE91-183*, pp.91-96, 1992.

(2) A. Matsutani, K. Iga, "Micro-Etching by Reactive Ion Beam Etch and Characterization of Induced Damage," *44th Group of Microoptics, The Optical Society of Japan, MICROOPTICS NEWS* vol. 10 No. 2, 65-70, 1992.

(3) H. Kuroda, Y. Ryu, T. Nishimura, K. Moriki, T. Sakaguchi, A. Matsutani and K. Iga, "1xN Optical Branching Device Using Diffraction in Polymer Waveguide," *Technical Report of IEICE, OQE93-170*, pp. 31-36, 1993.

(4) T. Mukaihara, N. Hatori, N. Ohnoki, A. Matsutani, F. Koyama and K. Iga, "Low threshold operation of micro-cavity InGaAs/GaAs vertical-cavity surface emitting lasers," *LQE, Technical Report of I IEICE of Jpn.*, 1995.

(5) M. Hamasaki, P. Kaewplung, T. Baba, A. Matsutani, F. Koyama and K. Iga," Short Cavity Semiconductor Lasers with Vertical Multiple Reflectors," *Technical Report of IEICE, OPE95-135, LQE95-129*, 1996.

E. Books

(1) A. Matsutani, F. Koyama and K. Iga, "Micro Dry Etching Process for Vertical Surface Emitting Lasers," *American Vacuum Society Series 10, American Institute of Physics, New York*, pp. 112-115, 1991.

(2) A. Matsutani, T. Tadokoro, F. Koyama and K. Iga, "Reactive Ion Beam Etching for Microcavity Surface Emitting Laser Fabrication: Technology and Damage Characterization," *Material Science Forum, @ 1993 Trans Tech Publications, Switzerland*, vol. 140-142, pp. 641-658, 1993.